Reviews in Mineralogy & Geochemistry
Vol. 84 pp. 393–459, 2018
Copyright © Mineralogical Society of America

Thermodynamics of Element Volatility and its Application to Planetary Processes

Paolo A. Sossi
Institut de Physique du Globe de Paris
1 rue Jussieu, F-75005
Paris
France
sossi@ipgp.fr

Bruce Fegley, Jr.
Planetary Chemistry Laboratory
Department of Earth and Planetary Sciences
and
McDonnell Center for the Space Sciences
Washington University
St. Louis, Missouri
USA
bfegley@wustl.edu

INTRODUCTION

Despite its importance in geological sciences, our understanding of interactions between gas and condensed phases (comprising solids and liquids) remains clouded by the fact that, often, only indirect evidence remains for their occurrence. This arises from the tendency for the vapor phase to escape from the condensed phase with which it interacts, owing to its much lower density and thus greater volume. For a gas that is sufficiently tenuous that interactions do not occur between its constituent molecules, this relationship is quantified in the ideal gas law (Clapeyron 1834):

$$PV = n\mathrm{R}T \quad (1)$$

where P is the total pressure exerted by the gas, V its volume, n is the number of moles, R the gas constant (8.3145 $\mathrm{Jmol^{-1}K^{-1}}$, Horstmann 1873) and T the absolute temperature. One mole of an ideal gas at 273.15 K and 10^5 Pa (standard temperature and pressure for gases)[1] has a molar volume of 22,711 $\mathrm{cm^3/mol}$, $10^3\times$ greater than typical silicate liquids or minerals. As a result, vaporization processes in nature are often informed by chemical and textural evidence remaining in the condensed phase. Such evidence points to the influence of vapor-condensed phase interaction at a variety of scales and geological settings, both in our solar system and beyond (Nagahara 2018, this volume). Although also important in terrestrial processes such as volcanism (see Symonds and Reed 1993; Henley and Seward 2018, this volume) and impact events (Koeberl 1986; King et al. 2018, this volume), we present in this chapter an overview of how elements can record gas-condensed phase interactions as they apply to planetary processes that include, but are not limited to:

1. Degassing of planetary magma oceans (section *Evaporation in the presence of major volatiles H, C, S and halogens*)
2. Atmospheres on existing bodies (section *Evaporation in the presence of major volatiles H, C, S and halogens*)

[1] Standard pressure was changed by IUPAC in 1982 from 760 mm Hg barometer (Partington 1950; Ewing et al. 1994)

1529-6466/18/0084-0011$10.00 (print)
1943-6266/18/0084-0011$10.00 (online)
http://dx.doi.org/10.2138/rmg.2018.84.11

3. Evaporation on small planetary bodies (section *Volatility during planetary formation*)
4. Evaporation during giant impacts (section *Volatility during planetary formation*)

To constrain the conditions under which these processes occur necessitates thermodynamic data of gaseous- and condensed species. Therefore, a review of our knowledge and lack thereof, is also presented (section *Thermodynamics of evaporation/condensation of metal oxides in simple, complex and natural systems*). Much of our information on thermodynamic quantities of gaseous species comes from spectrometric measurements, undertaken from the 1950s onwards, largely on simple (binary and ternary) systems (e.g., see Brewer 1953; Margrave 1967; Lamoreaux et al. 1987, and the section *Thermodynamics of evaporation/condensation of metal oxides in simple, complex and natural systems*). This information is now readily available in compilations of thermodynamic data such as JANAF (Chase 1998) or IVTAN (Glushko et al. 1999). However, the application of these data to more complex, natural geological systems is less straightforward.

Instead, for lack of any other comprehensive volatility scale, 50% nebular condensation temperatures, T_c, (Grossman and Larimer 1974; Lodders 2003), which describe the temperature at which half of the abundance of an element is condensed in the solar nebula, are frequently used to discuss elemental volatility in planetary environments. However, these T_c are strictly relevant only at the pressure and temperature conditions of a solar-composition protoplanetary accretion disk (e.g., the solar nebula). Namely, at low total pressures ($P_T \lesssim 10^{-2}$ bar), solar or close to solar metallicity[2] (i.e., $P_T \sim P_{H_2} + P_H + P_{He}$), oxygen fugacities ~6 log bar units below the Iron–Wüstite (IW) buffer (due to the low H_2O/H_2 ratios, 5×10^{-4}; Rubin et al. 1988; Grossman et al. 2008). Boss (1998) and Woolum and Cassen (1999), to give two examples, used astronomical observations to model midplane temperatures in protoplanetary accretion disks in the planet-forming region and found temperatures <1600 K. Petrological observations of Calcium, Al-rich inclusions (CAI) with the highly fractionated group II rare-earth element (REE) pattern[3] (Mason and Taylor 1982) indicate they formed by fractional condensation (Boynton 1975; Davis and Grossman 1979) at temperatures of 1676 K, 1463 K, 1296 K at total pressures (P_T) of 10^{-3} bar, 10^{-6} bar, and 10^{-9} bar, respectively (Kornacki and Fegley 1986). At total pressures above $\approx 10^{-2}$ bar, liquids condense in place of solids (Ebel 2004) and departures from solar composition (e.g., by changes in metallicity or H-loss on a planetary body) lead to condensation temperatures different to those in a solar-composition system (Larimer and Bartholomay 1979; Lodders and Fegley 1999; Schaefer and Fegley 2010). Thus, the complexity of evaporation and condensation reactions are such that, at conditions outside this range, the relevant gas species, their equilibrium partial pressures and mechanisms driving their escape diverge greatly.

Potentially powerful tracers of the conditions under which these gas–liquid/solid processes occur are the moderately volatile elements (MVEs), defined as those that condense from a solar composition gas at temperatures between the major components (≈1320 K, Fe, Mg and Si) and troilite (≈660 K, FeS) at 10^{-4} bar total pressure (Palme et al. 1988). Their utility lies in their balanced partitioning between the gas and the condensed phase, such that significant quantities remain to permit their analysis. However, as these elements are typically present in trace quantities in planetary materials, knowledge of their thermodynamic properties in minerals and melts is frequently incomplete. In particular, our understanding of the mechanisms by which MVEs substitute into common high-temperature phases and of their activity coefficients in silicate liquids and minerals remain inadequate. Furthermore, how the complex chemical environments relevant to planetary systems affect the relative stability of gaseous molecules is poorly known. Thus, at present, these gaps in knowledge limit the information one can extract from the behavior of moderately volatile- and other rock-forming elements during high-temperature planetary processes.

[2] Metallicity is the mass proportion of elements heavier than He relative to H in a star.
[3] The Group II CAI comprise 38% of CAI analysed for REE (see Table 1 of Ireland & Fegley 2000) and are depleted in both the most volatile and the most refractory REE, taken as evidence of direct condensation from the solar nebula.

Here, we present an introductory thermodynamic treatment of vaporization/condensation reactions, which serves as a framework for the application of thermodynamic models to geological processes. The two end-member styles of evaporation/condensation, equilibrium and kinetic, are described in the sections *Equilibrium evaporation/condensation* and *Kinetic Evaporation*, respectively. Calculation of thermodynamic equilibrium is discussed, taking into account the effect of non-ideality in the gas phase, enthalpies and entropies of fusion and vaporization, and activity coefficients of melt oxide species (section *General treatment of equilibrium evaporation/condensation*). Information on equilibrium partial pressures of metal-bearing gas species, mainly in simple systems, is derived from Knudsen Effusion Mass Spectrometry (KEMS) (e.g., Copland and Jacobsen 2010) and other experimental techniques (transpiration, torsion effusion; e.g., Margrave 1967), though alternative methods, such as *ab-initio* calculations (Langhoff and Bauschlicher 1988), CALPHAD modelling (Saunders and Miodownik 1998) and free-energy minimization programs (e.g., HSC chemistry, Roine 2002; IVTANTHERMO, Belov et al. 1999) are becoming increasingly widespread (section *Equilibrium evaporation/condensation experimental techniques*). A primer on the geological applications of these techniques, and the thermodynamic data they provide, including evaporation of simple-, complex- and natural oxide systems, are presented in sections *Evaporation of binary metal oxides (MO_x)* through *Natural Systems*.

The kinetic treatment (section *General treatment of kinetic evaporation*) is based on the Maxwell–Boltzmann kinetic theory of gases, which is then applied to derive the Hertz–Knudsen–Langmuir (HKL) equation used to calculate evaporation rates from a surface (Chapman and Cowling 1970; and references therein). Using this equation, extraction of thermodynamic data may also be achieved, though less precisely, from free or Langmuir evaporation experiments, which are performed in furnaces under vacuum or in a controlled atmosphere (section *Kinetic evaporation experimental techniques*). The HKL equation serves as the basis for predicting element loss as a function of time, temperature, and equilibrium partial pressures for element evaporation from minerals and melts (see sections *Major elements* through *Other trace elements*). Much of the information of the evaporation of trace elements in geologically relevant systems comes from these methods (Wulf et al. 1995; Sossi et al. 2016a; Norris and Wood 2017; see section *Other trace elements*). These experiments highlight the differences between nebular condensation and evaporation of silicates under post-nebular conditions (Visscher and Fegley 2013).

At lower temperatures, higher pressures, or in systems that have not lost their complement of major volatiles, the formation of metal hydroxide, -halide, -carbonate, and/or -sulfate gas species becomes important (section *Evaporation in the presence of major volatiles H, C, S and halogens*). The volatility of metals in H_2O (or steam) atmospheres is enhanced relative to their volatilities in the binary metal–oxygen system (Schaefer et al. 2012; Fegley et al. 2016) and speciation of an element in the gas phase may change as a function of pressure, temperature and fugacity of other volatiles (see sections *Cu-bearing gases* through *Factors governing the stability of gas species*). As such, volatile loss of these species may engender depletions in the complementary condensed phase that are distinct from evaporation under volatile-poor conditions.

This information is reconciled together to summarize and interpret volatile element depletions observed in the terrestrial planets in the section *Volatility during planetary formation.* Here, we give an overview of how volatile element depletion in planetary materials can be quantified, and how they relate to the processes, both physical and chemical, that occur during the formation of meteorites and subsequently the planets (see section *Overview*). Since the conditions under which the planets form differ from those present during solar nebula condensation, the mechanisms responsible for volatile depletion leave imprints on planetary composition distinct from those found in chondritic meteorites[4] (see section *Planetary bodies*). Though the Earth is depleted in volatile elements with respect to chondritic meteorites, its current mass and atmospheric temperature effectively impedes atmospheric escape (Zahnle and Catling 2017), except in special cases, namely for H, ^{3}He, ^{4}He

[4] Chondritic meteorites—the most common meteorites—are undifferentiated rocks containing metal, silicate, and sulfide, so called for the millimeter-sized spherical objects named 'chondrules' that comprise them.

(Hunten and Donahue 1976; Torgesen 1989), such that this depletion likely occurred early in its history (see section *The Earth*). By comparison, the Moon and the asteroid 4-Vesta are even more impoverished than the Earth in these volatile elements, which is partially attributable to their much smaller masses, the composition of their source materials, and their individual thermal histories (see section *The Moon and Vesta*).

This chapter is intended as an introduction and as a reference to the thermodynamic approaches, methods and existing data relevant to evaporation/condensation processes of metal oxides and their application to planetary processes. The reader is encouraged to select the sections that are most relevant to them, and to delve into the references cited, which are themselves not exhaustive. Finally, throughout this chapter, we highlight promising avenues of future research in the field that may help in gaining a more quantitative understanding of gas-condensed phase interactions in planetary science.

THERMODYNAMICS OF EVAPORATION/CONDENSATION OF METAL OXIDES IN SIMPLE, COMPLEX AND NATURAL SYSTEMS

Evaporation is the (solid, liquid) to gas phase transition and condensation is the reverse process. Unless otherwise noted we do not distinguish between sublimation (solid to gas) and vaporization (liquid to gas). Metals are taken to broadly to encompass metals, metalloids, and semiconductors that remain in metallic form, form oxides and silicates, or combine with other ligands such as C, N, P, OH, chalcogens (S, Se, Te) or halogens (F, Cl, Br, I) in planetary materials. The cases of silicates, oxides and metals (liquids and solids), common in planets and chondrites, are considered henceforth, but other compounds are discussed where relevant. The review covers virtually all naturally occurring elements with an emphasis on the moderately volatile. The MVE occur on the inner right-hand side of the periodic table; transition metals in groups 11 and 12 (Cu, Zn, Ag, Cd), metals and metalloids of groups 13 and 14 (e.g. Ga, Sn, Pb, Sb) in addition to the alkali metals (Li, K, Na, Rb, Cs).

A description of the basic mechanics of evaporation are presented, followed by some of the ways in which evaporation rates and equilibrium partial pressures can be determined experimentally. Finally, examples are presented of natural materials in which volatile element loss by evaporation has been recorded, and the implications this has for their geologic history.

Equilibrium evaporation/condensation

General treatment of equilibrium evaporation/condensation. Evaporation can occur congruently or incongruently. The majority of metals in condensed phases, evaporate congruently (e.g., Brewer 1953; Ackermann and Thorn 1961; Lamoreaux et al. 1987; Table 1), where a condensed component, such as a metal oxide, M–O, evaporates to one (associative) or more (dissociative) species in the gas phase, with the same overall stoichiometry. Congruent dissociative evaporation involving oxygen can be written generally:

$$\left(M^{x+n}\frac{x+n}{2}\mathrm{O}\right)_{(s,l)} = \left(M^{x}\frac{x}{2}\mathrm{O}\right)_{(g)} + \frac{n}{4}\mathrm{O}_{2(g)} \qquad (2)$$

where M is the metal species, x its formal charge, and n the number of electrons in the redox equilibrium. The metal is present in metallic form if $x+n=0$, whereas if $x+n>0$, then an oxide compound is stable in at least the more oxidized of the two species. The latter case typifies evaporation of silicate material, where metals are generally present as $\left(M^{x+n}\frac{x+n}{2}\mathrm{O}\right)$ components in the condensed phase, and n is positive such that the metal becomes more volatile

under reducing conditions as $\left(M^x\frac{x}{2}\mathrm{O}\right)$. However, when n is negative, oxidizing conditions promote vaporization of the metal- or metal-oxide component in the condensed phase.

Incongruent evaporation is characterized by reactions in which $(x+n)_{(s,l)} \neq (x+n)_{(g)}$. That is, the M/O ratio is greater or less than unity in the vapor phase with respect to the condensed phase. Incongruence is manifest in a change in stoichiometry of the condensed phase, which may be small and result in defect formation (e.g., ZnO, Kodera et al. 1968), or larger and lead to the formation of a new phase (as is discussed later). Defect chemistry is not discussed further and the reader is referred to Kröger (1964). Incongruent evaporation involving the production of oxygen only can be written with Equation (2) where $\left(M^x\frac{x}{2}\mathrm{O}\right)$ is also condensed. For cases in which a metal-bearing gas species is produced, incongruent evaporation, for all $x \geq n$, may be expressed:

$$2\left(M^x\frac{x}{2}\mathrm{O}\right)_{(s,l)} = \left(M^{x+n}\frac{x+n}{2}\mathrm{O}\right)_{(s,l)} + \left(M^{x-n}\frac{x-n}{2}\mathrm{O}\right)_{(g)} \tag{3}$$

As per congruent evaporation, if $n > 0$, the speciation of the element in the gas is more reducing, and vice-versa.

Speciation of metals in oxides, silicate liquids or minerals can be combined with thermodynamic data for stable gas species (e.g., Lamoreaux et al. 1987) to write an equilibrium constant for a given volatilisation reaction:

$$K_{(2)} = \frac{f\left(M^x\frac{x}{2}\mathrm{O}\right)f\left(\mathrm{O}_2\right)^{n/4}}{a\left(M^{x+n}\frac{x+n}{2}\mathrm{O}\right)} \tag{4}$$

The a and f terms are the activity and fugacity of a species. The fugacity of a gas is the product of the partial pressure and fugacity coefficient ϕ of the gas,

$$f_i = \phi_i p_i \tag{5}$$

The fugacity coefficient is equal to unity for an ideal gas and is either <1 or >1 for a non-ideal (real) gas. The fugacity coefficient is unity to a very good first approximation for equilibrium evaporation reactions with total vapor pressures ≤1 bar. For example, the 2nd virial coefficient for pure O_2 gas (Levelt Sengers et al. 1972) at one bar total pressure is within 0.03% of unity from 500 to 2000 K. The total vapor pressures in the equilibrium evaporation experiments discussed here are ≤ 1 bar and thus ideal gas behavior can safely be assumed, and hence the approximation $f = p$ (i.e., $\phi = 1$) can be made.

The activity of a pure condensed solid or liquid is unity at a partial pressure equal to that of the saturated vapor, $p_{i,\,\mathrm{sat}}$,

$$a_i = \frac{p_i}{p_{i,\,\mathrm{sat}}} \tag{6}$$

The activity of a pure condensed phase is simply the ratio of its partial pressure to its saturated vapor pressure at the same temperature. If equilibrium evaporation takes place at high total pressure, e.g., due to a high pressure exerted by an inert gas, the effect of total pressure on activity of the condensed phase(s) has to be considered using the thermodynamic relationship

$$\mathrm{R}T\ln a_i = \int_{p^\circ}^{P} V_\mathrm{m}\,dP \tag{7}$$

where V_m is the molar volume of the condensed phase and the integration limits are the saturated vapor pressure of the pure phase (p^o) and the total pressure of the system (P). This relation is known as the Poynting correction and expresses the effect of total pressure on vapor pressure.

The equilibrium constant for reaction (2) is related to the standard Gibbs Free Energy of the reaction via the reaction isotherm

$$\Delta G = \Delta G^\mathrm{o} + \mathrm{R}T\ln K \tag{8}$$

At equilibrium $\Delta G = 0$ and we have the familiar relationship

$$\Delta G^\mathrm{o}_{(2)} = -\mathrm{R}T\ln K_{(2)} \tag{9}$$

The standard Gibbs Free energy of an evaporation reaction is given by the Gibbs–Helmholtz Equation,

$$\Delta G^\mathrm{o} = \Delta H^\mathrm{o} - T\Delta S^\mathrm{o} \tag{10}$$

The standard Gibbs energy, enthalpy, and entropy of formation are all functions of temperature, and the Gibbs–Helmholtz equation can be rewritten in terms of the heat capacities of the product and reactant species

$$\Delta G^\mathrm{o}_T = \Delta H^\mathrm{o}_{T,\mathrm{ref}} + \int_{T,\mathrm{ref}}^{T} \Delta C^\mathrm{o}_P\ \mathrm{d}T - T\left[\Delta S^\mathrm{o}_{T,\mathrm{ref}} + \int_{T,\mathrm{ref}}^{T} \frac{\Delta C^\mathrm{o}_P}{T}\mathrm{d}T\right] \tag{11}$$

The reference temperature (T,ref) is generally 298.15 K but any other convenient value can also be used. The ΔC^o_P is the difference between the heat capacity of the products and reactants with the appropriate stoichiometric coefficients. This expression can be considerably simplified using the Gibbs energy function defined (typically at a reference temperature of 298.15 K) as

$$\frac{G^\mathrm{o}_T - H^\mathrm{o}_{298}}{T} = \frac{\left(H^\mathrm{o}_T - H^\mathrm{o}_{298}\right)}{T} - S^\mathrm{o}_T \tag{12}$$

Substituting this back into the expression for $\Delta \mathrm{G}^\circ_T$ gives

$$-\mathrm{R}\ln K_{(2)} = \frac{\Delta G^\mathrm{o}_T}{T} = \Delta\left[\frac{\left(G^\mathrm{o}_T - H^\mathrm{o}_{298}\right)}{T}\right] + \frac{\Delta H^\mathrm{o}_{298}}{T} \tag{13}$$

The Gibbs energy functions for a given compound tabulated in the JANAF Tables or other thermodynamic data compilations generally take solid-state phase changes (polymorphs, $\mathrm{solid}_1 \rightarrow \mathrm{solid}_2$) and fusion ($\mathrm{solid} \rightarrow \mathrm{liquid}$) into account, but if this is not the case then the Gibbs energy function of the liquid species must be calculated using an equation such as

$$\Delta_\mathrm{fus} G^\mathrm{o}_T = \Delta_\mathrm{fus} H^\mathrm{o}_{T_\mathrm{m}} + \int_{T_\mathrm{m}}^{T} \Delta C^\mathrm{o}_P\ \mathrm{d}T - T\left[\Delta_\mathrm{fus} S^\mathrm{o}_{T_\mathrm{m}} + \int_{T_\mathrm{m}}^{T} \frac{\Delta C^\mathrm{o}_P}{T}\mathrm{d}T\right] \tag{14}$$

The melting point is T_m, $\Delta_{fus}H^o_{T_m}$ and $\Delta_{fus}S^o_{T_m}$ are the standard molar enthalpy and entropy of fusion, and ΔC^o_P is the heat capacity difference between the solid and liquid oxide. Rewriting in terms of Gibbs energy functions this equation becomes

$$\frac{\Delta_{fus}G^o_T}{T} = \Delta\left[\frac{\left(G^o_T - H^o_{T_m}\right)}{T}\right] + \frac{\Delta_{fus}H^o_{T_m}}{T} \tag{15}$$

If the ΔC^o_P is not known and cannot be estimated, it is common to use the approximation

$$\frac{\Delta_{fus}G^o_T}{T} = \frac{\Delta_{fus}H^o_{T_m}}{T} - \Delta_{fus}S^o_{T_m} = \frac{\Delta_{fus}H^o_{T_m}}{T} - \frac{\Delta_{fus}H^o_{T_m}}{T_m} \tag{16}$$

Assuming ideality, it is clear from Equation (4) that the relative stabilities of the gas/condensed phase will depend on i) the $fO_2^{(n/4)}$) and ii) the equilibrium constant, K, as given by the standard state entropy, enthalpy and volume change of the reaction. However, mixing of elements in silicate melts are generally non-ideal and the activity of a component is related to its mole fraction via an activity coefficient γ_i

$$a_i = \gamma_i X_i \tag{17}$$

Use of thermodynamic properties obtained on pure compounds is only applicable to vaporization reactions from silicate minerals or melts if the non-ideality of the metal oxides in the condensed phase are considered (see sections *Activity measurements in binary metal oxide—silicate systems (MO_x–SiO_2)* through *Natural Systems*.)

Equilibrium evaporation / condensation experimental techniques. Techniques for acquiring thermodynamic data for evaporation reactions relevant to the geosciences include Knudsen Effusion Mass Spectrometry (KEMS), transpiration and torsion effusion, where partial pressures or gas species are detected by various spectroscopic methods (e.g., infra-red, Raman, and photoelectron spectroscopies), weight-loss or -gain, and mass spectrometry. Detailed descriptions of each of these techniques can be found in the reviews on high-temperature vapors by Margrave (1967), Hastie (1981) and Wahlbeck (1986), and only a brief primer is given here.

The most widely used technique is KEMS, which is predicated upon chemical and thermal equilibration of gaseous species with each other and with the condensed phase during heating of sample material inside a Knudsen cell in a vacuum (typically 10^{-4} to 10^{-10} bar) due to the small size of the cell and of the pinhole orifice relative to the large mean free path of gases at such low pressures. Thus, a Knudsen cell approximates a closed system. The gas, which has chemically and thermally equilibrated with sample of surface area A_s, effuses out of the pinhole orifice of area A_o. The equilibrium vapor pressure inside the cell (p_e) relative to that calculated by mass loss via the HKL equation (p_m) is given by the Whitman–Motzfeldt equation

$$p_e = p_m\left[1 + \frac{W_o A_o}{A_s}\left(\frac{1}{\alpha_e} + \frac{1}{W_c} - 2\right)\right] \tag{18}$$

where W_o and W_c are the Clausing factors for the orifice and cell body, respectively (Fig. 1a). The orifice therefore should ideally have a diameter and thickness that are infinitesimally small relative to the cell dimensions, A_s. A portion of the effusing gas is then ionized and the resulting positively charged ions are separated according to their mass/charge ratio in quadrupole time-of-flight or magnetic sector mass spectrometers (e.g., Drowart and Goldfinger 1967; Margrave 1967; Cater 1970; Copland and Jacobson 2010).

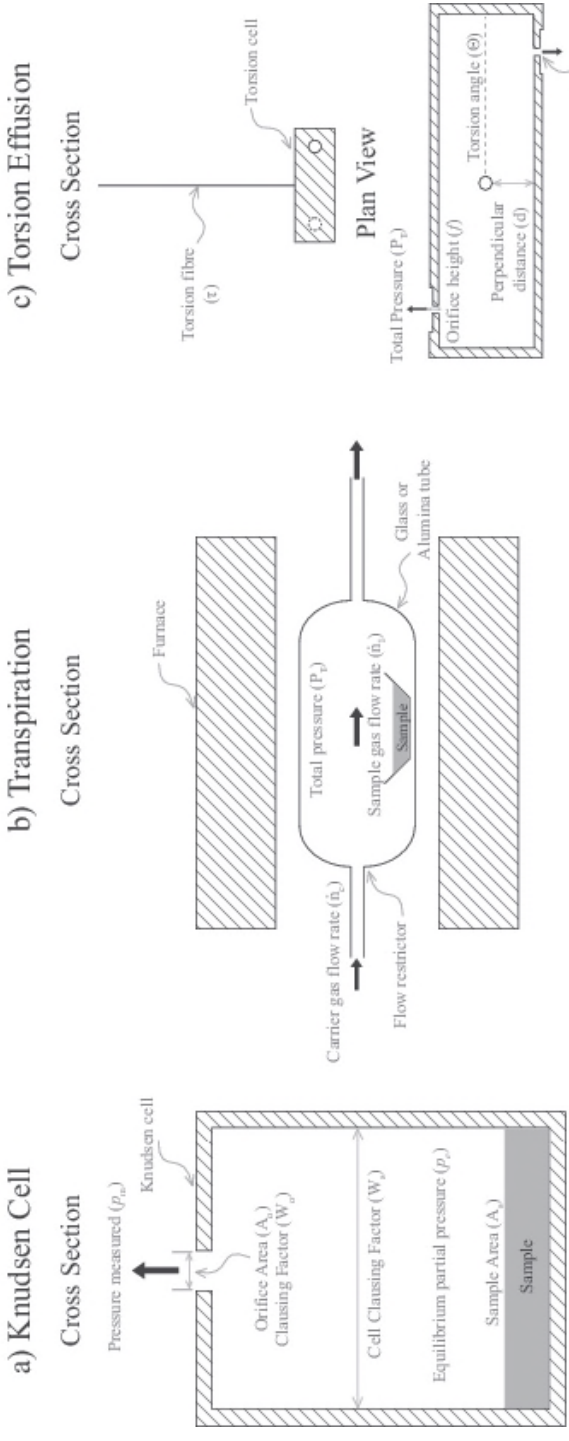

Figure 1. Schematic illustrations of the three types of apparatus used for measuring equilibrium vapor pressures. Only the essential components of each are represented here. **a)** Knudsen cell. See Chatillon et al. (1975); Copland and Jacobson (2010); Wetzel et al. (2012.) **b)** Transpiration apparatus. See Merten and Bell (1967); Wahlbeck (1986); Holstein (1993). **c)** Torsion effusion cell apparatus. See Pratt and Aldred (1959); Munir and Searcy (1964); McCreary and Thorn (1968); Viswanadham and Edwards (1975); Wahlbeck (1986).

Merten and Bell (1967) describe the transpiration method in which either an inert or reactive gas flows over a sample held in the isothermal hot zone of a tube furnace at gas flow rates such that the weight loss is independent of gas flow rate (see Fig. 4 of Belton and Richardson 1962; Fig. 1b). The partial pressure of an evaporating species, p_i, is given by:

$$p_i = \frac{n_i}{n_i + n_c} P_T \tag{19}$$

where n_i and n_c are the molar flow rates of the evaporating species and carrier gas, respectively. At low flow rates, $n_i/(n_i+n_c)$ becomes large and n_i is partially controlled by gas-phase diffusion, whereas n_i is unable to reach equilibrium values at high flow rates due to kinetic effects. Transpiration experiments have provided thermodynamic data for number of metal oxide, -chloride, -hydroxide, and -oxyhydroxide gases and have clarified vaporization behavior of numerous metals and their oxides (e.g., Darken and Gurry 1946; Kitchener and Ignatowicz 1951; Gilbert and Kitchener 1956; Ackermann et al. 1960; Alcock and Hooper 1960; Cubicciotti 1960; Meschi et al. 1960; Caplan and Cohen 1961; Shchukarev et al. 1961a,b; Cordfunke and Mayer 1962; Alexander et al. 1963; Altman 1963; Berkowitz et al. 1960; Berkowitz-Mattuck and Büchler 1963; Belton and McCarron 1964; Stafford and Berkowitz 1964; Belton and Jordan 1965; Faktor and Carasso 1965; Kim and Belton 1974; Sano and Belton 1974; Tetenbaum 1975; Sasamoto et al. 1979; Matsumoto and Sata 1981; Rau and Schnedler 1984; Rego et al. 1985; Hashimoto 1992; Holstein 1993a,b; Hashizume et al. 1999; Jacobson et al. 2005; Meschter et al. 2013; Myers et al. 2016; Nguyen et al. 2017).

The torsion effusion method, as first developed by Volmer (1931), and summarized by Freeman (1967), is predicated on the relationship between torsional force exerted on a cell suspended at its midpoint by a molecular vapor effusing horizontally from two antipodal orifices (A_1 and A_2) that displace the cell by a perpendicular distance d_1 and d_2 to an angle Θ against the restoring force of the fiber with a torsion constant τ (Fig. 1c). The total pressure, P_T, is given by momentum loss

$$P_T = \frac{2\tau\Theta}{\left(A_1 d_1 f_1 + A_2 d_2 f_2\right)} \tag{20}$$

where *f*s are the force recoil factors that account for the finite dimensions of the orifice. Some early works yielded data for *A*s (Rosenblatt and Birchenall 1960), Fe halides (Sime and Gregory 1960) and Ga (Munir and Searcy 1964). Later studies (Viswanadham and Edwards 1975; Edwards 1981; Botor and Edwards 1985; Govorchin 1986; Edwards et al. 1989) combine weight loss measurements by Knudsen effusion with torsion effusion approaches in the same apparatus as a means of verifying vapor pressure measurements. Several groups have measured vapor pressures of metal oxides via torsion effusion or Langmuir effusion (e.g., Hildenbrand et al. 1963, Peleg and Alcock 1966, Alcock and Peleg 1967, Piacente et al. 1972, Hildenbrand and Lau 1993).

These techniques were used extensively in the 1950s to 1980s to measure thermodynamic quantities of materials relevant to military applications, and leading to the construction of the JANAF (Chase 1998) and IVTAN (Glushko et al. 1999) databases in the US and former USSR. Some of this work was also relevant to the ceramic and steelmaking industries for understanding phase equilibria (Muan and Osborn 1965). More recent studies have combined experimental measurements with ab-initio calculations that enable prediction of geometries, vibrational frequencies, and free energies of formation of molecular species (Opila et al. 2007; Gong et al. 2009; Nguyen et al. 2017; Xiao and Stixrude 2018) and represent a fruitful future direction.

Evaporation of binary metal oxides (MO_x). Thermodynamic data for refractory oxides and their evaporation products were instrumental in understanding the major element mineralogy, trace element abundances, and rare earth element (REE) abundance patterns in Ca, Al-rich inclusions (CAIs) in the Allende CV3 chondrite and other meteorites (e.g., Grossman 1972, 1973, Grossman and Larimer 1974, Boynton 1975, 1978, Davis and Grossman 1979, Fegley and Palme 1985, Kornacki and Fegley 1986, Ireland and Fegley 2000). The same data are now useful for modelling atmosphere–surface interactions on hot rocky exoplanets such as CoRoT-7b and Kepler-10b (e.g., Schaefer and Fegley 2009a; Kite et al 2016) and chemistry in the proto-lunar disk (Visscher and Fegley 2013).

Table 1 lists the metal bearing gases in the saturated vapor over ~ 80 binary metal oxides, both volatile and refractory, based on experimental measurements and/or thermodynamic calculations. Bold type indicates the most abundant metal-bearing gas; others are listed in descending order. Monatomic and/or diatomic oxygen are also present in all cases but are not listed. The temperature range of each study and the melting point of each oxide are also listed, e.g., 2327 K for Al_2O_3.

Many oxides evaporate congruently such as Al_2O_3, CdO, Ga_2O_3, GeO_2, MnO, NiO, SiO_2, SnO_2, Ti_3O_5, V_2O_3, WO_3 ($T \leq 1550$ K). In these cases evaporation involves the production of oxygen and is dissociative, in which the gaseous species each have different stoichiometry than the condensed phase, but the bulk composition of the vapor is the same. Some oxides evaporate mainly as gases with the same stoichiometry as the solid or liquid oxide (congruent associative evaporation), e.g., As_4O_6, B_2O_3, BaO, Cs_2O, OsO_4, P_4O_{10}, Re_2O_7, Sb_4O_6, and Tl_2O, but even in these cases other metal-bearing gases with different stoichiometry are present in non-negligible amounts (Table 1). However several oxides do evaporate incongruently with different metal/oxygen ratios in the saturated vapor and the condensed phase, which may vary with temperature. Examples of this behavior include Fe oxides, TiO, TiO_2, Ti_2O_3 VO, V_2O_4, V_2O_5, CuO, Ag_2O, La_2O_3, Ce_2O_3, Y_2O_3, WO_2, WO_3 ($T > 1550$ K), ThO_2, and UO_2 (Ackermann et al. 1956, 1963, 1970; Ackermann and Rauh 1963, 1971a,b; Kodera et al. 1968; Farber et al. 1972b). In addition, Taylor and Hulett (1913) and Otto (1964, 1965, 1966a,b) measured manometrically the equilibrium O_2 dissociation pressures over HgO (mercuric oxide), Mn_2O_3 (manganic oxide), MnO_2 (pyrolusite), Ag_2O, and PbO_2 (plumbic oxide). With the exception of HgO, which vaporizes to $Hg_{(g)} + O_{2(g)}$, the total vapor pressure for these oxides, as well as $Fe_{1-x}O$, Fe_3O_4, Fe_2O_3 (Chizikov et al. 1971) and CuO (Kodera et al. 1968) is effectively the O_2 pressure.

Table 1. The metal bearing gases in the saturated vapour over 77 pure oxides.

Oxide	Temperature (K)	Gas Species	References
α-$Al_2O_{3(s,l)}$ 2327 K	2309–2605[a] 1500–1800[b] 2188–2594[c] 1900–2600[d] 2300–2600[e] 2450[f] 2200–2318[g] 2105–2800[h] 3500–4700$_{(l)}$[i] 2300–2600[j]	**Al**, AlO, Al_2O, AlO_2[d,g], Al_2O_2	[a]Brewer & Searcy 1951 [b]Porter et al. 1955a [c]Drowart et al. 1960 [d]Farber et al. 1972a [e]Chervonnyi et al. 1977 [f]Paule 1976 [g]Ho & Burns 1980 [h]Milushin et al. 1987 [i]Hastie et al. 2000 [j]Chervonnyi 2010
$As_2O_{3(s,l)}$ arsenolite 551 K	367–429[a] 400–1700[b] 375–415[c]	**As_4O_6** ≫ As_4O_5, As_4O_4, As_2O_3, AsO	[a]Behrens & Rosenblatt 1972 [b]Brittain et al. 1982 [c]Kazenas & Petrov 1997

Oxide	Temperature (K)	Gas Species	References
$B_2O_{3(l)}$ 723 K	1300–1500[a] 1410–1590[b] 1200–1440[c] 1170–1400[d]	**B_2O_3**, B_2O_2, BO, B	[a]Inghram et al. 1956 [b]Hildenbrand et al. 1963 [c]Büchler & Berkowitz-Mattuch 1963 [d]Jacobson & Myers 2011
$BaO_{(s)}$ 2246 K	1200–1500[a] 1150–1390[b] 1530–1758[c] 1365–1917[d] 1340–1660[e]	**BaO**, Ba, Ba_2O_3, Ba_2O_2, Ba_2O	[a]Claasen & Veenemans 1933 [b]Pelchowitch 1954 [c]Inghram et al. 1955 [d]Newbury et al. 1968 [e]Hilpert & Gerads 1975
$BeO_{(s)}$ 2851 K	1900–2400[a] 2300–2500[b]	**Be**, $(BeO)_3$, $(BeO)_4$, BeO, $(BeO)_2$, $(BeO)_5$, $(BeO)_6$, Be_2O[b]	[a]Chupka et al. 1959 [b]Theard & Hildenbrand 1964
$Bi_2O_{3(s,l)}$ 1098 K	1003–1193[a] 987–1017[b]	**Bi**, BiO, Bi_4O_6, Bi_2, Bi_2O_3 Bi_3O_4, Bi_2O_2, Bi_2O	[a]Sidorov et al. 1980 [b]Oniyama & Wahlbeck 1998
$CaO_{(s)}$ 3172 K	2080–2206[a] 1500–1900[b] 1923–2227[c]	**Ca**, CaO	[a]Farber and Srivastava 1976a [b]Sata et al. 1982 [c]Samoilova & Kazenas 1995
$CdO_{(s)}$ 1755 K, dec.	1150–1374[a] 873–1056[b] 1014–1188[c] 886–1090[d] 980–1334[e]	**Cd** ≫ CdO	[a]Gilbert & Kitchener 1956 [b]Kodera et al. 1968 [c]Miller 1975 [d]Behrens and Mason 1981 [e]Kazenas et al. 1984a
$CeO_{2(s)}$ 2753 K	1825–2320[a] 1736–2067[b] 1700–2200[c]	**CeO_2**, CeO ≫ Ce	[a]Ackermann & Rauh 1971b [b]Piacente et al. 1973 [c]Marushkin et al. 2000
$Ce_2O_{3(s)}$ 2523 K	1825–2320[a] 1850–2050[b]	**CeO**, CeO_2 ≫ Ce	[a]Ackermann & Rauh 1971b [b]Marushkin et al. 2000
$CoO_{(s)}$ 2103 K	1578–1744[a] 1617–1818[b]	**Co**, CoO	[a]Grimley et al. 1966 [b]Kazenas and Tagirov 1995
$Cr_2O_{3(s)}$ 2603 K	1839–2059[a] 1690–2020[b]	**Cr**, CrO, CrO_2, CrO_3	[a]Grimley et al. 1961 [b]Chizikov et al. 1972
$CrO_{3(s)}$ 470 K	423–523[a] 440–480[b]	**$(CrO_3)_n$,** (n = 3–5), Cr_xO_{3x-2}	[a]McDonald and Margrave 1968 [b]Kazenas & Samoilova 1995
$Cs_2O_{(s,l)}$ 768 K	443–1000[a] 1070–1170[b] 298–2500[c] 620–1100[d]	**Cs_2O**, Cs, Cs_2O_2, CsO	[a]Tower 1969 [b]Nicolosi et al. 1979 [c]Glushko et al. 1982 [d]Lamoreaux & Hildenbrand 1984
$Cu_2O_{(s)}$ 1517 K	1280–1450[a] 1210–1452[b]	**Cu**	[a]Kazenas et al. 1969 [b]Kodera et al. 1968
$CuO_{(s,l)}$ 1599 K	873–1173[a] 873–1273[b] 1200–2000[c]	**Cu,** Cu_2, CuO	[a]Kodera et al. 1968 [b]Mack et al. 1923 [c]IVTAN code & database
$Dy_2O_{3(s)}$ 2680 K	2432–2637[a] 2000–2500[b]	**DyO**, Dy	[a]Ames et al. 1967 [b]Panish 1961b
$Er_2O_{3(s)}$ 2691 K	2492–2687[a] 2000–2500[b]	**ErO**, Er	[a]Ames et al. 1967 [b]Panish 1961b
$Eu_2O_{3(s)}$ 2623 K	1984–2188[a] 1950–2350[b]	Eu, EuO[a,b] **EuO** ≫ Eu[c]	[a]Ames et al. 1967 [b]Panish 1961a [c]Dulick et al. 1986
$Fe_{1-x}O_{(s)}$ wüstite 1650 K $FeO_{(l)}$[c]	1776 $_{(l)}$[a] 1773–1867 $_{(l)}$[b] 1600–1750$_{(s,l)}$[c] 1543–1573[d] 1930–1950 $_{(l)}$[e]	**Fe** > FeO	[a]Brewer & Mastick 1951 [b]Washburn 1963 [c]Chizikov et al. 1971 [d]Shchedrin et al. 1978 [e]Kazenas and Tagirov 1995

Oxide	Temperature (K)	Gas Species	References
$Fe_3O_{4(s)}$ 1870 K	1400–1600[a] 1373–1673[b]	**Fe**[b]	[a]Chizikov et al. 1971 [b]Shchedrin et al. 1978
$Fe_2O_{3(s,l)}$ 1730 K dec in 1 atm O_2	1030–1200[a] 1639–1764[b]	**Fe**[b], FeO[b], FeO_2[b]	[a]Chizikov et al. 1971 [b]Hildenbrand 1975
$Ga_2O_{3(s)}$ 2080 K	1073–1273[a] 2068[b] 1013–1841[c]	**Ga_2O**, Ga, GaO	[a]Frosch & Thurmond 1962 [b]Burns 1966 [c]Shchukarev et al. 1969
$Gd_2O_{3(s)}$ 2693 K	2000–2500[a] 2350–2590[b] 2400–2550[c] 2100–2350[d]	**GdO** ≫ Gd	[a]Panish 1961b [b]Messier 1967 [c]Ames et al. 1967 [d]Alcock & Peleg 1967
$GeO_{2(s)}$ 1388 K	758–859[a] 1313–1373[b] 744–1373[c] 1213–1347[d] 965–1144[e]	**GeO**, Ge, Ge_2O, $(GeO)_2$, $(GeO)_3$	[a]Jolly & Latimer 1952 [b]Shimazaki et al. 1957 [c]Drowart et al. 1965b [d]Kazenas et al. 1973 [e]Rau & Schnedler 1984
$HfO_{2(s)}$ 3073 K	2246–2600[a] 2150–2500[b] 2200–2900[c]	**HfO** > HfO_2 ≫ Hf	[a]Panish & Reif 1963 [b]Alcock & Peleg 1967 [c]Belov & Semenov 1985
$Ho_2O_{3(s)}$ 2686 K	2487–2711[a] 2000–2500[b]	**HoO**, Ho	[a]Ames et al. 1967 [b]Panish 1961b
$In_2O_{3(s)}$ 2186 K	1290–1490[a] 1269–1539[b] 1300–1500[c] 1539–1631[d] 873–1223[e] 1322–1520[f]	**In_2O**, In, InO	[a]Shchukarev et al. 1961b [b]Burns et al. 1963 [c]Burns 1966 [d]Shchukarev et al. 1969 [e]Valderraman and Jacob 1977 [f]Gomez et al. 1982
$K_2O_{(s,l)}$ 1013 K[b]	1087–1186[a] 1037–1184[b] 580–825[c] 298–3000[d]	**K**, K_2O, KO, K_2O_2[d], K_2[d], KO_2[d]	[a]Ehlert 1977 [b]Simmons et al. 1977 [c]Byker et al. 1979 [d]Lamoreaux and Hildenbrand 1984
$La_2O_{3(s)}$ 2586 K	2230–2440[a] 2234–2441[b] 1778–2427[c]	**LaO** ≫ La	[a]Walsh et al. 1960 [b]Goldstein et al. 1961 [c]Ackermann & Rauh 1971a
$Li_2O_{(s)}$ 1711 K	1000–1600[a] 1494–1669[b] 1447–1662[c] 1300–1700[d] 1225–1507[e]	**Li ~ Li_2O** > LiO > Li_3O[d,e], Li_2O_2[d,e]	[a]Berkowitz et al. 1959 [b]Hildenbrand et al. 1963 [c]White et al. 1963 [d]Kudo et al. 1978 [e]Kimura et al. 1980
$Lu_2O_{3(s)}$ 2763 K	2615–2700[a] 2000–2500[b] 2700[c]	**LuO** ≫ Lu (LuO/Lu ~ 4)[c]	[a]Ames et al. 1967 [b]Panish 1961b [c]Lopatin & Shugurov 2014
$MgO_{(s)}$ 3100 K	1950[a] 1720–1960[b] 2020–2160[c] 1573–1973[d] 1820–1983[e]	**Mg**, MgO	[a]Porter et al. 1955b [b]Alcock & Peleg 1967 [c]Farber & Srivastava 1976b [d]Sata et al. 1978 [e]Kazenas et al. 1983
$MnO_{(s)}$ 2115 K	1767[a] 1618–1815[b] 1858–1999[c] 1535–1782[d]	**Mn**, MnO, MnO_2[c]	[a]Brewer & Mastick 1951 [b]Kazenas et al. 1984b [c]Hildenbrand & Lau 1994 [d]Matraszek et al. 2004
$MoO_{2(s)}$ 1373 K dec.	1481–1777[a] 2262–2466[b]	**MoO_3**, $(MoO_3)_2$, MoO_2, $(MoO_3)_3$, MoO[b]	[a]Burns et al., 1960 [b]DeMaria et al. 1960

Oxide	Temperature (K)	Gas Species	References
$MoO_{3(s)}$ 1074 K	800–1000[a] 980–1060[b]	**$(MoO_3)_3$**, $(MoO_3)_n$ n=4,5	[a]Berkowitz et al. 1957b [b]Ackermann et al. 1960
$Na_2O_{(s)}$ 1405 K	987–1114[a] 1144–1304[b] 984–1056[c] 873–1003[d]	**Na**, Na_2O, NaO, NaO_2[c]	[a]Hildenbrand and Murad 1970 [b]Piacente et al. 1972 [c]Hildenbrand and Lau, 1993 [d]Popovic et al. 2012
$NbO_{(s,l)}$ 2210 K	1773–2473$_{(s,l)}$[a] 2032–2125[b] 1971–2175[c]	**NbO_2 ~ NbO**	[a]Shchukarev et al. 1966 [b]Kamegashira et al. 1981 [c]Matsui & Naito 1982
$NbO_{2(s,l)}$ 2175 K 2188 K[b]	1773–2473[a] 1963–2323[b]	**NbO_2**, NbO	[a]Shchukarev et al. 1966 [b]Kamegashira et al. 1981
$Nb_2O_{5(s,l)}$ 1785 K	1726–2271	**NbO_2**	Matsui & Naito 1983
$Nd_2O_{3(s)}$ 2593 K	2250–2400[a] 2255–2408[b] 1950–2350[c] 2155–2485[d]	**NdO** ≫ Nd	[a]Walsh et al. 1960 [b]Goldstein et al. 1961 [c]Panish 1961a [d]Tetenbaum 1975
$NiO_{(s)}$ 2228 K	1782–1816[a] 1575–1709[b] 1400–1570[c] 1587–1730[d]	**Ni**, NiO	[a]Brewer & Mastick 1951 [b]Grimley et al. 1961b [c]Kodera et al. 1968 [d]Kazenas and Tagirov 1995
$OsO_{4\ (l)}$ 314 K	1100–1750	**OsO_4**, OsO_3 ≫ OsO_2	Grimley et al. 1960
$P_4O_{10(s)}$ 699 K	333–923[a] 313–773[b] 370–423[c]	**P_4O_{10}** ≫ P_4O_9, P_4O_8, P_4O_7, P_4O_6	[a]Hashizume et al. 1966 [b]Muenow et al. 1970 [c]Kazenas & Petrov 1997
$PbO_{(s)}$ 1160 K	1000–1150[a] 1010–1105[b] 810–1040[c]	**PbO**, Pb, $(PbO)_n$ (n=2–6)	[a]Drowart et al. 1965a [b]Kazenas & Petrov 1996 [c]Kobertz et al. 2014
$Pr_2O_{3(s)}$ 2573 K	1950–2350[a] Calculated[b]	**PrO** ≫ Pr	[a]Panish 1961a [b]Dulick et al. 1986
$Rb_2O_{(s,l)}$ 900 K	1020–1135[a] 298–3000[b]	**Rb**, Rb_2, Rb_2O, RbO, Rb_2O_2	[a]Nicolosi et al. 1979 [b]Lamoreaux and Hildenbrand 1984
$Re_2O_{7(s)}$ 570 K	327–463	**Re_2O_7**, ReO_3, ReO_2, Re_2O_6, Re_2O_5	Skinner and Searcy, 1973
$Sb_2O_{4(s)}$ 1524 K dec.	1090	**Sb_4O_6**, Sb_3O_4, Sb_2O_3, Sb, Sb_2O_2	Asryan et al. 2003
$Sb_2O_{3(s,l)}$ orthorhombic[a,b] 928 K cubic[a,c] 843 K T_{trans}	742–829 (cubic)[a] 742–917 (orthorh)[a] 929–1073 (liq)[a] 627–732 (orthorh)[b] 580–730 (cubic)[c]	**Sb_4O_6**[a,b,c] (+ Sb_4O_5, Sb_3O_4, Sb_2O_2, SbO)[c]	[a]Hincke 1930 [b]Behrens and Rosenblatt 1973 [c]Semenov et al. 1983
$Sc_2O_{3(s)}$ 2762 K	2555–2693[a] 2481–2740[b] 2521–2768[c]	**ScO**, Sc	[a]Ames et al. 1967 [b]Belov et al. 1987 [c]Rostai & Wahlbeck 1999
SiO_2 cristobalite 1996 K $SiO_{2(l)}$[g]	1840–1951[a] 1200–1950[b] 1600–1754[c] 1823–1983[d] 1833–1877[e] 1887–1988[f] 1800–2200[g]	**SiO**, SiO_2 ≫ Si	[a]Brewer & Mastick 1951 [b]Porter et al. 1955c [c]Nesmeyanov & Firsova 1960 [d]Nagai et al. 1973 [e]Zmbov et al. 1973 [f]Kazenas et al. 1985 [g]Shornikov et al. 1998

Oxide	Temperature (K)	Gas Species	References
$Sm_2O_{3(s)}$ 2613 K	2333–2499[a] 1950–2350[b]	**SmO**, Sm	[a]Ames et al. 1967 [b]Panish 1961a
$SnO_{2(s)}$ 1903 K	1254–1538[a] 1315–1660[b] 1296–1672[c] 1160–1450[d]	**SnO**, Sn_2O_2[a,d]	[a]Colin et al. 1965 [b]Hoenig and Searcy, 1966 [c]Kazenas et al. 1996 [d]Zimmermann et al. 1999
$SrO_{(s)}$ 2805 K	1575–1750[a] 2100[b] 2010–2102[c] 1905–1996[d]	**Sr ~ SrO**	[a]Pelchowitch 1954 [b]Porter et al. 1955b [c]Farber and Srivastava 1976 [d]Samoilova & Kazenas 1994
$Ta_2O_{5(s,l)}$ 2145 K	2019–2314[a] 1573–2073[b] 1924–2268[c] 1880–2525[d] 2043–2262[e]	**TaO_2**, TaO ≫ Ta	[a]Inghram et al. 1957 [b]Kofstad 1964 [c]Krikorian & Carpenter 1965 [d]Smoes et al. 1976 [e]Kazenas et al. 1994
$Tb_2O_{3(s)}$ 2682 K	2000–2500	**TbO** ≫ Tb	Panish 1961b
$ThO_{2(s,l)}$ 3650 K	2050–2250[a] 2170–2400[b] 2000–3000[c] 2170–2500[d] 2400–2800[e] 1782–1940[f] 2390–2950[g] 5140–6230[h]	**ThO_2**, ThO ≫ Th	[a]Shapiro 1952 [b]Wolff & Alcock 1962 [c]Ackermann et al. 1963 [d]Peleg & Alcock 1966 [e]Ackermann & Rauh 1973 [f]Murad & Hildenbrand 1974 [g]Belov & Semenov 1979 [h]Joseph et al. 2002
$TiO_{(s,l)}$ 2023 K	1840[a] 2023–2153[b]	**TiO**, Ti, TiO_2	[a]Berkowitz et al. 1957d [b]Gilles et al. 1968
$Ti_2O_{3(s,l)}$ 2115 K	2194[a] 1675–1768[b]	**TiO ~ TiO_2** ≫ Ti	[a]Berkowitz et al. 1957d [b]Wu & Wahlbeck 1972
$Ti_3O_{5(s,l)}$ 2050 K	1870–2000[a] 1837–2040[b] 2097–2143[c]	**TiO_2 ~ 2×TiO**	[a]Hampson & Gilles 1971 [b]Wahlbeck and Gilles 1967 [b]Gilles et al. 1968
TiO_2 (rutile,l) 2143 K	1881[a] 2193[b] 1850–2540[c]	**TiO_2 ~ TiO** ≫ Ti	[a]Berkowitz et al. 1957d [b]Gilles et al. 1968 [c]Semenov 1969
$Tl_2O_{(s,l)}$ 852 K	620–770[a] 820–940[b]	**Tl_2O** ≫ Tl_3O, Tl_4O_2	[a]Cubicciotti 1969, 1970 [b]Holstein 1993a
$Tl_4O_{3(s,l)}$ 990 K	~773[a] 920–1080[b]	**Tl_2O**	[a]Wahlbeck & Myers 1997 [b]Holstein 1993a
$Tl_2O_{3(s)}$ 1107 K	915–1030[a] 803–948[b] 657–773[c] 880–1060[d]	**Tl_2O**, Tl, TlO	[a]Shchukarev et al. 1961a [b]Cubicciotti & Keneshea 1967 [c]Wahlbeck et al. 1991 [d]Holstein 1993a
$Tm_2O_{3(s)}$ 2683 K	2450–2641[a] 2000–2500[b]	**Tm**, TmO	[a]Ames et al. 1967 [b]Panish 1961b
$UO_{2(s,l)}$ 3123 K	1600–2800[a] 2200–2800[b] 2025–2343[c] 2500–5000$_{(s,l)}$[d] 4715, 5708 $_{(l)}$[e] 2800–3400$_{(s,l)}$[f]	**UO_2**, UO_3, UO	[a]Ackermann et al. 1956 [b]Ohse 1966 [c]Matsui & Naito 1985 [d]Joseph et al. 1996 [e]Joseph et al. 2002 [f]Pflieger et al. 2011
$U_3O_{8(s)}$ 2010 K (in 1 kb He)	1230–1700[a] 840–1450[b]	**UO_3**	[a]Ackermann et al. 1960 [b]Ackermann & Chang 1973

Oxide	Temperature (K)	Gas Species	References
$VO_{(s)}$ 2063 K	1680–1950[a] 1803–1999[b]	**VO**, V ≫ VO_2	[a]Berkowitz et al. 1957a [b]Banchorndhevakul et al. 1986
$V_2O_{3(s)}$ 2340 K	2270[a] 1914–2182[b] 1839–2105[c]	**VO ~ VO_2**, V	[a]Farber et al. 1972b [b]Banchorndhevakul et al. 1985 [c]Wang et al. 2010
$V_2O_{4(s,l)}$ 1818 K	1673–2273[a] 2063–2270[b]	**VO_2**, VO, V_4O_{10}, V	[a]Frantseva & Semenov 1969 [b]Farber et al. 1972b
$V_2O_{5(s,l)}$ 943 K	1680–1950[a] 1003–1205[b]	**V_4O_{10}**, V_4O_8, V_6O_{14}, V_6O_{12}, V_2O_4	[a]Berkowitz et al. 1957a [b]Farber et al. 1972b
$WO_{3(s)}$ 1745 K	1368–1492[a] 2188–2475[b] 1300–1600[c] 1400–3150[d]	**W_3O_9**, W_4O_{12}, W_5O_{15} W_2O_6, WO_3, WO_2, WO,W_3O_8, W_3O_9 (over W)[b,d]	[a]Berkowitz et al. 1957c [b]DeMaria et al. 1960 [c]Ackermann & Rauh 1963 [d]Schissel & Trulson 1966
$Y_2O_{3(s,l)}$ 2712 K	2500–2700[a] 2492–2697[b] 2170–2500[c] 1400–2100[d] 1600–2700[e] 3500–5000 $_{(l)}$[f]	**YO** ≫ Y	[a]Walsh et al. 1960 [b]Ames et al. 1967 [c]Alcock & Peleg 1967 [d]Ackermann et al. 1970 [e]Ackermann & Rauh 1973 [f]Hastie et al. 2000
$Yb_2O_{3(s)}$ 2707 K	2000–2500[a] 2371–2626[b] 2000–2500[c] 2290–2580[d]	**Yb**, YbO	[a]Panish 1961b [b]Ames et al. 1967 [c]Alcock & Peleg 1967 [d]Stolyarova et al. 2014
$ZnO_{(s)}$ 2248 K	1229–1259[a] 1321–1632[b] 1023–1473[c] 1200–1540[d]	**Zn** ≫ ZnO[d]	[a]Anthrop and Searcy 1964 [b]Hoenig 1964 [c]Kodera et al. 1968 [d]Kazenas et al. 1984
$ZrO_{2(s)}$ 2950 K	1700–2500[a] 1800–2390[b] 2060–2875[c] 1790–2430[d] 2600–2820[e]	**ZrO ~ ZrO_2** ≫ Zr	[a]Chupka et al. 1957 [b]Peleg & Alcock 1966 [c]Ackermann et al. 1975 [d]Murad & Hildenbrand 1975 [e]Belov et al. 1981

Figure 2 shows vapor pressure curves for some metal-oxide systems listed in Table 1. The interested reader is encouraged to consult the references cited for details regarding metal-oxide vapor pressure measurements and the thermodynamic data. Early summaries of vaporization studies of oxides can be found in Brewer and Mastick (1951), Brewer (1953), Ackermann and Thorn (1961), Ackermann et al. (1961), Margrave (1967), Brewer and Rosenblatt (1969), Pedley and Marshall (1983), Lamoreaux and Hildenbrand (1984), and Lamoreaux et al. (1987). Margrave (1967) is a superb book that is still relevant today.

Activity measurements in binary metal oxide–silicate systems (MO_x–SiO_2). The application of Knudsen effusion, KEMS, torsion effusion, or transpiration measurements to natural geologic compositions has so far been limited, with a few exceptions, and has instead been used extensively to study binary glass-forming melts (borates, germanates, phosphates, and silicates; Stolyarova 2001). Electromotive force measurements, solubility measurements, and partitioning of a solute between two phases have also been used to measure activities in binary silicate melts. Kubaschewski and Alcock (1979) describe numerical calculation of activities and activity coefficients from all of these methods. Several of the papers listed below also give good descriptions of the underlying principles. The most activity data are available for Na_2O–SiO_2 and K_2O–SiO_2 melts: (e.g., Kröger and Sörström 1965; Charles 1967; Frohberg et al. 1973; Eliezer et al. 1978a; Sanders and Haller 1979; Plante 1981; Rego et al. 1985; Zaitsev et al. 1999, 2000). Some data are available for CaO–SiO_2, FeO–SiO_2,

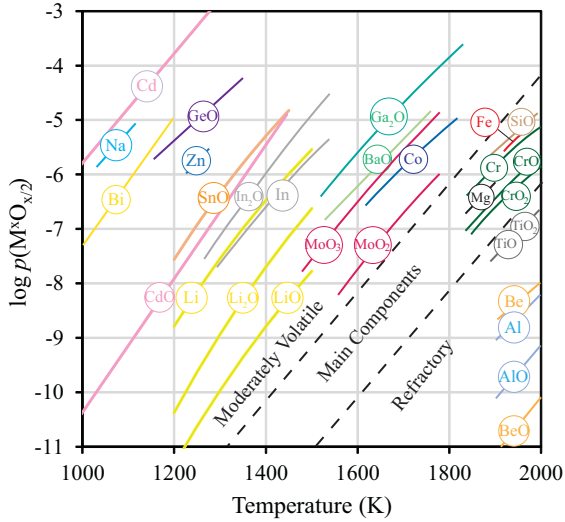

Figure 2. Equilibrium partial pressures of major metal-bearing gas species (listed in circles) over selected pure oxides during their evaporation in a vacuum. Not shown is $Tl_2O_{(s)}$ where $\log p(Tl_2O) = -3$ at 870 K Cubicciotti (1970); $CdO_{(s)}$, Behrens and Mason (1981); $Na_2O_{(s)}$, Hildenbrand and Murad (1970); $Bi_2O_{3(s)}$, Sidorov et al. (1980); $GeO_{2(s)}$ Drowart et al (1965); $ZnO_{(s)}$, Anthrop and Searcy (1964); $SnO_{2(s)}$, Zimmermann et al. (1999); $In_2O_{3(s)}$, Burns et al. (1963); Li_2O, Kimura et al. (1980); $Ga_2O_{3(s)}$, Shchukarev et al. (1969); $BaO_{(s)}$, Inghram et al. (1955); $MoO_{2(s)}$, Burns et al. (1960); $CoO_{(s)}$, $FeO_{(s)}$ Kazenas and Tagirov (1985); $SiO_{2(s)}$, Kazenas et al. (1985); $Cr_2O_{3(s)}$, Grimley et al. (1961); $MgO_{(s)}$, Kazenas et al. (1983); $TiO_{2(s)}$, Semenov 1969; $BeO_{(s)}$, Chupka et al. (1959); $Al_2O_{3(s)}$, Farber et al. (1972).

and MgO–SiO_2 melts (e.g., Schuhmann and Ensio 1951; Bodsworth 1959; Distin et al 1971; Zaitsev and Mogutnov 1995, 1997; Zaitsev et al. 2006). Apparently only a few studies exist for vaporization of $Li_2SiO_{3(s,l)}$ (Penzhorn et al. 1988; Asano and Nakagawa 1989). They show Li is the major Li-bearing gas with other LiO_x gases being significantly less abundant. Kim and Sanders (1991) computed Redlich–Kister parameters for the Rb_2O–SiO_2 and Cs_2O–SiO_2 binaries, based on the phase diagrams of Alekseeva (1963, 1966). Aside from the classic work of Kracek (1930) on the silica liquidus and of Alekseeva (1963, 1966) cited above, we are unaware of any other experimental studies on the Rb_2O–SiO_2 and Cs_2O–SiO_2 binaries. Thus, further work is urgently needed on these two systems to measure experimentally the activities of the Rb and Cs oxide components as a function of *T*, *P*, and composition.

Activity measurements for multicomponent silicate systems. Carmichael et al (1977) and Bottinga and Richet (1978) are the pioneering studies on computations of activity coefficients in multicomponent silicates. A large amount of subsequent work was done on thermochemical properties of silicate glasses and melts (e.g., Stebbins et al 1984; Richet and Bottinga 1986; Lange and Navrotsky 1992, 1993). Most work on activity measurements in multicomponent silicate systems focused on alkali-bearing aluminosilicates (e.g., Eliezer et al 1978b; Hastie et al. 1982; Kassis and Frischat 1981; Rammensee and Fraser 1982; Fraser et al. 1983, 1985; Chastel et al. 1987; Fraser and Rammensee 1987) with applications to granitic systems. There is also a large body of metallurgical literature in which the activities of silica and other major rock-forming oxides have been measured, generally at one or a few isotherms, e.g., the silica activity measurements of Kay and Taylor (1960) for the CaO–Al_2O_3–SiO_2 system which is relevant to the mineralogy of Ca, Al-rich inclusions; FeO–MgO–SiO_2 melts (Plante et al. 1992) and the CMAS system (Rein and Chipman 1965), that has been applied to model the phase equilibria of terrestrial basalts (Osborn and Tait 1952; Presnall et al. 1978), as well as olivine (Dohmen et al. 1998; Costa et al. 2017).

Aside from the major oxide components (i.e., SiO_2, TiO_2, Al_2O_3, FeO, $FeO_{1.5}$, CrO, $CrO_{1.5}$, MgO, CaO, $NaO_{0.5}$, $KO_{0.5}$, $LiO_{0.5}$, $PO_{2.5}$ and H_2O; Chipman 1948; Fincham and Richardson 1954; Rein and Chipman 1965; Charles 1967; Carmichael et al. 1977; Ryerson 1985; Ghiorso and Sack 1995; O'Neill 2005), whose activities can be constrained by phase equilibria (e.g., buffering of $a\mathrm{SiO_2}$ of a silicate liquid by olivine and orthopyroxene, Kushiro 1975), and a handful of trace elements (e.g., Mo, W, Co, Mn, Ni, Cu, In, Pb; Hirschmann and Ghiorso 1994; O'Neill and Eggins 2002; O'Neill et al. 2008; Wood and Wade 2013), the nature of metal oxide species (and of their activity coefficients) in complex silicate melts is poorly known and should be an experimental target in future. Table 2 lists determinations for some metal oxide activity coefficients in complex silicate melts. These should only be used as guide and the interested reader is referred to the relevant paper for further information as to how the activity coefficients were calculated and how they vary with melt composition, temperature, and oxygen fugacity.

Attempts to quantify the effects of composition on activity coefficients commonly apply single-value melt parameter models such as the relative proportion of Non-Bridging Oxygens to Tetrahedral cations (NBO/T; e.g., Mysen and Virgo 1980; Kohn and Schofield 1994) or optical basicity, which describes the tendency for the sum of the species in a melt

Table 2. Metal oxide activity coefficients of 28 species in complex silicate melts.

Oxide	Temperature (K)	Composition	Activity Coefficient	References
$AlO_{1.5}$	1573–1773	CMAS (An–Di)	0.28–0.37	Ghiorso & Sack 1995
$AsO_{1.5}$	1573	FCS	0.03–0.56	Chen & Jahanshahi 2010
$BiO_{1.5}$	1573	FCS	0.3–0.5	Paulina et al. 2013
CaO	1873	CMAS (0.55 < Basicity < 0.65)	≈0.001–0.15	Beckett 2002
CoO	1573–1873[a] 1673[b]	(F)CMAS[a] CMAS[b]	0.5–2.2[a] 0.8–1.8[b]	[a]Holzheid et al. 1997 [b]O'Neill & Eggins 2002; O'Neill & Berry 2006
CrO	1773	CAS	1.9–7.2	Pretorius & Muan 1992
$CrO_{1.5}$	1773	CAS	23–42	Pretorius & Muan 1992
$CuO_{0.5}$	1573[a] 1923[b]	(F)CMAS[a] CMAS[b]	9–11[a] 3.5[b]	[a]Holzheid & Lodders 2001 [b]Wood & Wade 2013
FeO	1600[a] 1573–1873[b] 1673[c] 1923[c]	SKAnF[a] (F)CMAS[b] CMAS[c, d]	0.6–2.3[a] 1.2–2.1[b] 0.9–1.8[c] ≈0.5–2.5[d]	[a]Doyle 1988 [b]Holzheid et al. 1997 [c]O'Neill & Eggins 2002 [d]Wood & Wade 2013
GeO	1423–1523	FCAS	1.44–2.55	Yan & Swinbourne 2013
GeO_2	1573	FCMS	0.24–1.50	Shuva et al. 2016
$InO_{1.5}$	1923	CMAS	0.02	Wood & Wade 2013
$KO_{0.5}$	1573	KFCAS* * with $KAlSiO_{4(s)}$	6.3×10^{-5}–7.1×10^{-4}	Hastie et al. 1981
MgO	1873	CMAS (0.55 < Basicity < 0.65)	≈0.25–4	Beckett 2002
MnO	1823–1923[a] 1873[b]	FCMS(P)[a] CAS[b]	0.7–3.5[a] 0.5–7.2[b]	[a]Suito & Inoue 1984 [b]Ohta & Suito 1995
MoO_2	1673[a] 1923[b]	CMAS[a, b]	67–227[a] ≈5–100[b]	[a]O'Neill & Eggins 2002 [b]Wood & Wade 2013

Oxide	Temperature (K)	Composition	Activity Coefficient	References
MoO_3	1673	CMAS	$0.1–0.8^*$ $^*\log\gamma MoO_3 = 1.49(\log\gamma MoO_2) - 3.59$	O'Neill & Eggins 2002
$NaO_{0.5}$	1623[a] 1673[b]	CMAS[a] CMS[b]	[a]10^{-3} [b]$8.4\times10^{-4}–2.2\times10^{-3}$	[a]Mathieu et al. 2008 [b]Mathieu et al. 2011
NiO	1573–1873[a] 1673[b] 1923[c]	(F)CMAS[a] CMAS[b, c]	1.3–3.5[a] 2.0–4.3[b] ≈1.5–3.0[c]	[a]Holzheid et al. 1997 [b]O'Neill & Eggins 2002; O'Neill & Berry, 2006 [c]Wood & Wade 2013
$PO_{2.5}$	1823–1923	CMFS	$10^{-6}–10^{-10}$	Turkdogan (2000)
PbO	1923	CMAS	0.22	Wood & Wade 2013
SiO_2	1573–1773	CMAS (An-Di)	0.9–1.1	Ghiorso & Sack 1995
SnO	1573	FCS	5–6.2	Takeda & Yazawa 1989
TiO_2	1573–1773	CMAS	1.5–1.7	Ghiorso & Sack 1995
V_2O_3	1900 2000 2100	CMAS CMAS CMAS	1.2–20.8 0.3–5.2 0.05–1.65	Wang et al. 2010
WO_2	1673	CMAS	$7.4–45^*$ $^*\log\gamma WO_2 = \log\gamma MoO_2 - 2.20$	O'Neill et al. 2008
WO_3	1673[a] 1923[b]	CMAS[a, b]	$0.02–0.3^{a*}$ $^*\log\gamma WO_3 = \log\gamma MoO_3 - 1.42$ $\approx 0.001–0.05$ [b]	[a]O'Neill et al. 2008 [b]Wood & Wade 2013
ZnO	1673–1823	CAS	0.25–0.58	Reyes & Gaskell 1983

Notes: A = Al_2O_3; An = Anorthite; C = CaO; Di = Diopside; F = FeO; K = K_2O; M = MgO; P = P_2O_5; S = SiO_2

to donate electrons (e.g., O'Neill and Eggins 2002; Burnham and O'Neill 2016), and then typically only in CMAS, CaO–MgO–Al_2O_3–SiO_2, (±Na_2O, TiO_2) systems. More complex formulations, such as the combined linear-quadratic fit of Wood and Wade (2013) are empirical and generally more tractable in these simple systems. Similarly, understanding the underlying mechanisms controlling the activity coefficients of melt components via quasi-chemical Gibbs Free energy approaches (Pelton et al. 2000; Björkvall et al. 2000; Schmid-Fetzer et al. 2007; Glibin and King 2015) remain restricted to binary and ternary systems, though free-energy minimization programs in multi-component silicate melts (e.g., MELTS; Ghiorso and Sack 1995) and ab-initio simulations hold promise for modelling the properties of complex silicate melts (Guillot and Sator 2007). As such, quantifying the evaporation/condensation of trace elements (notably, the moderately volatile elements) remains an empirical exercise for lack of a large of body of concerted experimental and theoretical work in complex, geological systems.

Once the metal oxide activities are known the partial vapor pressures can be computed using computer codes that take non-ideality of the melt into account and also simultaneously solve gas phase and gas–melt chemical equilibria (e.g., the FactSage code; Bale et al. 2002).

Natural Systems. Sample return from the Moon following the Apollo missions precipitated a push to understand the depletions of volatile metals (particularly Na and K) in a wide variety of lunar lithologies (O'Hara et al. 1970; Ringwood and Essene 1970; Baedecker et al. 1971). To aid in interpretation of these distinctive chemical signatures relative to terrestrial basalts, a small

body of evaporation studies on lunar compositions, mainly using KEMS, were undertaken, largely in the early 1970s (De Maria and Piacente 1969; Balducci et al. 1971; De Maria et al. 1971; Naughton et al. 1971; Gooding and Muenow 1976; Markova et al. 1986). These authors report measured vapor pressures of volatile elements as a function of temperature. Imperative in these experiments is to measure vapor pressures over a finite time and temperature range corresponding to the initial vaporization of the element, lest its concentration in the condensed phase falls such that its evaporation rate decreases and the data obtained no longer refer to a single well-defined composition. The measured equilibrium vapor pressures $p\left(M^{x}\frac{x}{2}\mathrm{O}\right)$ are instructive for simulating the composition of the atmosphere developed upon heating. However, as these elements are not evaporating from pure condensed phases, the measured $p\left(M^{x}\frac{x}{2}\mathrm{O}\right)$ is not indicative of element volatility unless the activities of the oxides in the melt are known from some independent information (see Table 2). Much of this information is available in the metallurgical literature, e.g., from equilibrium measurements such as those of Rein and Chipman (1965), but, in many cases, has not been appropriately exploited. Rather, in order to determine volatilities of components in silicate rocks, the vapor pressure is divided by the concentration of the element initially present in the sample:

$$\log\frac{p\left(M^{x}\frac{x}{2}\mathrm{O}\right)}{X\left(M^{x+n}\frac{x+n}{2}\mathrm{O}\right)}=\log K-\frac{n}{4}\log f\left(\mathrm{O}_2\right)+\log\gamma\left(M^{x+n}\frac{x+n}{2}\mathrm{O}\right) \tag{21}$$

This information is shown in Figure 3, for the KEMS data of De Maria et al. (1971), acquired upon heating of lunar mare basalt 12022 between 1250 and 2500 K. The most volatile of the major silicate components are the alkalis, Na and particularly K, and hence constitute the dominant metal-bearing component of the vapor evolved from natural basalts at low

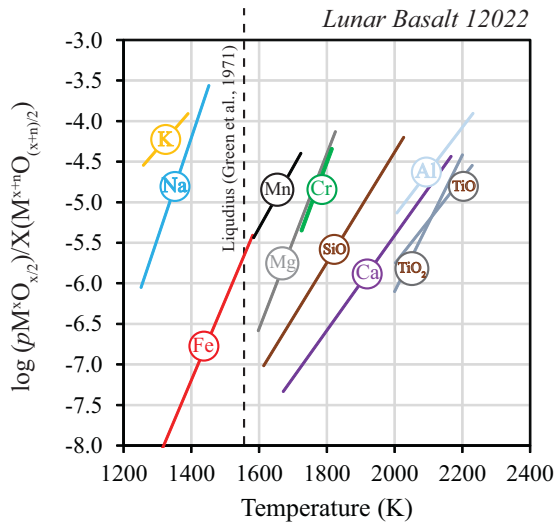

Figure 3. The calculated equilibrium partial vapor pressures ($p\,M^{x}\mathrm{O}_{x/2}$) of an element above lunar basalt 12022 relative to its initial concentration in the condensed sample ($X M^{x+n}\mathrm{O}_{(x+n)/2}$). The speciation of the metal in the gas phase is shown in the circle. Data from DeMaria et al. (1971).

temperatures. This order of evaporation is consistent with that of pure Na_2O and K_2O oxides where pK > pNa, a tendency also observed in the data of Gooding and Meunow (1976) on Knudsen evaporation of a Hawaiian basalt between 1175 and 1250 K. In these compositions, alkali volatility is 10^4 times greater than the next most volatile components measured, Fe and Mn. Both transition metals are divalent in silicate melts, occurring as $FeO_{(l)}$ and $MnO_{(l)}$ and predominantly as the monatomic gas in the vapor phase (Table 1), however, thermodynamic data for the pure Mn–O and Fe–O systems from the JANAF tables (Chase 1998) show that pMn > pFe at the same fO_2. The evaporation of $MgO_{(l)}$ and $CrO_{(l)}$ (since $Cr^{2+}/\sum Cr \approx 0.9$ at the fO_2 recorded in lunar basalts; Berry et al. 2006) also occur in a similar manner, and are both more volatile than SiO_2. The notionally 'refractory' components, CaO, Al_2O_3 and TiO_2 (lunar glass was found to have no Ti^{3+}; Krawczynski et al. 2009), enter the gas phase appreciably only above 1900 K. Phosphorus, a minor element that was not measured in the experiment of De Maria et al. (1971), is also volatile (Muenow et al. 1970) and is inferred to vaporize as $PO_{(g)}$ and $PO_{2(g)}$ gas species from silicate liquids (Markova et al. 1986), though the activity coefficients of $PO_{2.5}$ in steel-making slags can be very small (Table 2).

Owing to the high volatility and abundance of the alkalis relative to other volatile metals, their vaporization reactions determine the fO_2 of gas vaporized from silicate material at "low" temperatures where most of the major oxides remain involatile (e.g., see Schaefer and Fegley 2004a). With increasing temperature ($\gtrsim$ 2000 K) and/or with fractional vaporization at constant temperature, the less volatile but more abundant elements Fe, Si, and Mg vaporize in larger amounts and it is their respective gas species that then define the bulk properties of the gas at super-liquidus temperatures. The evaporation reaction

$$SiO_{2(l)} = SiO_{(g)} + \frac{1}{2}O_2 \tag{22}$$

produces an oxygen fugacity 2 log units below the Fayalite–Magnetite–Quartz (FMQ) buffer (O'Neill 1987) or 1.5 log units above the Iron–Wüstite (IW) buffer, at temperatures above the silicate liquids, >1600 K (Nagai et al. 1973; Kazenas et al. 1985; Shornikov et al. 1998). The oxygen pressures measured in the experiments of De Maria et al. (1971) correspond to an fO_2 buffered near FMQ + 0.5 over the temperature range 1396–1499 K (Fig. 4). That the fO_2 does not change appreciably over the temperature range of alkali-dominated ($K_{(g)}$, $Na_{(g)}$) at 1400 K to Fe-dominated gas by 1500 K implies that alkali evaporation also results in fO_2 close to FMQ. By contrast, evaporation of Fo_{93} olivine (Costa et al. 2017), with the same three major metal-bearing gas species, $Fe_{(g)}$, $Mg_{(g)}$ and $SiO_{(g)}$ produces oxygen fugacities close to $\approx$ FMQ − 1.5 at ≈1900 K (Fig. 4). A clear dependence with temperature is evident over the temperature range covered, becoming more reduced relative to FMQ from 1830 K (FMQ−1.4) to 1970 K (FMQ − 1.8). Extrapolating this trend linearly versus inverse temperature intersects the data of DeMaria et al. (1971) at 1450 K (Fig. 4), allowing consistency between the two datasets, and hinting that the entropy change associated with silicate vaporization is smaller than that of the FMQ buffer. The decrease of fO_2 relative to (the extrapolated) FMQ buffer at higher temperature may be related to the dissociation of oxygen:

$$O_2 = O + O \tag{23}$$

which proceeds to the right with increasing temperature, thereby decreasing fO_2. Nevertheless, even at temperatures in excess of 2000 K, thermodynamic calculations of evaporation of dry (H-, S-, C- and halogen-free) silicate mantles show that the fO_2 of the vapor phase is very close to that produced by evaporation of pure silica (Visscher and Fegley 2013; Fig. 4).

Lunar basalt 12022 has a liquidus temperature of ≈1300 °C (1573 K; Green et al. 1971), and hence evaporation of Na, K, and Fe occurred sub-liquidus. This makes accurate extraction

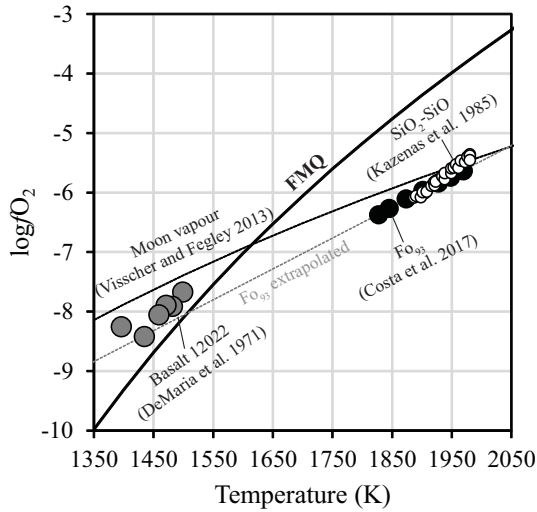

Figure 4. Calculated $\log fO_2$ as a function of temperature upon evaporation of silicate materials; lunar basalt 12022 (grey; De Maria et al. 1971), Fo_{93} olivine (black, Costa et al. 2017) and pure SiO_2 (white, Kazenas 1985). A model atmosphere by evaporation of a bulk silicate moon composition (Visscher and Fegley 2013) is shown by the stippled black line. The fO_2 defined by the Fayalite–Magnetite–Quartz (FMQ) buffer (O'Neill 1987) is shown in black.

of thermodynamic quantities from such experiments difficult, however, their partial pressures can be compared with those predicted from evaporation in the pure system, if the corresponding evaporation reaction is known. The activity of the *M*–O species in the pure phase is always equal to unity (Raoult's law). Because the gas is ideal in both the pure and complex systems, the activity coefficient of the metal oxide species in the liquid can be calculated from the ratio of the equilibrium constant (Eqn. (4)) of the reaction in the complex system, K^*, to that in the pure system, K at a given temperature, pressure and fO_2:

$$\gamma_i = \frac{K^*}{K} \tag{24}$$

The references cited above for activity data in binary and ternary alkali oxide melts and the results of DeMaria et al. (1971) show that alkali oxides dissolved in silicate melts are strongly non-ideal. The studies summarized in Table 1 show Na_2O and K_2O vaporization proceeds primarily via the reaction

$$\left(\mathrm{Na,K}\right)\mathrm{O}_{0.5(l)} = \left(\mathrm{Na,K}\right)_{(g)} + \frac{1}{4}\mathrm{O}_2 \tag{25}$$

The calculated activity coefficients of melt species from the data of De Maria et al. (1971) of $NaO_{0.5}$ and $KO_{0.5}$ are 10^{-3} and 5×10^{-5}, respectively (Fig. 5). Both of the calculated activity coefficients depend on the temperature, decreasing from 4.5×10^{-3} at 1500 K to 1.8×10^{-4} at 1300 K for $\gamma NaO_{0.5}$, while the decrease for $\gamma KO_{0.5}$ is milder, from 3.5×10^{-5} to 7.2×10^{-5}, respectively, and both are consistent with values in Table 2. A similar decrease in γMgO with falling temperature is observed in olivine (Costa et al. 2017), whereas SiO_2 shows the opposite trend (Fig. 5). All major components in olivine are close to unity, but, in detail, vary by a factor of 2 (greater for Fe, smaller for Mg).

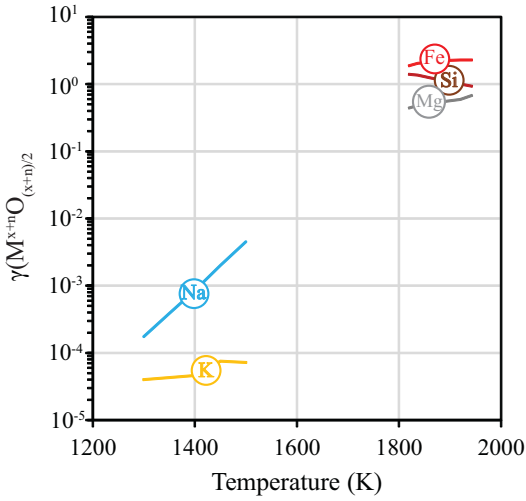

Figure. 5. Calculated activity coefficients for volatile melt species, $\gamma(M^{x+n}O_{(x+n)/2})$ as a function of temperature in the experiments of DeMaria et al. (1971) (Na, K) in a lunar basalt, and Costa et al. (2017) (Fe, Si, Mg) in olivine.

The conclusion is that equilibrium vapor pressures in liquid and solid silicates differ from those predicted from evaporation of the pure phase and require experimental data if their behavior during evaporation of silicate materials is to be understood. Aside from the role of activity coefficients of metal oxides in silicate melts which could be informed by systematic experimental studies in over a range of compositions in complex systems, the difference may also be related to interdependent vaporization equilibria, which often, but not always, involve production of O_2 and/or O gas. Thus the O_2 produced by vaporization of one oxide affects the vaporization of other oxides because of the law of mass action.

Kinetic Evaporation

General treatment of kinetic evaporation. The condition for kinetic, free or Langmuir evaporation is met when the partial pressure of the vaporizing species is such that the average distance travelled between collisions, the mean-free path, ℓ, is greater than the length scale over which the evaporation occurs, where:

$$\ell = \frac{\mathrm{k}T}{\sqrt{2}p_i\sigma} \tag{26}$$

and k is Boltzmann's constant and σ is the collisional cross-sectional area, which can be described by a Lennard-Jones 12–6 potential function that models the van der Waals forces between molecules (e.g., Neufield 1972).

The Hertz-Knudsen-Langmuir (HKL) equation describes the flux of particles striking a surface (Hertz 1882; Knudsen 1909; Langmuir 1916; Hirth and Pound 1963; Nussinov and Chernyak 1975; Richter et al. 2002), and is derived from the Maxwell–Boltzmann kinetic theory of gases given an ideal, isothermal gas:

$$\frac{\mathrm{d}n_i}{\mathrm{d}t} = -A\frac{\alpha_\mathrm{e}p_{i,\mathrm{sat}} - \alpha_\mathrm{c}p_i}{\sqrt{2\pi \mathrm{R}M_iT}} \tag{27}$$

Here, A is the surface area, $p_{i,\mathrm{sat}}$ is the equilibrium partial pressure of the gas species of element i, p_i is its actual partial pressure at the surface, M_i its molar mass, α_e and α_c the Langmuir coefficients for evaporation and condensation respectively, R the gas constant, T the absolute temperature and $\frac{\mathrm{d}n_i}{\mathrm{d}t}$ the evaporation rate in mol/s.

Equilibrium conditions prevail for the condition $p_{i,\mathrm{sat}}=p_i$. However, for all other conditions, evaporation is partially kinetic in nature, reaching the end-member case for which $p_i=0$, or pure Langmuir evaporation. This situation may physically occur for evaporation into a vacuum, or a scenario in which the gas is being transported away from the evaporation surface before it can be replenished. If this condition is demonstrated, then Equation (27) may be simplified by setting $p_i=0$. For evaporation of a molten sphere, which approximates the geometry of the melt on the wire-loops in the widely used experimental petrology method (e.g., Tsuchiyama et al. 1981) then:

$$\mathrm{d}n_i = -4\pi r^2 \frac{\alpha_e p_{i,\mathrm{sat}}}{\sqrt{2\pi \mathrm{R} M_i T}} \mathrm{d}t \tag{28}$$

In order to determine the extent of elemental loss (a change in concentration) experienced by a spherical body, Equation (28) is divided by the total number of moles in a sphere, $n_T^0 = \frac{4\pi r^3 \rho}{3M}$, yielding $\left(\frac{n_i}{n_T^0}\right) = X_i$, the concentration of element i. Equation (28) then becomes:

$$\mathrm{d}X_i = -\alpha_e p_{i,\mathrm{sat}} \frac{3}{r\rho}\sqrt{\frac{M_i}{2\pi \mathrm{R} T}}\ \mathrm{d}t \tag{29}$$

Here, r is the radius of the melt sphere and ρ its density.

Though grounded in statistical mechanics, the applicability or otherwise of the HKL equation to experimental and natural processes nonetheless remains equivocal because the assumptions used it in its derivation may be invalid. Knudsen's work on the kinetic theory of gases generated intense interest among chemists and physicists in the early 20th Century and led to a large number of subsequent experimental and theoretical studies that verified his ideas, e.g., Loeb (1961). Much of the ambiguity stems from the meaning of the evaporation coefficient, α_e, which is an empirical term describing the non-ideality of evaporation. Since the HKL equation quantifies only the number of molecules striking a surface over time, Langmuir coefficients therefore express the energy required in the transformation of a condensed component into a gaseous molecule (or vice-versa), and may depend upon several factors including crystal structure, surface roughness, chemical composition, temperature and gas species. The HKL equation is derived from an equilibrium distribution of gas molecules at a single temperature, and is therefore applicable when the evaporating flux is null, such that the introduction of non-equilibrium coefficients a posteriori undermines this assumption (Ackermann et al. 1967). Ab-initio approaches to this inconsistency may consider a non-Maxwellian gas distribution, as attempted by Schrage (1953) whose equation yields evaporation rates double those of the HKL equation, but does not satisfy momentum- or energy conservation.

The HKL equation as written in Equation (27) assumes that the temperature in the gas is equivalent to that in the condensed phase, as pointed out by Littlewood and Rideal (1956). They investigated various organic molecules at low temperatures and found that when the temperature difference across the interface was accounted for, the agreement between α_e and the ideal case ($\alpha_e = 1$) improved significantly. Persad and Ward (2016), extend this argument, though they largely focused on liquids (water, silicone oil) that have high vapor pressures at low temperatures, as well as vapor species with large dipole moments (Langmuir 1932;

Wyllie 1949). An alternative law based on statistical rate theory is proposed to better account for these complexities (Persad and Ward 2016), because they give rise to conditions that diverge from those under which the HKL equation should be applied by exacerbating temperature differences between the gas and condensed phase, decreasing the mean-free path and enhancing polar interactions between molecules (see also Bond and Struchtrup 2004).

These departures from ideal conditions are mitigated in high-temperature geological applications, and variation in α_e appears to be smaller, typically between 0.05-1 (Wolff and Alcock 1962; Alcock and Peleg 1967; Krönert and Boehm 1972; Srivastava and Farber 1981; Fedkin et al. 2006; Richter et al. 2011; Shornikov 2015), with those for liquids being closer to unity (Burns 1966; Fedkin et al. 2006; Safarian and Engh 2009) which may reflect low heats of vaporization relative to thermal energies. Schaefer and Fegley (2004a) give a convenient summary of vaporization coefficients for several minerals and melts in their Table 10. Nevertheless, further experimental testing of the HKL equation at high temperatures is required in order to better understand its applicability and the nature of evaporation coefficients. Therefore, although the HKL equation should only strictly be applied under equilibrium conditions to ideal gases, it can provide an accurate description of Langmuir evaporation processes in controlled experiments at high temperatures, provided the caveats mentioned above are considered.

Kinetic evaporation experimental techniques. Thermodynamic data on equilibrium partial vapor pressures of elements evaporating from natural silicate melts or solids are very scarce (see section *Natural Systems*). Information garnered on metal volatility in multicomponent systems predominantly comes from kinetic, or Langmuir evaporation experiments. As opposed to the Knudsen Cell, kinetic evaporation experiments are typically conducted in alumina tube furnaces that are capable of reaching ≈ 1800 °C with $MoSi_2$

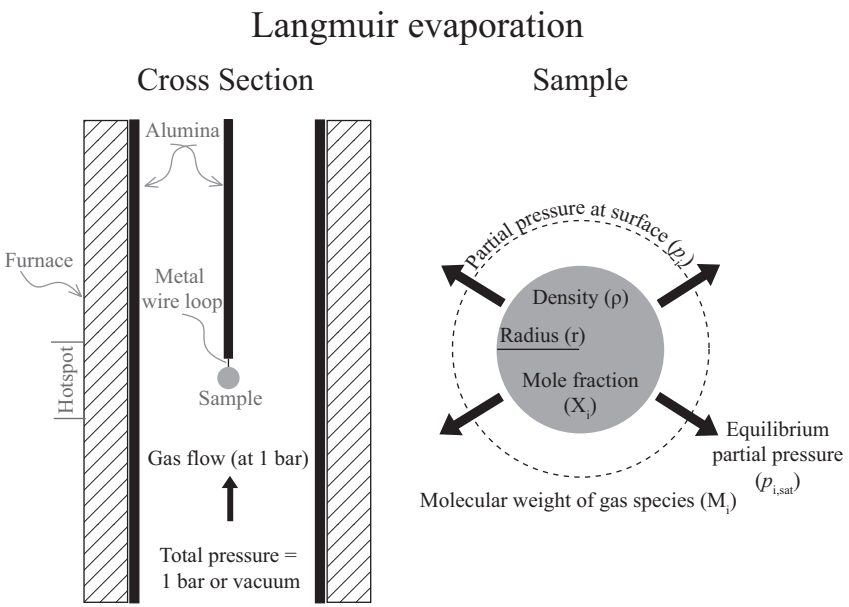

Figure 6. Schematic illustration of an alumina tube furnace in which a sample is suspended from a metal wire loop or levitated and equilibrated at high temperatures with a gas flow or under vacuum. See Donaldson (1979); Tsuchiyama et al. (1981), Hashimoto (1983); Nagahara and Kushiro (1989); Richter et al. (2002); O'Neill and Eggins (2002); Pack et al. (2010).

heating elements in their ≈3–5 cm 'hot zone', in which a sample is suspended on a wire loop or crucible (Fig. 6). In these experiments, the temperature (≈±2 °C) and pressure (1 bar) are fixed, but also the oxygen fugacity, by means of CO/CO_2 (e.g., O'Neill 2005) or CO_2/H_2 (e.g., Donaldson 1979) gas mixtures to better than ≈±0.1 log unit, depending on the mixing ratio (Huebner 1987). Equally, experiments in this apparatus can also be conducted under vacuum (e.g., Hashimoto 1983; Richter et al. 2002; Yu et al. 2003; Nagahara, this volume). Laser-heated aerodynamic levitation apparatuses, in which the atmosphere composition may also be controlled by changing the composition of the gases used to levitate the sample, are becoming increasingly employed for Langmuir evaporation experiments (Pack et al. 2010; Macris et al. 2016). This method has the advantage being able to heat samples in excess of 2000 °C via a CO_2 laser, temperatures that are amenable to the study of the vaporization of refractory elements. The major difference with respect to equilibrium techniques is that these experiments take place in an open system, where the evolved gas loses contact with the condensed phase, either from expansion into a vacuum or by a continual flux of gases at typical gas flow rates of 10–200 sccm through the furnace tube or chamber, leading to a strong dependence of the volatile content of the condensed phase with time (e.g., Richter et al. 2002), see Equation (27). Furthermore, an open system means that the evolved gases are subsequently lost from the system. Therefore, vapor pressures of evaporating components must be calculated from the concentration of the element remaining in the condensed phase, by weight loss or by target collection, rather than measured as for effusion techniques.

Some of the kinetic evaporation experiments in the geochemical literature are similar to Langmuir evaporation experiments (e.g., Gibson and Hubbard 1972; Storey 1973; Donaldson 1979; Tsuchiyama et al. 1981; Hashimoto 1983), while others are similar to transpiration experiments (e.g., Jacobson et al. 2005). Langmuir vaporization experiments for geochemically important metal oxides (e.g., Al_2O_3, HfO_2, MgO, REE sesquioxides, SiO_2, ThO_2, ZrO_2) are described in several papers (e.g., Wolff and Alcock 1962; Peleg and Alcock 1966; Alcock and Peleg 1967; Krönert and Boehm 1972). Sata et al. (1982) conducted both Langmuir vaporization and transpiration experiments involving CaO. Their paper illustrates the utility of and differences between the two methods (their figures 1 and 3 and associated text). Given the uncertainty in evaporation coefficients (section *General treatment of kinetic evaporation*), data obtained from Knudsen effusion or other equilibrium techniques are generally preferred. As per the equilibrium experiments, the vast majority of studies in the geochemical literature deal primarily with the alkalis (Gibson and Hubbard 1972; Storey 1973; Donaldson 1979; Tsuchiyama et al. 1981; Kreutzberger et al. 1986; Tissandier et al. 1998) or the major silicate components (Hashimoto 1983; Floss et al. 1996; Richter et al. 2007).

Major elements. For a recent, comprehensive summary of the kinetic evaporation of major components (Fe, Mg, Si, Al, Ca) from silicate melts, the reader is referred to Davis and Richter (2014). In brief, as per the equilibrium case, Fe is shown to be the most volatile component of FCMAS melts (Hashimoto 1983; Floss et al. 1996; Richter et al. 2011), in which FeO dissolved in a silicate liquid evaporates according to:

$$\mathrm{FeO_{(l)}} = \mathrm{Fe_{(g)}} + \frac{1}{2}\mathrm{O_2} \tag{30}$$

However, work by several groups cited earlier (Table 1) shows that pure wüstite ($Fe_{1-x}O$), magnetite (Fe_3O_4), and hematite (Fe_2O_3) evaporate incongruently with lower Fe/O atomic ratios in the vapor than in the condensed phase. It is still uncertain whether or not pure molten FeO vaporizes congruently; Darken and Gurry (1946) report the congruently vaporizing composition has O/Fe = 1.116 but Smoes and Drowart (1984) consider that the congruently vaporizing composition is stoichiometric FeO. Further work is needed to resolve this question.

In either case, Fe vaporization and transport may result in subsequent oxidation of the silicate residue if the evolved oxygen remains behind. Initially, the next most volatile component is SiO_2, which volatilizes as SiO, Equation (22). However, as, evaporation proceeds, the activity coefficient of SiO_2 decreases, such that the equilibrium partial pressure of $SiO_{(g)}$ falls below that of $Mg_{(g)}$ (Richter et al. 2002, 2007), whose vaporization reaction occurs by congruent dissociation of MgO to $Mg_{(g)}+½O_2$, as shown by Kazenas et al. (1983). Calcium oxide and Al_2O_3 behave conservatively over the range of temperatures investigated by Hashimoto (1983), up to 2000 °C. Forsterite evaporation occurs congruently, whether in the liquid or solid state (Mysen and Kushiro 1988; Hashimoto 1990; Wang et al. 1999), however, this congruent vaporization involves several gas species (dissociative), according to the reaction:

$$Mg_2SiO_4 = 2Mg_{(g)} + SiO_{(g)} + \frac{3}{2}O_2 \quad (31)$$

Forsterite–fayalite solid solutions were shown to evaporate incongruently by Nagahara and Ozawa (1994), who found the residual condensed olivine was Mg-richer post-vaporization, resulting from preferential loss of $Fe_{(g)}$ relative to $Mg_{(g)}$, as confirmed by KEMS measurements of the vapor above Fo_{93} (Costa et al. 2017). Plagioclase also evaporates incongruently, in which Na is more volatile than Ca leaving a more anorthitic residue (Nagahara and Kushiro 1989). This behavior is likely a general property of binary isomorphous solid solutions with complete miscibility (i.e., cigar shaped phase diagrams). It is also possible that other melts will display azeotropic[5] behavior upon evaporation (Heyrman et al 2004), though this has not been rigorously tested experimentally. See the chapter by Nagahara in this volume for further information on the evaporation of forsterite and of other minerals relevant to the solar nebula.

Alkali metals. For the pure oxides, thermodynamic data (e.g., Brewer 1953; Margrave 1967; Lamoreux and Hildenbrand 1984) indicates the following order of alkali volatility (least volatile) Li < Na < K < Rb < Cs (most volatile). This sequence is not universally confirmed from evaporation of alkalis from more complex silicates with different bulk compositions, however.

Shimaoka and Nakamura (1989, 1991) and Shimaoka et al. (1994) find that, upon evaporation of fine-grained (< 10 μm) chondrites, Na is more volatile than K and Rb, between 1200–1400 °C at 8×10^{-6} torr (10^{-8} bar), with Rb evaporation marginally favored relative to K at lower temperatures (1200 °C). Although these experiments were performed sub-solidus, Donaldson (1979) also observed more rapid loss of Na than K from an alkali olivine basalt ($T_{liquidus} = 1232 \pm 2$ °C) between 1236 °C and 1293 °C and $\log fO_2$ between −3.3 and −11.9 (FMQ+4.5 to FMQ−4), as did Storey (1973) from an Fe-rich quartz tholeiite between 1160 and 1210 °C.

In a similar study, Kreutzberger et al. (1986), investigated alkali (Na, K, Rb, Cs) evaporation from An–Di melt at 1400 °C, in which evaporation followed the sequence expected from the pure oxides, i.e., Na < K < Rb < Cs (Fig. 7). This hierarchy holds for evaporation in air, at the IW buffer (FMQ − 3.6 at 1400 °C) and under vacuum (<10^{-6} bar). Furthermore, Gibson and Hubbard (1972), whose experiments on lunar basalt 12022 (20 wt.% FeO) at 3×10^{-9} bar were conducted from 950 °C to 1400 °C, also show that pRb > pK > pNa, where their volatilities become more dissimilar at lower temperatures. Hastie and Bonnell (1985) measured alkali vaporization from NIST SRM glass and dolomitic limestone samples. They found pNa > pK for the Fe-free glass (their Fig. 9), but pK > pNa for the low Fe limestone (their Fig. 10).

The changing order of volatility among alkalis evaporating from silicate relative to their pure oxides led Donaldson (1979) to postulate that differences in $NaO_{0.5}$ and $KO_{0.5}$ activity coefficients (i.e., $\frac{\gamma_{NaO_{0.5}}}{\gamma_{KO_{0.5}}} > 1$) must act to enhance Na volatility relative to K in order to explain the data. Indeed,

[5] An azeotrope is defined by the conditions at which the bulk composition of the vapor and the condensed phase is identical.

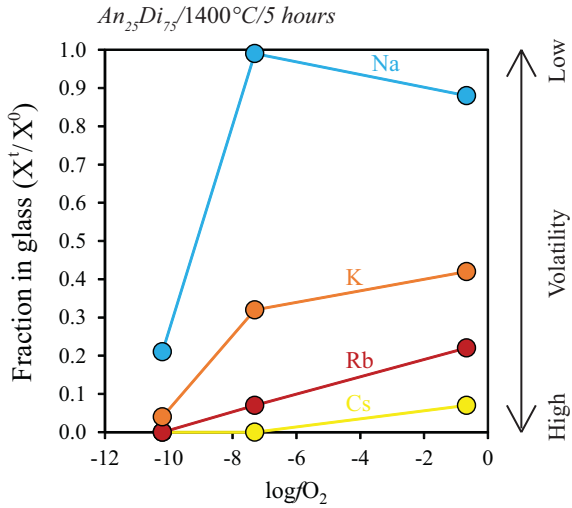

Figure 7. The fraction remaining of a trace element after 5 hours with respect to its initial amount (X^t/X^0) in an $An_{25}Di_{75}$ melt as a function of logfO_2 after heating at 1400 °C for 5 hours (Kreutzberger et al. 1986). The vacuum experiment is predicted to define a logfO_2 = −7.3 using the trend of logfO_2 with temperature for evaporation in a vacuum from Figure 4.

this behavior occurs in binary M_2O–SiO_2 (Charles 1967; Wu et al. 1993), ternary Na_2O–K_2O–SiO_2 melts (Chastel et al. 1987) and multicomponent M_2O-bearing melts (Hastie et al. 1981; Borisov 2009; Mathieu et al. 2011). The key point from these studies is that the depression of $\gamma MO_{0.5}$, which acts to decrease volatility, when combined with SiO_2- or $Al_2O_3 + SiO_2$-bearing melts is proportional to their volatilities as pure oxides. Alkali aluminates are very stable compounds, and increasing $X_{AlO_{1.5}}$ in the liquid causes negative deviations from ideality in the order Na < K < Rb (O'Neill 2005; Yazhenskikh et al. 2006, 2011; Borisov 2009). As illustrated by the KEMS data of De Maria et al. (1971), this does also appear to be the case in natural compositions, with Na becoming more volatile than K above 1200 °C (Fig. 3). At present only limited data are available, and it therefore remains unclear as to what controls the alkali element volatility hierarchy in silicate melts and minerals. Solutions to this question require a better understanding of alkali metal activity coefficients in silicate melts as a function of *P*, *T* and *X*.

Other trace elements. Systematic studies of the evaporation behavior of trace elements from silicate materials are exceedingly sparse, restricted to the studies of Notsu et al. (1978), Masuda and Tanaka (1979), and Wulf et al. (1995), joined recently by that of Sossi et al. (2016a) and Norris and Wood (2017). Other works are unrefereed abstracts and include Shaffer et al. (1991); Ertel-Ingrisch and Dingwell (2010); Ertel-Ingrisch et al. (2012); Speelmans (2014), and Humayun and Crowther (2015).

Early studies on the kinetic vaporization of natural rocks dealt predominantly with meteorites. A series of studies on the heating of chondritic meteorites were published, mainly in the 1970s, by the group of M.E. Lipschutz (e.g., Ikramuddin et al. 1976; Matza and Lipschutz 1977; Bart et al. 1980). These experiments provide information on the volatility sequence of trace elements during meteorite metamorphism. Although they were initially carried out in 10^{-5} atm H_2 to replicate nebular conditions, their interpretation is not straightforward for several reasons. Namely, due to the poorly constrained fugacities for oxygen, sulfur, and halogens; the relative importance of diffusion versus volatility, and uncertainty regarding the extent of equilibration during stepwise heating (Wulf et al. 1995; Schaefer and Fegley 2010). Furthermore, Wulf et al. (1995) in attempting to replicate these experiments, found

that significant quantities of Na, K and Ga had entered the quartz tube containing the samples following heating. Nevertheless, experiments of this type are instructive for discerning between element mobility by diffusion and volatility, and reasonable agreement is found between volatilities and the most labile elements in their experiments. For example, In, Tl, Bi and Cd are invariably the most depleted (e.g., Bart et al. 1980) and are among the most volatile in nebular environments (Lodders 2003; Schaefer and Fegley 2010), broadly matching their abundances in metamorphosed chondrites (Wang and Lipschutz 2005).

Notsu et al. (1978) carried out DC arc heating experiments on the Allende CV3 chondrite liquid at 2000 °C in air, as well as on a basalt (JB – 1) by Mo resistance heating at 0.01 bar, and measured the residual composition after Langmuir evaporation. Masuda and Tanaka (1979) performed heating experiments in a vacuum ($\approx 5 \times 10^{-8}$ bar) on JB – 1 heated to ≈ 2000 °C by a W filament and measured the concentration of each element precipitated on a condensation plate. In both studies, Al, Ca, Ti, Sc and the REE behave in a refractory manner, becoming enriched in vaporization residues. Masuda and Tanaka (1979) note that La, and particularly Eu and Yb are relatively more volatile than their neighboring REEs, consistent with Boynton (1975). Vanadium content is roughly constant, while Cr, Fe and Mn are originally refractory before decreasing in abundance beyond 20% vaporization, being reduced to negligible levels by 90%. Magnesium only decreases in concentration after 80% vaporization of the starting material, and is initially less volatile than SiO_2 but is depleted more rapidly thereafter, as also observed by Richter et al. (2002). Sodium is the most volatile metal studied by Notsu et al. (1978), though K is similarly volatile and Rb more so in Masuda and Tanaka (1979), while Ni, Co, Ir and Au are also all quantitatively lost within 40–50% vaporization (Notsu et al. 1978). The volatility of these ordinarily non-volatile siderophile metals comes about due to the oxidizing conditions under which the experiments were performed (air). Wänke et al. (1984) also observe that the volatility of refractory siderophile elements Re, Os, W and Mo, in addition to halogens and chalcogens are enhanced in an oxidizing, H_2O-steam atmosphere relative to a more reducing N_2-rich atmosphere, whereas Zn and In show the opposite behavior. The systematics of element volatility as a function of the atmosphere under which they evaporate is expanded upon below.

Wulf et al. (1995) studied the loss of trace elements from two natural carbonaceous chondrites (Murchison and Allende) over a range of oxygen fugacities ($\log fO_2 = -16.5$ to air) and temperatures (1050–1300 °C; always sub-liquidus) at atmospheric pressure (Fig. 8). Wulf et al. (1995) did their work at sub-liquidus temperatures and suggested elemental volatility was controlled by a combination of equilibrium partial pressures and stability of the MVE host phases. Therefore, for trace elements locked in a phase whose decomposition depends on

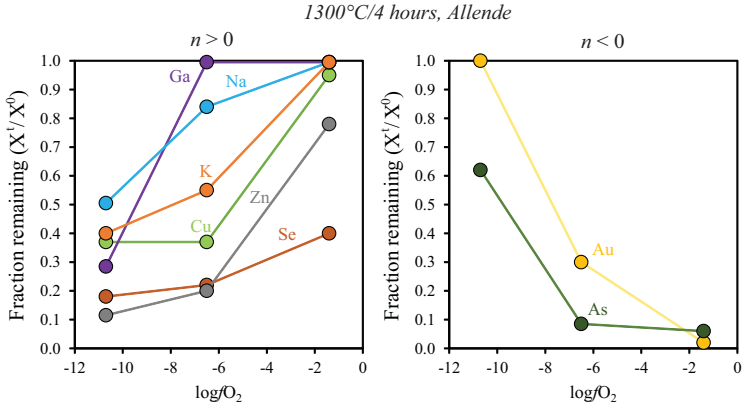

Figure 8. The fraction remaining of a trace element after 4 hours with respect to its initial amount (X^t/X^0) in bulk Allende chunks as a function of $\log fO_2$ after heating at 1300 °C for 4 hours (Wulf et al. 1995). These conditions were chosen as equilibrium is more likely to have been reached in these higher-temperature experiments.

the thermodynamics of other major elements, these experiments give only qualitative insight into their volatility, as discussed for platinum-group metals in alloys trapped in silicates. The experiments of Norris and Wood (2017) were undertaken on a natural MORB liquid at a single temperature, 1300 °C, with varying $\log fO_2$ from −7 to −13 (FMQ + 0.3 to IW − 2.3), using a Ni stirrer to mitigate the potential for incomplete diffusive equilibration of the liquid phase during evaporation (see also Dingwell et al. 1994). Volatile loss of different elements in their experiments is not systematic as a function of time, and so they deduced empirical 'volatility factors' for a constant run time (Fig. 9).

In both studies, the fO_2 of the gas (and silicate melt in Norris and Wood 2017) was externally buffered by a continuous flow of CO–CO_2 gas mixture inside the furnace tube, a situation that diverges from natural systems, in which the fO_2 of the gas is defined by the partial pressures of the evolved gas species from the heated material. The telling result from Wulf et al (1995) and Norris and Wood (2017) is this: elemental volatility depends strongly on the fO_2 of the gas into which elements are evaporating (Figs. 8a,b, 9). This dependence is not equivalent for all elements, nor would one expect it to be so from knowledge of vaporization stoichiometry of the pure oxides (see Table 1). For example, certain elements become more volatile at oxidizing conditions, whereas for others, reducing conditions promote evaporation. The former group are comprised of largely highly siderophile noble metals that exist in metallic form in chondrites, notably Au, As, Re, and Os (Fig. 8b). By contrast, lithophile and chalcophile elements, such as the alkalis, Cu, Zn, Sn, Sb, Pb and Ga are more readily lost at low fO_2 (Fig. 8a; Fig. 9). Fegley and Cameron (1987) discussed this type of behavior for Ce (vs. other REE) and U and Pu (vs Th).

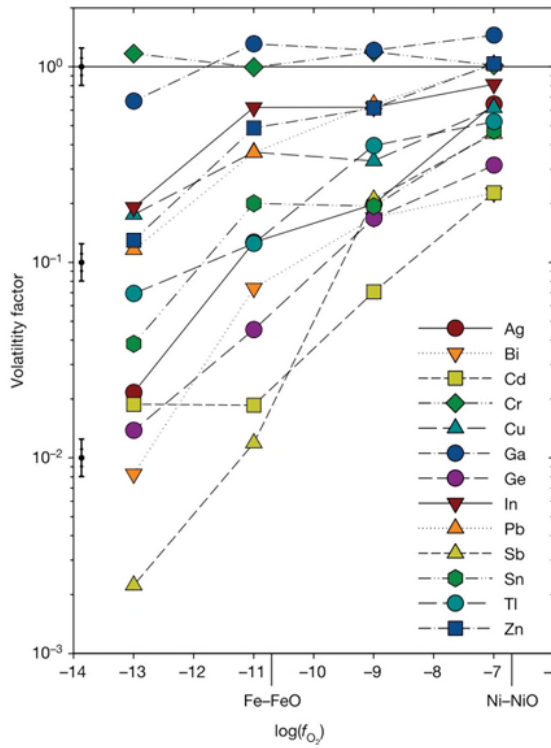

Figure 9. The volatility factor (fraction of the element remaining in the glass) for selected moderately volatile elements as a function of $\log fO_2$ at 1300 °C and 60 minutes. Reproduced from Norris and Wood (2017).

This contrasting behavior may be understood by the reaction shown in Equation (2). For the first group of elements, $n<0$, meaning the element in the gas phase is more oxidized than in the condensed phase. Chalcophile and particularly lithophile elements mostly exist as oxides in natural rocks, and their gas species tend to be more reduced, yielding $n>0$. For many moderately volatile elements, such as Na, K, Rb, Zn, Cu, Ge, Sn, Cd, Ag, Mn, Fe, Mg, Si a single (though different) metal-bearing species predominates in both phases over a wide range of temperature and fO_2 (e.g., Lamoreaux et al. 1987; Table 1). Some elements may exist in multiple oxidation states, in the condensed and/or the gas phase, such that several equilibria akin to Equation (2) must be written to describe the overall volatility behavior of an element.

In this way, Sossi et al. (2016a) showed that the vapor pressures of the evaporating species for a given element may be calculated from the concentration of that element remaining in the residual condensed phase (in their case, a liquid), $X\left(M^{x+n}\frac{x+n}{2}\mathrm{O}\right)$. Re-arranging the equilibrium constant, Equation (4), to solve for the partial pressure of the metal species yields:

$$p\left(M^{x}\mathrm{O}_{\frac{x}{2}}\right)=\frac{K_{(2)}X\left(M^{x+n}\mathrm{O}_{\frac{x+n}{2}}\right)\gamma\left(M^{x+n}\mathrm{O}_{\frac{x+n}{2}}\right)}{f\left(\mathrm{O}_2\right)^{n/4}} \tag{32}$$

Substituting Equation (32) into Equation (29) allows it to be integrated with respect to time and concentration to yield the relative loss of the element from the sphere over a given time interval:

$$\frac{X_i^t}{X_i^0}=\exp\left(-\frac{\alpha_e\gamma\left(M^{x+n}\mathrm{O}_{\frac{x+n}{2}}\right)K_{(2)}}{f\left(\mathrm{O}_2\right)^{n/4}}\frac{3}{r\rho}\sqrt{\frac{M_i}{2\pi\mathrm{R}T}}\left(t-t_0\right)\right) \tag{33}$$

where t_0 is the time at which the element begins evaporating, and X_i^t and X_i^0 its concentration at t and t_0, respectively (Sossi et al. 2016a). Tsuchiyama et al. (1981) and Humayun and Koeberl (2004) derived an expression with a similar functional form. This analysis requires implicit knowledge of the speciation of the element in at least one of the condensed- or the gas phase, and hence cannot uniquely identify its speciation. Rather, speciation must be inferred from the dependence of $\frac{X_i^t}{X_i^0}$ with fO_2. This analysis becomes complicated if volatiles such as water, halogens, or sulfur (important for MVE speciation at higher pressures; see section *Evaporation in the presence of major volatiles H, C, S and halogens*) and is thus applied only to anhydrous materials herein. As neither α_e nor the activity coefficient of the oxide species are known a priori, a new equilibrium constant, K^* is defined, where $K^*=\alpha_e\gamma K$. It is clear that the loss of an element by kinetic evaporation still strongly depends on its equilibrium partial pressure, $p_{i,\mathrm{sat}}$, in addition to other, non-equilibrium (or 'kinetic') factors, most notably the radius and density of the evaporating body, the time for which it is evaporating, and the square root of the molar mass of the evaporating species (Eqn. 33). To a first approximation (i.e., no concentration gradients in the evaporating material, and temperature–independent enthalpy of vaporization and activation energy), kinetic evaporative loss depends on the temperature in an Arrhenian fashion, and hence linear arrays are anticipated in plots of $ln\frac{X_i^t}{X_i^0}$ vs. t. In detail, the rate constants of evaporation reactions are not exactly constant with $1/T$ (Benson 1960), but,

predominantly, because $p_{i,\mathrm{sat}}$ decreases as the abundance of the element in the condensed phase (X_i^t) decreases, evaporation rate slows with time, and linearity over time is never achieved.

In a plot of $\frac{X_i^t}{X_i^0}$ vs. $\log fO_2$ for a given time, the data define a sigmoidal curve, where the range of $\log fO_2$ over which the element passes from fully condensed to fully vaporized is proportional to the number of electrons (n) in the reaction. The more n diverges from 0, the sharper this transition is. Therefore, in this way, the speciation of the element in the gas phase can be inferred from the slope of the sigmoid. An example for the case of Cu and Zn evaporation is shown below (Fig. 10).

The volatility of Cu is, at low oxygen fugacity, lower than that of Zn (compare the amount of each remaining in the glass at $\log fO_2 = -8$, Fig. 10a,b). However, as oxygen fugacity increases, Cu becomes more volatile relative to Zn, such that, in air, the proportion of Cu and Zn remaining in the glass is equivalent. Using Equation (33) to fit the experimental data shows that Cu evaporation is consistent with an $n=1$ transition, whereas Zn conforms to an $n=2$ reaction. Given knowledge of their respective speciation in silicate melts, their volatilisation reactions are:

$$\mathrm{ZnO_{(l)}} = \mathrm{Zn_{(g)}} + \frac{1}{2}\mathrm{O_2} \tag{34}$$

and for Cu,

$$\mathrm{CuO_{0.5(l)}} = \mathrm{Cu_{(g)}} + \frac{1}{4}\mathrm{O_2} \tag{35}$$

The different colored points and curves correspond to different temperatures at a given run time, and illustrate that higher temperatures result in more extensive volatile loss. This effect may be quantified by a change in the $\log K^*$ value, which shifts the curves to the left (lower temperature) or right (higher temperature) along the $\log fO_2$ axis. Higher values correspond to greater stability of the products (i.e., the volatile species). The stoichiometry of ZnO and $CuO_{0.5}$ vaporization from silicate melts deduced from this method is consistent with those in Table 1.

The $\log K^*$ for each volatilisation reaction used to fit the data can be converted into an effective Gibbs Free Energy, ΔG^* using Equation (9). Sossi et al. (2016a) performed their experiments between 1300 °C and 1550 °C. For their data, the variation of ΔG^* of a

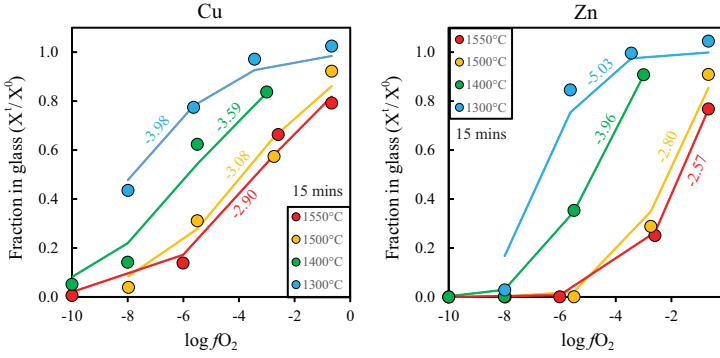

Figure 10. The fraction remaining in the melt (X^t/X^0) at $t = 15$ mins, where $X =$ **a)** Cu and **b)** Zn as a function of $\log fO_2$. Colors correspond to the temperature of the experiment (blue = 1300 °C; green = 1400 °C; yellow = 1500 °C and red = 1550 °C). Curves are calculated using Equation (33) and the numbers are their associated $\log K^*_{(r)}$. Data from Sossi et al. (2016a).

volatilisation reaction against the absolute temperature, T in an Arrhenius plot, results in a straight line (Fig. 11). This confirms that a reproducible, thermally activated process is controlling elemental loss, namely, their equilibrium partial pressures.

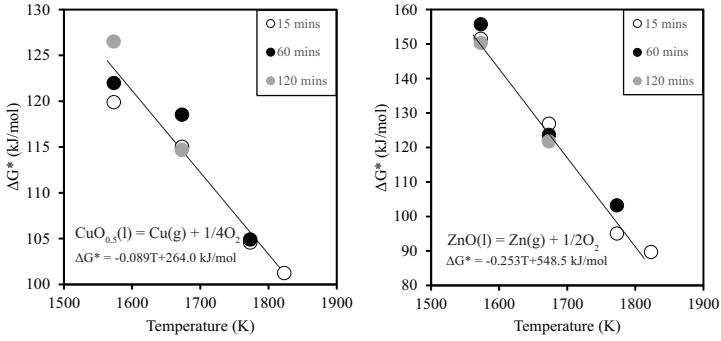

Figure 11. The calculated $\Delta G^*_{(r)}$ for **(a)** Cu and **(b)** Zn as a function of temperature for given run times (white = 15 mins; black = 60 mins; grey = 120 mins). Data from Sossi et al. (2016).

At constant total pressure, the Gibbs–Helmoltz equation is given by Equation (10), and hence, the slope of the line is equivalent to $-\Delta S^*$ and its intercept, ΔH^*, which are average values determined for the mid-point temperature over the temperature range. This is a 2nd law treatment of the vaporization data and is analogous to the integration of the Clausius–Clapeyron Equation generally used for interpretation of vapor pressure data (Drowart and Goldfinger 1967; L'vov 2007). It implicitly assumes that ΔH^* is much greater than the product of ΔC_P^o and temperature over the interval of interest, see Equation (11), such that slopes can be approximated as linear within experimental uncertainty.

Relative volatilities and evaporation temperatures can be calculated from these thermodynamic data; including the activity coefficients of melt oxide species in the silicate melt (Sossi et al. 2016a).

Table 3 qualitatively illustrates the differences in the volatility behavior of the elements calculated for the solar nebula (Lodders 2003) and observed in Langmuir evaporation experiments of molten basalt (Sossi et al. 2016a; Norris and Wood 2017). Changes in relative element volatility reflect the distinct thermodynamic conditions that typify the two environments; the high pressures (1 bar; though note that Equation (33) is applicable to any total pressure, it is the partial pressure of the individual gas species that matter) compared to 10^{-4} bar assumed for the solar nebula calculations (see also section *Evaporation in the presence of major volatiles H, C, S and halogens*), in addition to the higher relative fO_2 (IW − 7 and IW, respectively) and

Table 3. Qualitative order of element volatilities, from least to most, in the solar nebula (IW−7; 10^{-4} bar) and from evaporation of silicate melts at 1573 K near the IW buffer at 1 bar.

Solar nebula (Lodders 2003)	Mo < Cr < Mn ≈ Li < Cu < K ≈ Ag < Sb ≈ Ga ≈ Na < Ge < Rb < Bi ≈ Pb ≈ Zn ≈ Sn < Cd < In < Tl
Evaporation of ferrobasalt (Sossi et al. 2016a)	Mn < Mo < Cr < Li < Ga ≈ Na < K < Cu ≈ Rb < Zn ≈ Ge < Pb < Ag < Cd
Evaporation of MORB (Norris & Wood 2017)	Cr ≈ Ga < In < Zn < Cu ≈ Pb < Sn < Tl ≈ Ag < Bi < Ge < Cd < Sb

different bulk composition. Low total pressures in the solar nebula promote the formation of solid minerals relative to liquids (Ebel 2004), with many moderately volatile elements condensing into FeS (e.g., Ag, Cd, In, Pb, Zn) or Fe metal (Bi, Ga, Ge, Cu, Sb), whereas the alkalis partition into feldspar aside from Li which, like Mn, condenses into forsterite and enstatite (Lodders 2003). By contrast, these elements are probably all dissolved as oxide components in silicate melts. As a result, their activity coefficients will differ from those in solid phases, especially if those solids are metals or sulfides. This phenomenon can explain why In becomes less volatile, and Cu more so in the experiments of Sossi et al. (2016a) and Norris and Wood (2017); the $\gamma InO_{1.5}$ in FCMAS melts is 0.02, while $\gamma CuO_{0.5}$ is 3.5 at 1650 °C (see Wood and Wade 2013 for a discussion). A similar interpretation holds for the decreased volatilities of the alkalis relative to other elements such as Cu and Ag, as the alkalis have very low activity coefficients that stabilize them in silicate melts relative to the gas phase (see Table 2, see section *Alkali metals*). Additionally, the speciation of the element in the gas may be affected by the more oxidizing conditions of the Langmuir evaporation experiments; notably, the Group VI metals Cr, Mo, and W form stable oxide species that enhance their volatilities at oxidizing conditions (Fegley and Palme 1985; Sossi et al. 2016a; Table 1) and become even more volatile at fO_2s > IW. Some other elements are sensitive to the presence of volatiles, such as S, that stabilize $GeS_{(g)}$ and $SnS_{(g)}$ in the solar nebula, but, during evaporation of sulfur-free halogen-free basaltic magma, are constrained to form oxides (see section *Evaporation in the presence of major volatiles H, C, S and halogens* for a discussion).

It is emphasized that this behavior is relevant to volatile-poor systems that lack major gas species found in many terrestrial (and extra-terrestrial) magmatic systems, notably H_2O, SO_2, CO_2, CO, CH_4, H_2S, in addition to halogens such as Cl and F. These species can preferentially complex metallic elements, thereby stabilizing them in the gas phase relative to the nominally 'dry' case (Symonds and Reed 1993; Matousek 1998; Meschter et al. 2013; Fegley et al. 2016; Renggli et al. 2017). Although these volatiles are readily degassed or lost during high temperature vaporization processes, such that they may be nearly absent at the temperatures sufficient to vaporize metallic elements, they were also probably extant on primordial planetary atmospheres (section *Evaporation in the presence of major volatiles H, C, S and halogens*). This thermodynamic framework for interactions between gas and condensed phases is then reconciled to provide information as to how planetary bodies acquired (or then subsequently lost) their volatile element budgets during their formation (section *Volatility during planetary formation*).

EVAPORATION IN THE PRESENCE OF MAJOR VOLATILES H, C, S AND HALOGENS

Overview

Very few natural materials are truly anhydrous and completely free of other volatiles—even the Moon contains halogens, sulfur, and at least trace water (Tartèse et al. 2013; Hauri et al. 2015; McCubbin et al. 2015)—so the relative importance of fO_2 versus the fugacities of these other volatiles for evaporation of the MVE requires consideration.

Henley and Seward discuss volcanic gas chemistry in their chapter in this volume and it is not our purpose to do so here. But to a first approximation the observed composition (H_2O, CO_2, SO_2, H_2S, H_2, CO, HCl, HF) of terrestrial volcanic gases (e.g., Table 6.13 in Lodders and Fegley 1998; Tables 3–5 in Symonds et al. 1994) is similar to that of BSE–steam atmosphere models for the early Earth (e.g., Fig. 15 of Fegley et al. 2016). Thus we use observations and calculations of volcanic gas chemistry to help illustrate important points about the factors controlling volatility of the MVE on the early Earth and its precursor planetesimals.

Cu-bearing gases. Taking copper as an example, band spectra show CuCl gas in volcanic flames at Kilauea (Murata 1960), and Nyiragongo (Delsemme 1960). These observations agree with equilibrium calculations showing CuCl is the major Cu-bearing species in terrestrial volcanic gases from several different volcanoes (e.g., Symonds et al. 1987—Merapi;

Quisefit et al. 1989—Momotombo; Symonds and Reed 1993—Mount St Helens; Brackett et al. 1995; Mather et al. 2012—Kilauea; Churakov et al 2000, Henley and Seward 2018—Kudryavy; Zelenski et al. 2013; Renggli et al. 2017—Erta Ale), volcanic gas with the same composition as the lower atmosphere of Venus (Schaefer and Fegley 2004b), laboratory experiments (Ammann et al. 1993) and primordial lunar volcanic gases with different assumed compositions, pressure, and temperature (Fegley 1991; Renggli et al. 2017).

The formation of CuCl gas from monatomic Cu gas occurs via

$$Cu_{(g)} + ½\ Cl_{2(g)} = CuCl_{(g)} \tag{36}$$

The equilibrium constant for this reaction, assuming ideality of all gases is

$$K_{(36)} = \frac{p_{CuCl}}{p_{Cu}} \frac{1}{f_{Cl_2}^{1/2}} \tag{37}$$

One could write this reaction in terms of $Cu_{(g)}$ and $HCl_{(g)}$, which is the major Cl species observed in terrestrial volcanic gases, but there is no guarantee that HCl would be the major Cl-bearing gas on a heated planetary body undergoing outgassing and/or evaporation reactions. For example, as shown in Table 4, the major Cl-bearing gas evolved from H-chondritic material during heating at low pressure is NaCl, not HCl (Schaefer and Fegley 2010). Also, the major Cl-bearing gas changes from HCl to NaCl (at $P \sim 3$ bar) to Cl (at $P \sim 2 \times 10^{-5}$ bar) at 2000 K and otherwise constant conditions for the BSE (bulk silicate earth)–steam atmosphere model of Fegley et al. (2016). Thus we use the Cl_2 fugacity, which is a fundamental variable computed iteratively from the partial pressure sum for all Cl-bearing gases (see below).

However, our use of the Cl_2 fugacity as a fundamental variable does not necessarily mean that Cl_2 is the major Cl-bearing gas. This is unlikely unless either (1) volcanic HCl is oxidized by the O_2 in air to form Cl_2—a reaction known as the Deacon process (Lewis 1906) or (2) chlorine is much more abundant than the elements that usually bond with it—H, the alkalis, and sulfur. Zelenski and Taran (2012) studied the Deacon process and showed it explains the Cl_2 emitted in air-rich fumarolic gas at Tolbachik in Kamchatka. Fegley and Zolotov (2000) explored the latter case where Cl/H, Cl/alkali, and Cl/S molar ratios are greater than unity in their calculations of alkali and halogen chemistry in volcanic gases on Io, the volcanically active satellite of Jupiter. However their preferred models—based on elemental abundances deduced from the Io plasma torus and other constraints—show chlorine is emitted as NaCl and KCl in Ionian volcanic gases. Lellouch et al. (2003) subsequently discovered NaCl gas in Io's atmosphere and concluded it was volcanic in origin. Moullet et al. (2013) tentatively observed KCl gas on Io and concluded it was also compatible with a volcanic origin.

Returning to the CuCl formation reaction above, we can rearrange the equilibrium constant expression to show that the CuCl/Cu molar ratio (X denotes mole fraction in the gas) is proportional to the square root of total pressure at otherwise constant conditions

$$\frac{X_{CuCl}}{X_{Cu}} = K_{(36)} \sqrt{X_{Cl_2}} \sqrt{P_T} \tag{38}$$

Thus higher pressure favors $CuCl_{(g)}$ while lower pressure favors Cu^0 gas. The tabulated thermodynamic data for gaseous Cu and CuCl (e.g., JANAF or IVTAN) show K_{eq} for the Cu–CuCl reaction decreases (i.e., the $\Delta G°$ of reaction is less negative) with increasing temperature; hence at otherwise constant conditions Cu is favored at higher temperature. Figure 12 shows the pressure dependence of the CuCl/Cu ratio at 2000 K for the BSE–steam atmosphere model of Fegley et al (2016). This model uses a $CuO_{0.5}$ activity coefficient of 3.5 based on Wood and Wade (2013) and Holzheid and Lodders (2001); Fegley et al (2016)

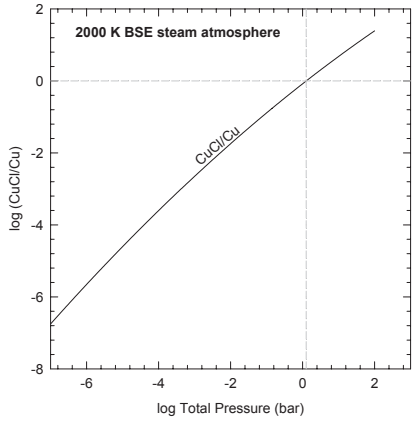

Figure 12. The CuCl/Cu molar ratio in the gas phase is plotted as a function of total pressure at 2000 K for the BSE–steam atmosphere model of Fegley et al (2016). The chemical equilibrium calculations are described in their paper. The CuCl/Cu ratio is unity at ~ 1.25 bar total pressure. Higher pressure and lower temperature favor CuCl while lower pressure and higher temperature favor monatomic Cu gas. See the text for a detailed discussion. Subsequent figures in this section are for the same model.

describe other details of the calculations, which consider chemical equilibrium in the magma, between gas and magma, and in the gas phase. Figure 12 shows that the 1:1 ratio occurs at ~ 1.25 bar with Cu dominant at lower pressures and CuCl dominant at higher pressures. The position of the 1:1 ratio will be different for this steam atmosphere model at different temperatures. It will also be different in gas mixtures of different composition, e.g., terrestrial volcanic gases, or the outgassed atmosphere on a heated planetesimal, because the Cl-bearing gas speciation and thus the Cl_2 fugacity will be different. But the general behavior—CuCl favored at higher *P* and lower *T* and Cu favored at lower *P* and higher *T* will be the same. Thus we expect Cu volatility at lower pressures/high temperatures is mainly due to its evaporative loss as Cu^0 while Cu volatility at higher pressures/low temperatures involves CuCl gas.

Calculations in a multicomponent gas mixture

Before continuing with another example we return to the Cl_2 fugacity and explain what it represents. This discussion is analogous to that given by Lodders (2003) for condensation calculations in the solar nebula. The partial pressure sum for chlorine in a multicomponent gas mixture—be it a volcanic gas, steam atmosphere on the early Earth, or an outgassed atmosphere on a planetesimal—is given by a mass balance equation such as

$$\begin{aligned} P_{\Sigma Cl} = X_{\Sigma\, Cl} P_T = &\left(P_{Cl} + P_{HCl} + P_{NaCl} + P_{KCl} + P_{CuCl} + \cdots\right) \\ &+2\left(P_{Cl_2} + P_{MgCl_2} + P_{FeCl_2} + \cdots\right) + 3\left(P_{CrCl_3} + \cdots\right) + 4\left(P_{Mn_2Cl_4} + \cdots\right) + \cdots \end{aligned} \tag{39}$$

This mass balance equation can be rewritten in terms of the Cl_2 fugacity and the equilibrium constants for forming each gas from its constituent elements in their reference states, and the thermodynamic activities and fugacities of other elements combined with Cl in gases

$$P_{\Sigma Cl} = \left(f_{Cl_2}\right)^{1/2} \begin{bmatrix} \left(K_{Cl} + K_{HCl} f_{H_2}^{1/2} + K_{NaCl} a_{Na} + K_{KCl} a_K + K_{CuCl} a_{Cu} + \cdots\right) \\ +2 f_{Cl_2}^{1/2}\left(K_{Cl_2} + K_{MgCl_2} a_{Mg} + K_{FeCl_2} a_{Fe} + \cdots\right) \\ +3 f_{Cl_2}\left(K_{CrCl_3} a_{Cr} + \cdots\right) + 4 f_{Cl_2}^{3/2}\left(a_{Mn}^2 K_{Mn_2Cl_4} + \cdots\right) + \cdots \end{bmatrix} \tag{40}$$

The actual mass balance sum contains as many Cl-bearing gases as are in the thermodynamic database of the code used to do the computations; typically several hundred Cl-bearing gases are considered. The equation above shows that chlorine chemistry is coupled to that of all other elements in the gas and the nonlinear system of mass balance equations for Cl and all other elements included in the computations must be solved iteratively. The

Cl_2 fugacity used to calculate Figure 12 is the value computed from such a mass balance equation and takes into account the distribution of Cl between all Cl-bearing gases in the steam atmosphere model of Fegley et al (2016). For example, Figures 15–24 in their paper show the more abundant Cl-bearing gases, which include NaCl, HCl, KCl, $(NaCl)_2$, $MgCl_2$, $FeCl_2$, $NiCl_2$, and $CaCl_2$; however many more Cl-bearing gases are in the partial pressure sum but are not abundant enough to appear in the figures in Fegley et al (2016).

Analogous considerations apply to the hydrogen, oxygen, fluorine, and sulfur fugacities in complex gas mixtures. In each case the elemental fugacity (fH_2, fO_2, fF_2, fS_2) is a fundamental variable that is computed from the mass balance expressions and chemical equilibrium abundances of all gases containing each element. For example, Table 4 below shows elemental fugacities from the computer calculations of Fegley et al (2016) for a BSE–steam atmosphere model (at 2000 K and one bar total pressure). The BSE composition was taken from Palme and O'Neill (2014) in their computations.

Table 4. Illustrative elemental fugacities for key volatiles (2000 K, one bar) steam atmosphere

fH_2	fO_2	fF_2	fS_2	fCl_2
9.02×10^{-2}	4.74×10^{-6}	6.00×10^{-18}	1.29×10^{-3}	4.16×10^{-10}

Zn-bearing gases

Zinc chemistry is analogous to that of copper, but there are no spectroscopic observations of zinc compounds in terrestrial volcanic gases. Chemical equilibrium calculations for terrestrial volcanic gases from several different volcanoes (Symonds et al. 1987; Quisefit et al. 1989; Symonds and Reed 1993; Churakov et al. 2000; Wahrenberger et al. 2002; Renggli et al. 2017) predict Zn is the major species at higher temperatures while $ZnCl_2$ is the major species at lower temperatures. Churakov et al (2000) give the transition temperature between these two species as 1223 K for their calculations modelling Kudryavy fumarolic gases.

The formation of $ZnCl_2$ from monatomic Zn gas occurs via the reaction

$$Zn_{(g)} + Cl_{2(g)} = ZnCl_{2(g)} \tag{41}$$

The equilibrium constant for this reaction, again assuming ideality for the gases, is

$$K_{(41)} = \frac{P_{ZnCl_2}}{P_{Zn}} \frac{1}{f_{Cl_2}} \tag{42}$$

Upon rearranging the equilibrium constant expression we see the $ZnCl_2$/Zn molar ratio is proportional to total pressure at otherwise constant conditions

$$\frac{X_{ZnCl_2}}{X_{Zn}} = K_{(41)} X_{Cl_2} P_T \tag{43}$$

This equation shows higher pressure favors $ZnCl_2$ while lower pressure favors monatomic zinc. The thermodynamic data for gaseous $ZnCl_2$ show it becomes less stable relative to Zn^0 at higher temperature. Figure 13 shows that the 1:1 ratio occurs at ~ 890 bar with Zn dominant at lower pressures and $ZnCl_2$ dominant at higher pressures. The behavior of the Zn–$ZnCl_2$ pair is analogous to that of the Cu–CuCl pair; the chloride is dominant at higher pressure and lower temperature and the monatomic gas dominates at lower pressure and higher temperature. Our calculations, those from the volcanic gas models cited earlier, and the evaporation studies reviewed in the section on *Thermodynamics of evaporation/condensation of metal oxides in simple, complex and natural systems* all imply that Zn volatility is governed by its evaporative loss as Zn^0.

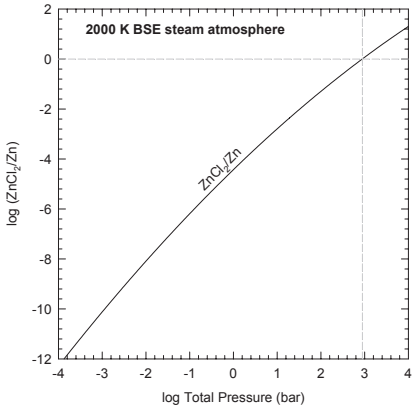

Figure 13. The $ZnCl_2$/Zn molar ratio in the gas phase is plotted as a function of total pressure at 2000 K for the same steam atmosphere model shown in Figure 12. The $ZnCl_2$/Zn ratio is unity at ~ 890 bar. Higher pressure and lower temperature favor $ZnCl_2$ while lower pressure and higher temperature favor monatomic Zn gas. See the text for a detailed discussion.

Factors governing the stability of gas species

Table 5 illustrates several trends as a function of pressure, temperature and composition. The columns for the solar nebula and H-chondrites are taken from our calculations for solar nebula condensation and ordinary chondrite metamorphism (Lodders 2003; Schaefer and Fegley 2010). The volcanic gas column is from published calculations (Symonds et al. 1992—Augustine, Churakov et al. 2000, Wahrenberger et al. 2002—Kudravy and Symonds and Reed 1993—Mt. St. Helens) and the ferrobasalt column is based on the Langmuir vaporization experiments of Sossi et al. (2016a). As shown in Table 5, the alkalis, Ag, Ga, In and Tl behave analogously to Cu; the chloride is dominant at higher pressure and lower temperature while the monatomic gas is dominant at lower pressure and higher temperature. Figure 14 shows Mn chemistry is like that of Zn but with the interesting complication that with decreasing pressure under otherwise constant conditions the major gas changes from $MnCl_2$ to MnCl to Mn. Volcanic gas chemical equilibrium calculations from the literature show several other elements (Bi, Cr, Fe, Mo, Pb, Sb) may exist as chlorides at one bar pressure and temperatures of 1143–1213 K (see Table 5). These trends are easily understood using the same reasoning as described above for the Cu–CuCl and Zn–$ZnCl_2$ equilibria.

Iron gas phase chemistry (see Table 3) exemplifies the competition between halide and hydroxide gases. (Hastie 1975, pp. 68–73) showed the relative abundances of halide and hydroxide gases in steam-rich systems with HCl and HF are controlled by exchange equilibria such as

$$FeCl_{2(g)} + 2\,H_2O_{\,(g)} = Fe(OH)_{2(g)} + 2\,HCl_{(g)} \tag{44}$$

The equilibrium constant expression for this reaction is

$$K_{(44)} = \frac{P_{Fe(OH)_2}}{P_{FeCl_2}} \left(\frac{P_{HCl}}{P_{H_2O}} \right)^2 \tag{45}$$

We can rearrange this to show that the hydroxide/chloride molar ratio is independent of the total pressure but varies with the square of the H_2O/HCl molar ratio in the gas

$$\frac{X_{Fe(OH)_2}}{X_{FeCl_2}} = K_{(44)} \left(\frac{X_{H_2O}}{X_{HCl}} \right)^2 \tag{46}$$

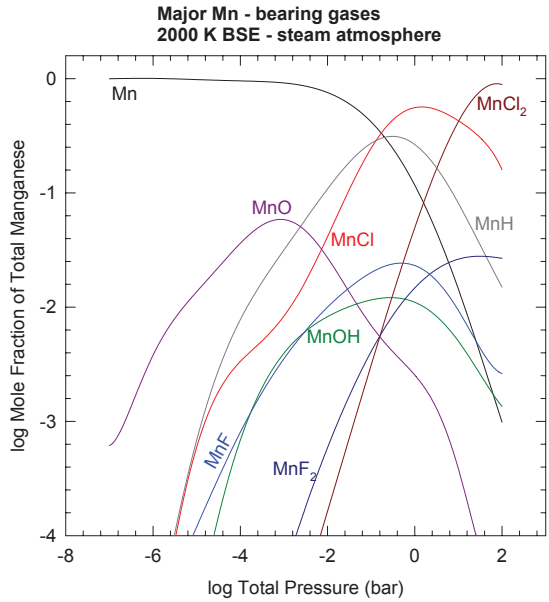

Figure 14. The speciation of manganese is plotted as a function of total pressure at 2000 K for the same steam atmosphere model shown in Figure 12. The major Mn-bearing gas shifts from $MnCl_2$ to MnCl to Mn with decreasing pressure. Higher pressure and lower temperature favor the Mn chloride gases while lower pressure and higher temperature favor monatomic Mn gas.

Similar competition between halide and hydroxide gases was calculated to be important for Al, Ca, K, and Na in the steam atmosphere models of Fegley et al (2016). As pointed out by Pokrovski et al. (2013), thermodynamic data may be lacking for trace elements that readily undergo gas phase hydrolysis (notably the Group VI metals), such that the full spectrum of gaseous species may not be represented in these calculations for H_2O-rich volcanic vapors. However, the monatomic gases are expected to be the major forms of Fe, K, and Na in the solar nebula (Table 5). Indeed, at high temperatures (>1200 K) even in volcanic vapors with high fS_2 and fCl_2, the monatomic gases (noted above) and oxide species (e.g. Group VI metals, As, Sb) begin to replace their chloride- and hydrated equivalents, respectively (see discussion in Churakov et al. 2000). The experiments of Sossi et al. (2016a) notably lack major volatile species, thereby simplifying chemical equilibria in the gas phase by lowering the stability of these –OH, –Cl and S-bearing species observed in volcanic vapors (Table 5). At low pressures (≤1 bar), these molecules are either sparingly soluble in silicate melts (Cl, Carroll and Webster 1995; Webster 1997; H_2O, Dixon et al. 1995) and/or highly volatile (S, Cl, F, H) that they may be near-absent in degassing magmas at high temperatures at low pressures, leaving O_2 as the major volatile species. Such conditions are likely found on heated planetesimals, on which the escape velocities are too low to retain an atmosphere comprised of light elements, such as H, C, or S, resulting in confining pressures of < 1 bar. Under these conditions complex halide or sulfide gases are predicted to be absent; indeed, the major gas species inferred from the experiments of Sossi et al. (2016a) are the monatomic gases (the alkalis, Zn, Cd, Ag, Pb, Cu, Fe, Mn and Ga), though notably some have stable di- or trioxide species (CrO_2, MoO_3), while others form monoxides at fO_2 close to air (LiO, GaO, PbO). Their vaporization behavior in passing from volatile-poor systems to lower-temperature volcanic gases can be generalised as: monatomic gases tend to form chlorides (e.g., alkalis, Cu, Zn), oxide species are hydrated (e.g., H_2CrO_2) and gas species of divalent chalcophile elements such as GeO and PbO substitute O_2^- with S_2^- (GeS, PbS).

Table 5. Speciation of major gases at these conditions.

Element	Solar nebula, 1500 K 10^{-4} bar	H-chondrite, 1500 K 10^{-4} bar	Volcanic gas 1143–1213 K 1 bar	Anhydrous ferrobasalt (Sossi et al. 2016a), 1573–1823 K 1 bar
Ag	Ag	Ag	Ag[8], (AgCl)[8]	Ag
As	As	AsS	AsS[5,7,8], AsO[7]	—
Au	AuS[1]	AuS	AuS[8]	—
Bi	Bi	Bi	Bi[6–8], (BiS[5,6], $BiCl^5$)	—
Br	HBr	NaBr	HBr[5–8]	—
Cd	Cd	Cd	Cd[5,7,8]	Cd
Cl	HCl	NaCl	HCl[5–8]	—
Cr	Cr	Cr	CrO_2Cl_2[5], CrO_2H_2[7]	CrO_2
Cs	Cs[2]	Cs	CsCl[7,8]	Cs[9]
Cu	Cu	Cu	CuCl[5–8]	Cu
F	HF	NaF	HF[5–8]	—
Fe	Fe	Fe	$Fe(OH)_2$[6–8], ($FeCl_2$[5,7])	Fe
Ga	Ga	GaF[3]	GaCl[6,7]	GaO, Ga
Ge	GeS	GeS	GeS[7]	GeO
H	H_2	H_2	H_2O[5–8]	
I	I	NaI	—	—
In	In	In	InCl[6,7]	—
K	K	K	KCl[5–8]	K
Li	Li	—	LiCl[5,7]	Li, LiO
Mn	Mn	Mn	$MnCl_2$[5,7,8]	Mn
Mo	Mo	—	H_2MoO_4[6–8], (MoO_2Cl_2[5])	MoO_3
Na	Na	Na	NaCl[5–8]	Na
O	CO[4]	CO	H_2O[5–8]	—
P	PO	P_4O_6	—	—
Pb	Pb	PbS	PbS[6–8], ($PbCl_2$[5])	PbO, Pb
Rb	Rb	Rb	RbCl[7,8]	Rb
S	H_2S	S_2	SO_2[5–8]	—
Sb	Sb	SbS	SbS[5,7,8], SbO[7],($SbCl_3$[5])	—
Se	Se	SeS	H_2Se[8]	—
Sn	SnS	SnS	SnS[6,7]	—
Te	Te	Te	Te[8]	—
Tl	Tl	Tl	TlCl[6,7]	—
Zn	Zn	Zn	Zn[7,8], ($ZnCl_2$[5])	Zn
log fO_2	–18.06	–12.48	–12.58 to –10.93	–10 to –0.67

[1]Au is about half as abundant as AuS

[2]If thermal ionisation is considered, Cs^+ is major Cs gas

[3]GaOH is almost as abundant as GaF

[4]$CO/H_2O \sim 0.86$ at this P and T

[5] Symonds et al. 1992, Augustine ($\log fO_2 = 12.58$; $T = 1143$ K)

[6] Wahrenberger et al. 2002, Kudryavy ($\log fO_2 = -10.99$; $T = 1173$ K)

[7] Churakov et al. 2000, Kudryavy ($\log fO_2 = -10.93$; $T = 1213$ K)

[8] Symonds and Reed 1993, Mt. St. Helens ($\log fO_2 = -11.39$; $T = 1203$ K)

[9] Kreutzberger et al. 1986

Gas species that are more stable at lower temperature and/or high Cl_2 fugacity are shown in brackets.

VOLATILITY DURING PLANETARY FORMATION

Overview

Chondritic (undifferentiated) meteorites are currently assumed to provide the best estimate for the bulk composition of the rocky planets. The CI carbonaceous chondrites are particularly useful, as they have relative abundances of rocky elements identical to solar photospheric abundances of these elements. Thus the elemental composition of the solar nebula is given by elemental abundances from CI chondrites and from the Sun (e.g., see Lodders 2003, 2008 and references therein for the details).

However, basaltic rocks and remote sensing measurements show that rocky bodies of the inner solar system, in addition to other chondrites, are depleted in MVEs (Dreibus and Wanke 1985; Palme et al. 1988; Mittlefehldt and Lindstrom 1990; Barrat et al. 2000; Ruzicka et al. 2001; O'Neill and Palme 2008). Element depletion is quantified by normalizing a volatile element to a refractory, lithophile element (typically Mg). This ratio is then divided by the same quantity in CI chondrites:

$$f_E = \frac{E_x / \mathrm{Mg}_x}{E_{CI} / \mathrm{Mg}_{CI}} \tag{47}$$

This exercise is performed for each element, E in a given planetary body, x. It has been the convention in cosmochemistry for 50 years (Larimer 1967) to plot these elemental depletion factors (f_E) against their nebular half-condensation temperatures[6], T_c (Fig. 15). The mid-plane pressure in the inner solar nebula is $\approx 10^{-4}$ bars and conditions are highly reducing (fO_2 is 10^7 times more reducing than Iron-Wüstite, IW− 7; Rubin et al 1988; Grossman et al. 2008). The moderately volatile elements, have T_c between the main components (Mg, Fe, Si, $T_c \approx 1320$ K) and FeS (660 K).

Quantitative condensation of a moderately volatile element occurs over a narrow range of <100 K (e.g., Lodders 2003). Should MVE abundances simply reflect nebular condensation temperatures, then the final temperature of accretion of chondrite components should sharply discriminate between those elements whose T_c is higher than that of last equilibration with the gas phase (fully condensed) from those with lower T_c, which reside entirely in the gas phase (as recognized by Larimer 1967). Rather, MVEs in chondritic meteorites vary monotonically with nebular condensation temperature, and tend to flatten out in the most volatile ($T_c < 650$ K), as noted by Wolf et al. (1980) and expanded upon by Humayun and Cassen (2000). This feature implies two superimposed processes i) the depletion of volatile elements in chondrites according to their condensation temperatures above 650 K and ii) mixing of a second component with its full complement of volatile elements in proportions that are sufficient to elevate the abundances of the highly volatile elements, but not to affect the trend of the moderately volatile elements (see also Anders 1964). The two physical reservoirs for these components are likely manifest in chondrules (volatile-depleted) and matrix (volatile-rich), see Grossman and Larimer (1974). Despite large variations in the chemistry of individual chondrules (e.g., Zanda 2004), the compositions of bulk chondrites are remarkably constant, arguing for complementarity of the two components (Bland et al. 2005; Hezel and Palme 2010; Friend et al. 2017).

Although, to a first order, elemental abundances in rocky bodies are correlated with nebular condensation temperatures (e.g., Humayun and Cassen 2000), in detail this picture becomes blurred. This may be due to each planet accreting different amounts of higher temperature (volatile-depleted) and lower temperature (volatile-rich) material in its feeding zone (e.g., see Barshay 1981 or the discussion of his modelling in Moynier and Fegley 2015), though the exact mechanisms remain uncertain. Alternatively, on the planetary scale if we consider only thermal escape (neglecting important non-thermal escape processes (see Tables 7.1, 7.2 of Chamberlain and Hunten 1989) that are very difficult to model), atmospheric loss from a body is described in

[6] T_c is the temperature at which half the mass of an element is calculated to condense in the solar nebula

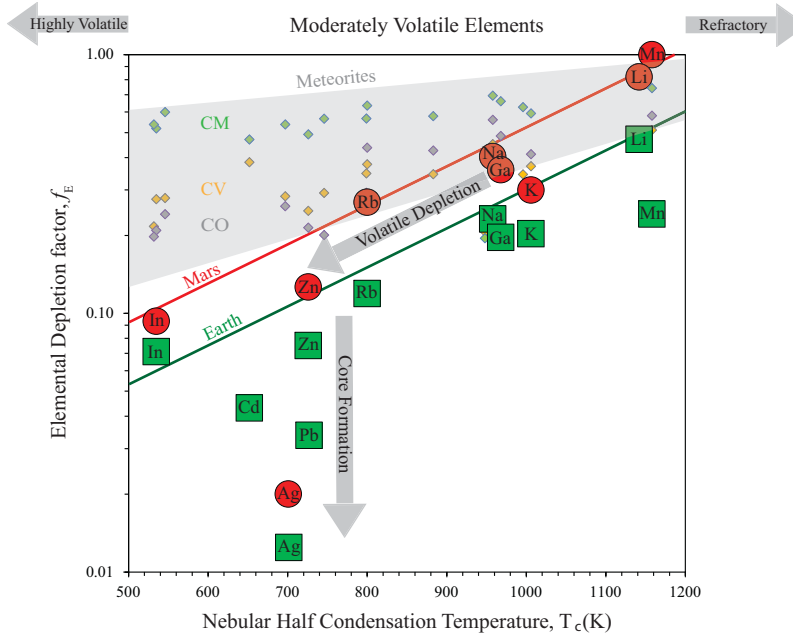

Figure 15. Depletion factors (f_E) of moderately-volatile elements in the Earth (Palme and O'Neill 2014; green squares), Mars (Dreibus and Wänke 1985; red circles) and carbonaceous chondrites; CM, CV and CO classes (Wasson and Kallemeyn 1988). Elements are plotted as a function of their nebular half-condensation temperatures, T_c (K) from Lodders (2003) except Ag (Kiseeva and Wood 2015). The trends labelled 'Mars' and 'Earth' are defined by abundances of elements that do not partition into metal, delineated by the 'volatile depletion' arrow. Depletion in Zn, Pb, Cd and Ag, is inferred to be caused by 'core formation'.

two regimes; Jeans escape (Jeans 1916) and hydrodynamic escape (Parker 1960). Jeans escape assumes a Maxwell–Boltzmann distribution of particles, in which the escape flux is:

$$\left(\frac{\mathrm{d}m}{\mathrm{d}t}\right)_J = n\left(\frac{2\mathrm{k_B}T}{\pi m}\right)^{\frac{1}{2}}\left(1+\lambda_{\mathrm{esc}}\right)e^{-\lambda_{\mathrm{esc}}} \tag{48}$$

where n is the particle number density, m the molar mass of the particle, and λ_{esc} is the escape parameter, the ratio of the thermal velocity of the particles to the escape velocity of the body, ν_{esc} (= $[2GM_{body}/r]^{1/2}$):

$$\lambda_{\mathrm{esc}} = \frac{mv_{\mathrm{esc}}^2}{2\mathrm{k_B}T} \tag{49}$$

When the mean thermal velocity of the Maxwell-Boltzmann distribution of particles begin to exceed the escape velocity of the planet (i.e., $\lambda_{esc}<1$; Genda and Abe 2003), the condition for hydrodynamic escape is met. Here, Equation (49) simplifies and the flux (kg/s) of atmosphere loss of a particle is given by the product of its density, surface area and the thermal velocity of the particle:

$$\left(\frac{\mathrm{d}m}{\mathrm{d}t}\right)_H = 4\pi r^2 \rho \varpi \tag{50}$$

The very old Pb and Sr isotope ages for eucrites and angrites (e.g., Amelin 2008; Hans et al. 2013) suggest at least some of the accreted material was differentiated and depleted in MVEs, either in the solar nebula or by these atmosphere escape mechanisms. From a mechanistic standpoint, equilibrium between the gas phase and the liquid is not mandated during gas-condensed phase interaction, and may depend on the scale at which the exchange occurs. Thus, whether the operative process of volatile depletion occurred at equilibrium or was kinetic in nature remains unconstrained. Add to this the difficulty in assessing the degree of volatile depletion experienced by differentiated bodies due to the dual siderophile/chalcophile nature of many MVEs (see Palme et al. 1988), the origin of volatile element depletion is poorly understood. Indeed, a clear departure of chalcophile elements relative to lithophile elements with similar condensation temperatures is observed in terrestrial samples (e.g., Ag and Pb; Schönbächler et al. 2010; Wood and Halliday 2010), implying that core formation also plays a role.

A possible solution to this paradox is the changing locus of volatile depletion with time. The relevance of nebular condensation temperatures is inherently rooted to the conditions of the solar nebula (i.e., that present during the formation of chondrites; and even then there are variations, e.g., Schaefer and Fegley 2010). However, planetary formation is more protracted (up to 100 My; Kleine et al. 2009; Jacobson and Morbidelli 2014), long after the dispersion of the nebular gas, which likely occurred within 5 My of the solar system's formation (Dauphas and Chaussidon 2011) but may have taken longer, perhaps up to 30 My based on astronomical observations of circumstellar disk dissipation (Cameron 1995). Thereafter, the volatility behavior of the elements are no longer bound to their nebular condensation temperatures, because the conditions under which evaporation occurs is markedly different in the post-nebular realm.

Planetary Bodies

Collisions between two embryonic planets, for example between the proto-Earth and a Mars-sized planetesimal thought to have resulted in the formation of the Moon, are highly energetic, reaching temperatures of ≈6000 K (e.g. Melosh 1990; Cameron and Benz 1991; Canup 2004; Nakajima and Stevenson 2014; Lock and Stewart 2017). Such temperatures not only far exceed those present in the solar nebula (<2000 K for any reasonable nebular pressure), but they lead to extensive melting, as they surpass the low-pressure peridotite liquidus (≈2000 K) and cause vaporization of silicate material (e.g., see the discussion in section 6.3.5 of Fegley and Schaefer 2014). Computational models that minimize the Gibbs free energy of both liquid and vapor species for major elements (Fegley and Cameron 1987; Schaefer and Fegley 2004a; Visscher and Fegley 2013) show that the composition of the gas evolved from molten peridotite (>3000 K) is dominated by SiO vapor, though Na predominates between 1800–3000 K, in both cases yielding oxygen fugacities $10^7\times$ more oxidizing than that of the nebular gas (Visscher and Fegley 2013; Fig. 16). Furthermore, the total pressure exerted by the

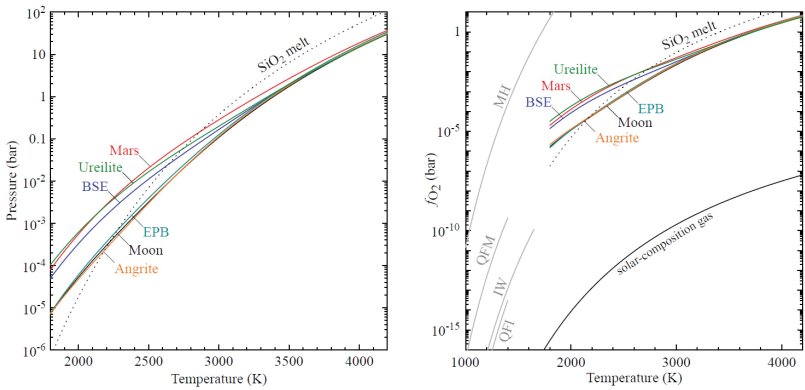

Figure 16. Evolution of the **a)** total pressure and **b)** oxygen fugacity as a function of temperature (in K) upon evaporation of planetary mantles of their own composition. Reproduced from Visscher and Fegley (2013).

gas increases with temperature as the partial pressures of gas species increase, reaching 10 bar, orders of magnitude higher than in the solar nebula, 10^{-4} bar (Fig. 16).

As illustrated by experimental work (section *Thermodynamics of evaporation/condensation of metal oxides in simple, complex and natural systems*), the order of element volatility must change in response to the different thermodynamic conditions. To this end, a recent push has seen the use of certain element pairs that should be sensitive to volatility under various conditions in order to help to distinguish between nebular and post-nebular volatile loss. Among the first was the study of O'Neill and Palme (2008) who exploited the lithophile behavior of Mn and Na (though Mn becomes weakly siderophile at high pressures and temperatures; Mann et al. (2009), to demonstrate that all small planetary bodies had undergone post-nebular volatile loss (Fig. 17). This conclusion is reached on the basis of their super-chondritic Mn/Na ratios. Manganese and Na are similarly volatile under nebular conditions (cf. the constancy of Mn/Na in chondrites with variable volatile depletion, monitored by the Mn/Mg ratio), but Na becomes relatively more volatile than Mn at more oxidized conditions:

$$MnO_{(l)} + Na_{(g)} = Mn_{(g)} + NaO_{0.5(l)} + \frac{1}{4}O_2 \qquad (51)$$

Equation (51) is a combination of the $n = 1$ reaction for Na evaporation, and an $n = 2$ reaction for Mn evaporation. As such, a preferential loss of Na relative to Mn, normalized to chondritic values, results from an increase in fO_2 relative to nebular conditions. Sitting conspicuously on the nebular array is the bulk silicate Earth (Fig. 17). An Mn/Mg ratio that is lower than any chondrite group firstly suggests that Earth is more volatile depleted than any other group (providing only minor Mn was lost to the core; Geßmann and Rubie 1998; Mann et al. 2009;

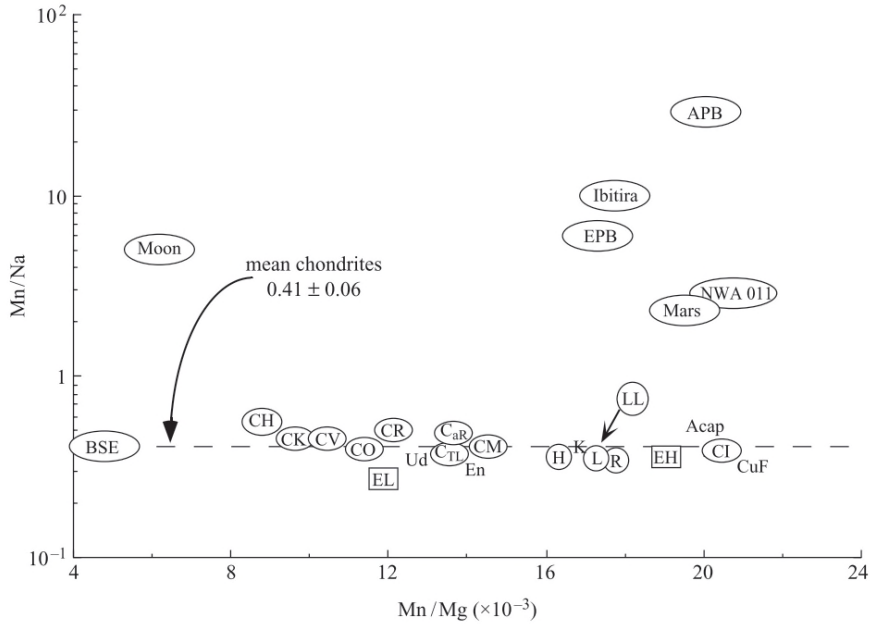

Figure 17. The Mn/Na vs. Mn/Mg ratio of planetary bodies (reproduced from O'Neill and Palme 2008). The Mn/Mg ratio tracks the degree of volatile depletion, with no effect of fO_2. Mn/Na ratios increase as a function of volatile depletion if the fO_2 is higher than that of the solar nebula. That Mn/Na is roughly constant in chondrites suggests that they were similarly volatile in the solar nebula. As the Earth plots on the chondritic array, its volatile depletion was inferred to have been nebular.

Siebert et al. 2018). A chondritic Mn/Na implies that Mn and Na were similarly volatile during their depletion from Earth. This behavior only occurs at very low fO_2, restricted to those found in the solar nebula, a conclusion supported by short-lived (3.7 My) Mn–Cr isotope system, in which the Earth falls on the isochron defined by chondritic meteorites (Moynier et al. 2007; Trinquier et al. 2008; see Palme and O'Neill 2014 for a discussion).

The Earth

The view that Earth's moderately volatile element budget was set in the solar nebula has been debated for some time (e.g., Ringwood 1966, 1979) and was recently challenged again by Norris and Wood (2017). They find that the depletion of moderately volatile elements is better correlated with their volatilities during evaporation from a silicate melt at IW – 1 than with nebular condensation temperatures. Three elements that are notable in this assessment are Zn, In and Cd, as their relative abundances are difficult to reconcile with core formation and nebular condensation temperatures. In an earlier study, this led Wang et al. (2016) to conclude that the Earth is non-chondritic. Their associated f_E are 0.075, 0.071 and 0.043 (Palme and O'Neill 2014) and calculated T_c are 726 K, 535 K and 650 K, respectively. Extrapolating the trend of f_E vs. T_c for lithophile volatile elements (Fig. 5 of Wang et al. 2016), yields expected f_E for Zn of 0.08; 0.06 for Cd and 0.035 for In. This observation may suggest the calculated condensation temperature of In is too low. Indeed, the CI- and Mg-normalized Zn/In ratio in carbonaceous chondrites is unity (0.96 ± 0.06; Wasson and Kallemeyn 1988), implying that In and Zn have similar volatilities in the solar nebula. This view extends to more oxidizing conditions and higher pressures, as supported by the volatilities inferred from Norris and Wood (2017), where Zn is slightly more volatile than In (see Fig. 9), citing the lack of S-bearing species in their experiments that stabilize $In_2S_{(g)}$ in the solar nebula. The key message is, if Zn and In depletion occurred exclusively by volatility, their depletion factors in the Earth should be very similar, as is observed.

Experimental studies show that element partitioning between silicate liquid and metal is ordered in the sequence $D = 1 \approx Zn < Cd \approx In = 10$ (Ballhaus et al. 2013; Wood et al. 2014; Wang et al. 2016); suggesting that core formation i) would deplete In to a significantly greater extent than Zn (which is not observed) and ii) would not appreciably fractionate Cd/In ratios. This, together with the observation that Zn and Cd have chondritic stable isotope ratios in the BSE (Wombacher et al. 2008; Sossi et al. 2018) and that they remain relatively impervious to other mass transfer processes during planetary formation such as collisional erosion (Carter et al. 2018) or partial melting (Witt-Eickschen et al. 2009), suggests that the abundances of these three elements should largely reflect fractionation attributed to volatility during Earth's formation, where (least volatile) $In \approx Zn < Cd$ (most volatile).

A departure from the canonical condensation temperature sequence was noted for the alkali elements by Jones and Palme (2000). In their treatment, a better correlation was found between f_E and the square-root of their masses (Fig. 18a) than with T_c (Fig. 18b). This correlation holds relatively well across other weakly siderophile MVEs, however, in detail, large discrepancies are apparent. For example, Zn (0.075), Ga (0.17), despite the heavier mass of the latter element, especially considering that Ga is more siderophile than Zn (e.g., Wood et al. 2014). Jones and Palme (2000) tentatively attributed this broad dependence on the square root of the mass to indicate the controlling influence of a transport process, namely Jeans escape, on the abundances of MVEs. For a Maxwell–Boltzmann distribution of kinetic energies, particles in a hot atmosphere will have mean velocities equal to:

$$\bar{v} = \sqrt{\frac{2RT}{M}} \tag{52}$$

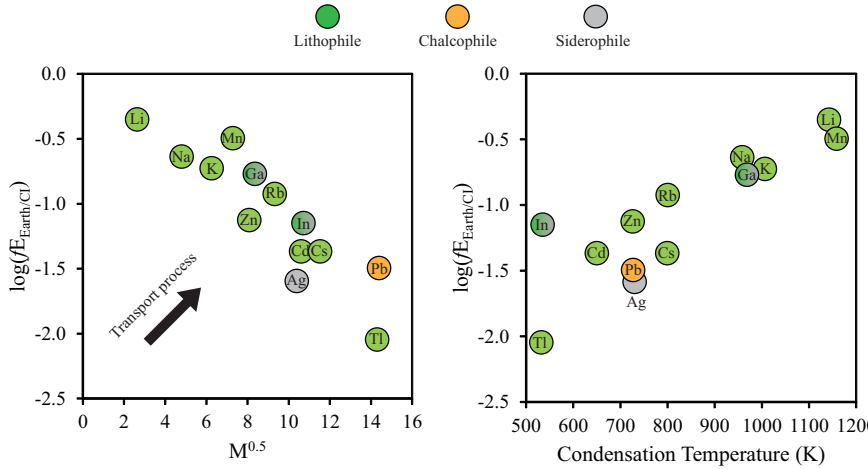

Figure 18. CI- and Mg-normalized elemental abundances (f_E) in the Earth's primitive mantle (Palme and O'Neill 2014), as a function of **a)** the square root of their atomic mass (arrow denotes fictive trend for loss controlled by a transport process) and **b)** nebular condensation temperature (Lodders 2003) and, Ag, (Kiseeva and Wood 2015). Green = lithophile; orange chalcophile, grey = siderophile.

where R is the gas constant, T the absolute temperature and M the molar mass. Where this velocity exceeds $\overline{v}_{esc}$, volatile loss occurs (see Eqn. 49). As such, lighter particles should be preferentially lost relative to heavier ones proportional to $M^{-0.5}$, the inverse of what is observed. Rather, the depletions in alkalis are positively correlated with the experimental results of Kreutzberger (1986), where the volatility sequence is, from least to most volatile, Na < K < Rb < Cs (see section *Alkali metals*, Fig. 7). As volatile depletion in their experiments is controlled by equilibrium partial pressures of alkali metals in the gas phase, so too do these depletions in the Earth likely reflect the same control at some stage of its evolution.

Whether volatile depletion on Earth was the result of gas-condensed phase interaction in the solar nebula or later during planetary formation, and to what degree equilibrium was attained, may be edified by ongoing experimental and isotopic work. The emerging picture from numerical modelling suggests that escape velocities for the Earth (11.1 km/s) are prohibitively large for thermal escape to occur. Indeed, even for hydrodynamic escape, which results from dissociation of H_2O in a hot Earth–Moon disk after a giant impact (Genda and Abe 2003; Desch and Taylor 2013), the escape of volatiles is retarded by their necessity to diffuse through a medium dominated by heavier molecules (e.g., $SiO_{(g)}$, $Na_{(g)}$, $NaCl_{(g)}$, see section *Evaporation in the presence of major volatiles H, C, S and halogens*) apparently rendering their loss by this mechanism ineffectual (Nakajima and Stevenson 2018). Nevertheless, proto-lunar disk models are still in flux and Gammie et al. (2016) argue "a hot magnetized disk could drive bipolar outflows that remove mass and angular momentum from the Earth–Moon system". Furthermore, Genda and Abe (2005) argue for enhanced atmospheric loss on the early Earth if oceans were present when impacts took place. Depending on which models are correct, post-nebular volatile loss by evaporation from silicate melts may be restricted to smaller planetesimals where escape velocities are lower (Charnoz and Michaut 2015; Hin et al. 2017). Alternatively, the Earth's MVE depletion was inherited from its constituents that had already lost volatiles in the solar nebula (O'Neill and Palme 2008; Dauphas et al. 2015; Sossi et al. 2016b).

The Moon and Vesta

Two such small, volatile depleted bodies are found in the form of the Moon and Vesta, which have radii of 1737 km and 263 km, respectively. Both bodies are volatile depleted and these depletions have some similarities (Fig. 19), but differ in detail (e.g., Dreibus and Wänke 1979, 1980, 2001; O'Neill 1991; Ruzicka et al. 2001). Jochum and Palme (1990) argued that the consistent K/La, Rb/Sm, Cs/U element correlations in eucrites would not be present if evaporative loss of alkalis occurred during volcanism or thermal metamorphism. A similar argument was presented for the lunar mare basalts (see Gooding and Muenow 1976), meaning that volatile depletion is a widespread characteristic of both bodies and likely occurred during their accretion. Several MVEs are depleted to similar extents in the two bodies (Fig. 19). Although reliable data on the composition of the bulk silicate Moon and Vesta are scarce, f_E appears to exhibit a log–linear decrease with decreasing T_c (Fig. 19). Clues on the nature of volatile metal depletion on Vesta may be found by considering the extent of alkali metal depletion. As per the Earth, alkalis are depleted on Vesta in the sequence Na < K < Rb < Cs; with f_E = 0.07, 0.07, 0.01, and 0.007, respectively. This therefore implies a strong control of equilibrium partial pressures of alkali species in determining the volatile abundances of Vesta, rather than any transport process. This conclusion is in line with the small size of Vesta (263 km radius), and associated escape velocity of 0.36 km/s. Heating of rocky material to minimum temperatures of 1000 K at 10^{-3} bar to liberate alkali metals (e.g., Margrave 1967) yields mean particle velocities, Equation (52), of between 0.96 km/s (Na) to 0.40 km/s (Cs), meaning all alkali thermal velocities exceed the contemporary escape velocity of Vesta. Lodders (1994) discussed thermal loss of alkalis during planetary accretion and modelled alkali loss (as MOH gas, M = Li to Cs) as a function of the ratio of escape/thermal velocities, showing loss by Jeans escape would occur in the sequence of Li > Na > K > Rb > Cs (most volatile but heaviest species), the opposite to that observed. Thus, earlier in its accretion history, heating of the Vestan mantle was likely associated with immediate loss of volatile metals proportional to their partial pressures.

The larger size of the Moon (r_{Moon} = 1737 km; v_{esc} = 2.38 km/s), and its different abundance pattern of volatile metals suggest other processes may have been at play. In detail, lunar volatile metal depletion is characterized by a 'step-wise' pattern, where three groups define plateaus in a T_c vs. f_E plot (Fig. 19). The weakly volatile elements, T_c > 1000 K, (Li, Mn) have $f_E \approx 0.4$, the moderately volatile, 700 < T_c (K) < 1000 with $f_E \approx 0.02$ and the highly volatile T_c < 700 K with

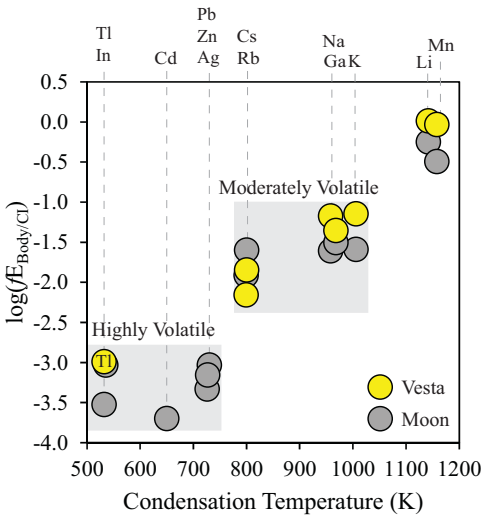

Figure 19. CI-, Mg-normalized depletion factors (f_E) of volatile metals in the Moon (grey) and Vesta (yellow) as a function of condensation temperature. Trace element abundances from Taylor and Wieczorek (2014), Tl, Cd, Cs, Rb, K and O'Neill (1991), Li, Mn, Na, Ga, Zn, Pb, In for the Moon and Ruzicka et al. (2001) for Eucrites. To calculate mantle composition incompatible element abundances (all except Li, Mn, Zn) were multiplied by La_{PM}/La_E, where La_E = 3.35 ppm (Eucrite), with La_{PM} = 0.683 ppm. Condensation temperatures from Lodders (2003) save for Ag (Kiseeva and Wood 2015).

$f_E \approx 0.0005$. Alkali metals on the Moon show a near-constant CI-, Mg-normalized depletion of 0.02, in disagreement with their partial vapor pressures. This feature is also observed for the so-called 'highly volatile' elements at $f_E \approx 0.0005$, Ag, Bi, Br, Cd, In, Sb, Sn, Tl and Zn, again with little dependence on their anticipated volatilities (Wolf and Anders 1980; O'Neill 1991; Taylor et al. 2006). Why the Moon should exhibit such a distinctive step-wise depletion pattern has not yet been understood, below several mechanisms are explored.

That Cs and Rb are not as impoverished in the Moon as might be expected from equilibrium partial pressures relative to other alkali metals has been recognized previously (Kreutzberger et al. 1986; O'Neill 1991; Jones and Palme 2000). O'Neill (1991) considered that this anomalous behavior may be due to the addition of a small fraction (4%) of H-chondrites to the Moon, which are also relatively rich in alkali metals compared to other MVEs (e.g., Wasson and Kallemeyn 1988). The abundances of HVEs (Zn, Tl, Ag, etc.) are an order of magnitude lower than the alkalis and, in this model, also reflect the H-chondrite contribution. A similar 'chondritic veneer', though this time with C-chondrites, was invoked by Wolf and Anders (1980) to explain the near-chondritic relative proportions of these highly volatile elements.

A 'double-depletion' scenario is favored by Taylor et al. (2006), in which the timing of the Moon's volatile depletion may have occurred in two stages. This hypothesis is grounded on a striking feature of lunar volatile depletion; it closely parallels that of the Earth (Ringwood and Kesson 1977; Taylor et al. 2006, their Fig. 1). Such depletion is taken as evidence for the inheritance of alkali metals from the Earth's mantle, or from the impactor, characterizing the first stage of volatile loss. An early alkali depletion event is signaled by the similar composition of BABI[7] and the earliest lunar rocks (e.g., Carlson and Lugmair 1988; Edmunson et al. 2009; Hans et al. 2013). Volatile depletion was then punctuated by a second event, presumably related to a giant impact, in which vapor loss occurred at a single threshold temperature of ≈1000 K, resulting in minimal accretion of elements present in the vapor (principally the highly volatile elements). A similar scenario had already been envisaged by O'Neill 1991, exploiting the observation that, relative to the Earth's mantle, Na falls to $1/10^{th}$ of its initial abundance in the Moon, whereas its neighboring alkali metal, Li, is essentially undepleted. Satisfying this constraint using thermodynamic data, for which the reaction may be written:

$$LiO_{0.5(l)} + Na_{(g)} = Li_{(g)} + NaO_{0.5(l)} \tag{53}$$

yields temperatures of ≈1400 K, lest Li is lost to greater than 10% for 90% Na loss (see Appendix 2 of O'Neill 1991). However, this assumes that solid $LiAlSi_2O_6$ (in clinopyroxene) and $NaAlSi_3O_8$ (in albite), approximate their components in a silicate melt (Ghiorso and Sack 1995). According to these studies, volatile depletion on the Moon was a low-temperature phenomenon occurring at a certain threshold temperature.

Canup et al. (2015), through dynamical and chemical models, provide a mechanism for the Moon's formation that evolves naturally to a state resulting in a wholesale loss of volatiles by incomplete condensation at a certain temperature. In their model, the Moon accretes initially rapidly (< 1 yr) from material outside the Roche limit[8] at 2.6 Earth radii. Over the subsequent 10^2 yr, tidal shearing of hot (> 2500 K) silicate material in the inner disk causes it to spread beyond the Roche limit and accrete to the nascent Moon. As such, in the model, the Roche limit represents a natural threshold that dictates the temperature at which volatile elements are lost, though as the study treats only Zn, K and Na, it is unknown as to whether this process results in step-wise lunar MVE depletion. In contrast to the earlier estimates cited above, Canup et al (2015) predict higher temperatures, ≈2500–3000 K, depending on the total atmospheric pressure (typically several bar). Their work used a *P–T* profile based on the vapor pressure of pure molten silica but also used the MAGMA code, which considers

[7] *Basalt Achondrite Best Initial*

[8] The Roche limit describes the closest distance to a planetary body beyond which its gravitational pull is so weak so as to allow condensed material to coalesce into a second body under its own gravity.

activity coefficients for Zn, Na, K, and major elements in the melt, to compute volatility of Zn, Na, and K from molten peridotite. Further work is needed to include Li, Rb, Cs, other MVE, halogens, water, and sulfur in the MAGMA code. Calculations with other codes give results in the same temperature range for the same total pressures (Petaev et al. 2016; Fegley and Lodders 2017). Complex melts, such as the molten bulk silicate proto-Earth (i.e., at the time of planetary accretion and/or lunar formation) probably evaporate incongruently until an azeotropic composition is reached, e.g., see Heyrman et al 2004; Petaev et al 2016; Fegley and Lodders 2017; Lock et al 2018). Whether these models hold for a non-canonical disk, in which the majority of the disk's mass already lies beyond the Roche limit (Nakajima and Stevenson 2014), or in a magnetized disk (Gammie et al. 2016) is yet to be assessed.

It is clear that the use of a single parameter (e.g., $M^{-0.5}$ or condensation temperature) fails to capture the entire complexity in describing the abundances of MVEs in planetary bodies. Instead, a combined approach is required that involves thermodynamic modelling to constrain temperatures, pressures and fugacities of major volatile species (O_2, Cl_2, S_2) during gas–vapor exchange, together with dynamical modelling that places constraints on the physical processes that moderate volatile escape.

CONCLUSIONS

Quantitative understanding of the conditions (pressure, temperature, composition) and processes (style of vaporization/condensation, volatile escape mechanism, equilibrium *vs.* kinetic) that produced the chemical signatures observed in planetary materials necessitates the application of appropriate thermodynamic data. To this end, the material covered in this chapter is summarized:

- At equilibrium, evaporation reactions of oxides and oxide components may either occur congruently, in which the M/O ratio in the gas is the same as that in the condensed phase, or incongruently, in which $M/O_{condensed} \neq M/O_{gas}$. For congruent vaporization, these reactions may also be associative (with identical speciation in both) or dissociative, where the condensed component decomposes into two or more species. These components in complex silicate melts likely evaporate congruently, though the bulk liquid may do so incongruently until reaching an azeotrope.
- A treatment is outlined for equilibrium thermodynamic calculations for evaporation reactions using existing data on pure oxides. Despite the accessibility of thermodynamic data for simple systems, they have not been properly exploited because their application to complex, multicomponent systems, requires knowledge of the activity coefficient of the species in the appropriate phase.
- Techniques for measuring equilibrium vapor pressures and thermodynamic quantities are briefly described, and comprise Knudsen cell effusion, torsion effusion, and transpiration methods, in which the partial pressures of vapor species are measured or characterized by mass spectrometry, spectroscopic techniques, or by momentum and/or weight loss or gain. Newer approaches include thermodynamic modelling and *ab-initio* calculations.
- Table 1 compiles the equilibrium speciation of metal-bearing gas species observed above $MO_{x(s,\,l)}$ phases for ~ 80 oxides, and serves as an indication for their behavior in more complex systems.
- Studies reporting thermodynamic data of metal oxides in binary-, ternary- and multicomponent silicate systems, with an emphasis on vapor-pressure measurements are summarized. For reference, a table showing approximate ranges of $28\,MO_x$ activity coefficients in multicomponent (>3) silicate melts is presented.

- Experimental data is reviewed for the evaporation of metal oxides in natural silicate systems, namely basaltic material and olivine, with the aim of quantifying the volatilities of the major silicate components, which are broadly K ≥ Na > Fe, Mn > Cr, Mg, Si > Al, Ca, Ti. The oxygen fugacity (fO_2) of the vapor phase above natural silicate material is close to the Fayalite–Magnetite–Quartz buffer and its influence on element volatility is discussed.
- The condition for kinetic or 'Langmuir' evaporation is presented, and the applicability of the Hertz–Knudsen–Langmuir (HKL) equation to quantify evaporation processes in experiments is evaluated. Providing caveats such as temperature gradients between the gas and the condensed phase are considered, the HKL equation can provide accurate descriptions of vapor pressures above silicate melts at high temperatures, although equilibrium methods are preferred and further testing is required.
- Experimental techniques that deal with kinetic vaporization are usually performed in a furnace under vacuum or with a continual flow of gases that buffer fO_2, and, in contrast to equilibrium techniques, volatilities are calculated from the fraction remaining in the condensed phase or by target collection.
- Evaporation of major elements from solids may be congruent (forsterite) or incongruent (olivine, plagioclase) and is reviewed in more detail in Nagahara (this volume).
- Alkali metals have very low activity coefficients in silicate melts that decreases their equilibrium partial pressures compared to those expected from pure alkali oxides. Their activity coefficients (Li > Na > K > Rb > Cs) are inversely proportional to their volatilities (Cs > Rb > K > Na > Li). Therefore, even though $K_2O_{(s)}$ is more volatile than $Na_2O_{(s)}$, Na and K are similarly volatile from silicate melts and $\gamma NaO_{0.5}$ and $\gamma KO_{0.5}$ are sensitive to composition.
- Evaporation of elements from a silicate melt at fixed pressure and temperature is controlled by the fO_2. This can be understood by the congruent evaporation of metal oxides and their speciation in the gas- and condensed phase. Lower fO_2 increases the vapor pressure of the metal-bearing gas species if it is more reduced than in the condensed phase, and vice-versa. Sossi et al. (2016a) show how the speciation of the element in the gas phase can be calculated by analysis of the condensed phase as a function of fO_2 in Langmuir evaporation experiments. These authors also describe a method based on the HKL equation that allows for quantitative extraction of free energies of vaporization and activity coefficients of metal oxides from silicate melts.
- The order of volatility during vaporization of silicate melts is discussed and contrasted with volatilities expected in the solar nebula. Reasons for differences between the two regimes include i) higher total pressures in evaporation experiments such that equilibrium is between liquid–gas rather than solid–gas in the solar nebula; ii) differences in phases e.g., silicate melt vs. minerals (feldspar, olivine, enstatite and Fe-Ni alloy) in the solar nebula and iii) the difference in the fugacity of volatile species (fO_2, fS_2) in the gas that may stabilize different gas species (e.g., CrO_2, MoO_3 at high fO_2 and SnS and GeS at high fS_2).
- The presence of other volatile species, particularly S_2, Cl_2 and H_2 in steam atmospheres above planetary bodies has the potential to complex metal-bearing gases. Increasing pressure and decreasing temperature increases the stability of the chloride species relative to the monatomic gas, where each ratio of $Zn/ZnCl_2$, Cu/CuCl, and $Mn/MnCl_x$ becomes unity at 890, 1.25 and 0.15 bar, respectively.

- The controls on the dominant speciation of 33 elements are contrasted in four different environments, between i) the solar nebula ii) an ordinary, H-chondrite composition, iii) terrestrial volcanic gases and iv) evaporation of an anhydrous ferrobasalt.
- Volatile element depletion in planetary materials is quantified by normalization to a refractory lithophile element (typically Mg) and then to the same ratio in CI chondrites, whose abundances for all but the most volatile elements approximate those of the Sun. Although the depletion of volatile elements in planetary bodies broadly correlates with nebular half condensation temperatures, this volatility scale is suitable only for understanding condensation as it applies to a gas of solar composition under canonical nebular conditions.
- By contrast, planetary bodies likely experienced volatile depletion at conditions distinct from those extant in the solar nebula. This is expected from results of equilibrium calculations of atmospheric compositions above planetary mantles that are dominated by Na below 3000 K and SiO above (compared to H_2 in the solar nebula), and edified by the superchondritic Mn/Na ratios of small planetary bodies that reflect more oxidizing conditions, with the notable exception of Earth.
- The Bulk Silicate Earth's abundances of Cd, In and Zn likely reflect their volatility rather than core formation, and suggest that the volatility of In is lower than supposed given its nebular half condensation temperature. A negative correlation between element abundance of moderately volatile elements and $M^{0.5}$ for the Earth show that a transport process (such as Jeans or Hydrodynamic escape) cannot have been responsible for their depletion, likely due to its high escape velocity.
- The Moon and Vesta are more strongly depleted in moderately volatile elements than the Earth, and is likely a global feature of both bodies. The loss of alkalis on Vesta in concert with their equilibrium partial pressures (Cs > Rb > K > Na > Li) points to a quantitative loss of the vapor due to the inability of Vesta to retain an atmosphere due to its small size.
- A step-wise depletion pattern is observed for the Moon, in which weakly volatile, moderately volatile, and highly volatile elements define plateaus of Mg, CI-normalized abundances of 0.4, 0.02 and 0.0005, respectively. Possible explanations for this pattern include inheritance from the Earth and an additional depletion event at 1100 K ('double depletion'); depletion at low temperatures (≈ 1400 K) and addition of a small amount (4%) of H-chondrite; or a high-temperature, high-pressure depletion event at 2500–3000 K.

ACKNOWLEDGMENTS

P.A.S. is grateful to the European Research Council under the Horizon 2020 framework grant #637503 (Pristine), and thanks Hugh O'Neill, Stephan Klemme, Nate Jacobson, Julien Siebert and Frédéric Moynier for discussions. B.F. acknowledges support by NASA Grant NNX17AC02G (XRP Program), NSF Astronomy Program Grants AST-1412175 and AST-1517541, thanks Dick Henley, Nate Jacobson, and Katharina Lodders for useful discussions, and thanks the staff of the Interlibrary Loan Service (ILL) of the Washington University Libraries for their superb support of his research work. We are grateful to Trevor Ireland, Nate Jacobson, Dick Henley, Penny King and an anonymous reviewer for far-reaching and comprehensive reviews on numerous aspects of this chapter that ultimately led to a much-improved contribution.

REFERENCES

Ackermann RJ, Chang AT (1973) Thermodynamic characterization of the U_3O_{8-z} phase. J Chem Thermo 5:873–890

Ackermann RJ, Rauh EG (1963) A thermodynamic study of the tungsten–oxygen system at high temperatures. J Phys Chem 67:2596–2601

Ackermann RJ, Rauh EG (1971a) A high temperature study of the stoichiometry, phase behavior, vaporization characteristics, and thermodynamic properties of the lanthanum+oxygen system. J Chem Thermo 3:445–460

Ackermann RJ, Rauh EG (1971b) A high temperature study of the stoichiometry, phase behavior, vaporization characteristics, and thermodynamic properties of the cerium + oxygen system. J Chem Thermo 3:609–624

Ackermann RJ, Rauh EG (1973) High-temperature properties of the Th-O system: revision of thermodynamic properties of $ThO_{(g)}$ and $ThO_{2(g)}$. High Temp Sci 5:463–473

Ackermann RJ, Tetenbaum M (1980) High-temperature vaporization behavior of oxygen-deficient thoria. *In:* Thermodynamics of Nuclear Materials 1979, vol I, IAEA, Vienna, pp. 29–43

Ackermann RJ, Thorn RJ (1961) Vaporization of oxides. *In:*Progress in Ceramic Science vol I, Oxford, NY, pp. 39–88

Ackermann RJ, Gilles PW, Thorn RJ (1956) High-temperature thermodynamic properties of uranium dioxide. J Chem Phys 25:1089–1097

Ackermann RJ, Thorn RJ, Alexander C, Tetenbaum M (1960) Free energies of formation of gaseous uranium, molybdenum, and tungsten trioxides. J Phys Chem 64:350–355

Ackermann RJ, Thorn RJ, Winslow GH (1961) Systematic trends in vaporization and thermodynamic properties. Planet Space Sci 3:12–23

Ackermann RJ, Rauh EG, Thorn RJ, Cannon MC (1963) A thermodynamic study of the thorium–oxygen system at high temperatures. J Phys Chem 67:762–769

Ackermann RJ, Thorn RJ, Winslow GH (1967) Some fundamental aspects of vaporization. *In:*Margrave JL (ed) The Characterization of High Temperature Vapors. John Wiley and Sons, Inc., New York, N.Y., pp 427–452

Ackermann RJ, Rauh EG, Chandrasekharaiah MS (1969) A thermodynamic study of the urania–uranium system. J Phys Chem 73:762–769

Ackermann RJ, Rauh EG, Walters RR (1970) Thermodynamic study of the system yttrium+yttrium sesquioxide. A refinement of the vapor pressure of yttrium. J Chem Thermo 2:139–149

Ackermann RJ, Rauh EG, Alexander CA (1975) The thermodynamic properties of $ZrO_{2(g)}$. High Temp Sci. 7:304–316

Alcock CB, Hooper GW (1960) Thermodynamics of the gaseous oxides of the platinum-group metals. Proc R Soc Lond A 254:551–561

Alcock CB, Peleg M (1967) Vaporization kinetics of ceramic oxides at temperatures around 2000 °C. Trans Br Ceram Soc 66:217–232

Alexander CA, Ogden JS, Levy A (1963) Transpiration study of magnesium oxide. J Chem Phys 39:3057–3060

Alekseeva ZD (1963) Equilibrium diagram of the $RbSiO_3$–SiO_2 system. Russ J Inorg Chem 8:741-744

Alekseeva ZD (1966) The Cs_2O–SiO_2 system. Russ J Inorg Chem 11:626-629

Altman RL (1963) Vaporization of magnesium oxide and its reaction with alumina. J Phys Chem 67:366–369

Amelin Y (2008) U–Pb ages of angrites. Geochim Cosmochim Acta 72:221–232

Ames LL, Walsh PN, White D (1967) Rare earths. IV. Dissociation energies of the gaseous monoxides of the rare earths. J. Phys. Chem. 71:2707-2718

Ammann M, Hauert R, Burtscher H, Siegmann HC (1993) Photoelectric charging of ultrafine volcanic aerosols: detection of Cu (I) as a tracer of chlorides in magmatic gases. J Geophys Res Solid Earth 98:551–556

Anders E (1964) Origin, age, and composition of meteorites. Space Sci Rev 3:583–714

Anthrop DF, Searcy AW (1964) Sublimation and thermodynamic properties of zinc oxide. J Phys Chem 68:2335–2342. doi: 10.1021/j100790a052

Asano M, Nakagawa H (1989) Vaporization of lithium metasilicate in a graphite Knudsen cell. J Nucl Mater 161:190–196

Asryan NA, Alikhanyan AS, Nipan GD (2003) Specifics of sublimation of antimony oxides. Dokl Phys Chem 392:221–226. doi: 10.1023/A:1025776803970

Baedecker PA, Schaudy R, Elzie JL, Kimberlin J, Wasson JT (1971) Trace element studies of rocks and soils from Oceanus Procellarum and Mare Tranquillitatis. Proc 2nd Lunar Sci Conf 1037–1061

Balducci G, Maria GD, Guido M, Piacente V (1971) Dissociation energy of FeO. J Chem Phys 55:2596–2598

Bale CW, Chartrand P, Degterov SA, Eriksson G, Hack K, Mahfoud RB, Melançon J, Pelton AD, Petersen S (2002) FactSage thermochemical software and databases. Calphad 26:189–228

Ballhaus C, Laurenz V, Münker C, Fonseca RO, Albarède F, Rohrbach A, Lagos M, Schmidt MW, Jochum KP, Stoll B, Weis U (2013) The U/Pb ratio of the Earth's mantle—A signature of late volatile addition. Earth Planet Sci Lett 362:237–245. doi: 10.1016/j.epsl.2012.11.049

Banchorndhevakul W, Matsui T, Naito K (1985) Vaporization study of V_2O_3 and two-phase mixture of V_2O_3 and VO by mass spectrometric method. Thermochim Acta 88:301–306

Banchorndhevakul W, Matsui T, Naito K (1986) Vaporization study on vanadium monoxide and two-phase mixture of vanadium and vanadium monoxide by mass-spectrometric method. J Nuc Sci Tech 23:602–611

Barrat JA, Blichert-Toft J, Gillet P, Keller F (2000) The differentiation of eucrites: The role of in situ crystallization. Meteoritics 35:1087–1100

Barshay SS (1981) Combined Condensation-Accretion Model of the Terrestrial Planets. PhD thesis, Department of Earth and Planetary Sciences, Massachusetts Institute of Technology

Bart G, Ikramuddin M, Lipschutz ME (1980) Thermal metamorphism of primitive meteorites-IX. On the mechanism of trace element loss from Allende heated up to 1400 °C. Geochim Cosmochim Acta 44:719–730. doi: 10.1016/0016-7037(80)90161-1

Beckett JR (2002) Role of basicity and tetrahedral speciation in controlling the thermodynamic properties of silicate liquids, part 1: The system $CaO–MgO–Al_2O_3–SiO_2$. Geochim Cosmochim Acta 66:93–107

Behrens RG, Mason CFV (1981) A mass spectrometric investigation of the vaporization thermodynamics and vapor composition of cadmium oxide. J Less-Common Met 77:169–184. doi: 10.1016/0022-5088(81)90168-5

Behrens RG, Rosenblatt GM (1972) Vapor pressure and thermodynamics of octahedral arsenic trioxide (arsenolite). J Chem Thermo 4:175–190

Behrens RG, Rosenblatt GM (1973) Vapor pressure and thermodynamics of orthorhombic antimony trioxide (valentinite). J Chem Thermodyn 5:173–188. doi: 10.1016/S0021-9614(73)80077-1

Belov AN, Semenov GA (1979) Mass spectrometric determination of the temperature dependence of the pressure of gaseous oxides over thorium and zirconium dioxides. Russ J Phys Chem 53:1752–1755

Belov AN, Semenov GA (1985) Thermodynamics of binary solid solutions of zirconium, hafnium, and yttrium oxides from high–temperature mass spectrometry data. Russ J Phys Chem 59:342–344

Belov AN, Semenov GA, Teterin GA, Shkol'nikova TM (1987) Evaporation and thermodynamic properties of Sc_2O_3 and of $ZrO_2–Sc_2O_3$ solid solutions according to high temperature mass spectrometry data I. Experimental. Russ J Phys Chem 61:464–468

Belov GV, Iorish VS, Yungman VS (1999) IVTANTHERMO for Windows–Database on thermodynamic properties and related software. CALPHAD 23:173–180

Belton GR, Jordan AS (1965) The volatilization of molybdenum in the presence of water vapor. J Phys Chem 69:2065–2071

Belton GR, McCarron RL (1964) The volatilization of tungsten in the presence of water vapor. J Phys Chem 68:1852–1856

Belton GR, Richardson FD (1962) A volatile iron hydroxide. Trans Faraday Soc 58:1562–1572. doi: 10.1039/tf9625801562

Benson SW (1960) The Foundations of Chemical Kinetics. 1st Edition. McGraw-Hill, New York, N.Y.

Berkowitz J, Chupka WA, Inghram MG (1957a) Thermodynamics of the V–O system: Dissociation energies of VO and VO_2. J Chem Phys 27:87–90. doi: 10.1063/1.1743723

Berkowitz J, Chupka WA, Inghram MG (1957b) Polymeric gaseous species in the sublimation of molybdenum trioxide. J Chem Phys 26:842–846. doi: 10.1063/1.1743722

Berkowitz J, Chupka WA, Inghram MG (1957c) Polymeric gaseous species in the sublimation of tungsten trioxide. J Chem Phys 27:85–86. doi: 10.1063/1.1743722

Berkowitz J, Chupka WA, Inghram MG (1957d) Thermodynamics of the $Ti–Ti_2O_3$ system and the dissociation energy of TiO and TiO_2. J Phys Chem 61:1569–1572

Berkowitz J, Chupka WA, Blue GD, Margrave JL (1959) Mass Spectrometric Study of the Sublimation of Lithium Oxide. J Phys 63:644–648. doi: 10.1021/j150575a002

Berkowitz J, Meschi DJ, Chupka WA (1960) Heterogeneous reactions studied by mass spectrometry. II. Reaction of $Li_2O_{(s)}$ with $H_2O_{(g)}$. J Chem Phys 33:533–540

Berkowitz-Mattuck JB, Büchler A (1963) A transpiration study of lithium hydroxide. J Phys Chem 67:1386–1388

Berry AJ, O'Neill HSC, Scott DR, Foran GJ, Shelley JMG (2006) The effect of composition on Cr^{2+}/Cr^{3+} in silicate melts. Am Mineral 91:1901–1908

Björkvall J, Sichen D, Seetharaman S (2000) Thermodynamic description of 'FeO'–MgO–SiO_2 and 'FeO'–MnO–SiO_2 melts—a model approach. High Temp Mat Proc 19:49–60

Bland PA, Alard O, Benedix GK, Kearsley AT, Menzies ON, Watt LE, Rogers NW (2005) Volatile fractionation in the early solar system and chondrule/matrix complementarity. PNAS 102:13755–13760

Bodsworth C (1959) The activity of ferrous oxide in silicate melts. J Iron Steel Inst 193:13-24

Bond M, Struchtrup H (2004) Mean evaporation and condensation coefficients based on energy dependent condensation probability. Phys Rev E—Stat Nonlin Soft Matter Phys 70:061605. doi: 10.1103/PhysRevE.70.061605

Borisov AA (2009) Influence of SiO_2 and Al_2O_3 on the activity coefficients of alkalis in melts: An experimental study. Petrology 17:579–590. doi: 10.1134/S0869591109060058

Boss AP (1998) Temperatures in protoplanetary disks. Ann Rev Earth Planet Sci 26:53–80

Botor JP, Edwards JG (1985) Vaporization chemistry and thermodynamics of the $MnS–In_2S_3$ system by the simultaneous Knudsen and torsion–effusion method. J Electrochem Soc 132:229–235

Bottinga Y, Richet P (1978) Thermodynamics of liquid silicates, a preliminary report. Earth Planet Sci Lett 40:382–400

Boynton WV (1975) Fractionation in the solar nebula: condensation of yttrium and the rare earth elements. Geochim Cosmochim Acta 39:569–584

Boynton WV (1978) Rare-earth elements as indicators of supernova condensation. Lunar Planet Sci Conf IX, pp 120–122

Brackett RA, Fegley B, Arvidson RE (1995) Volatile transport on Venus and implications for surface geochemistry and geology. J Geophys Res 100:1553–1563. doi: 10.1029/94JE02708

Brewer L (1953) The thermodynamic properties of the oxides and their vaporization processes. Chem Rev 52:1–75

Brewer L, Margrave J (1955) The vapor pressures of lithium and sodium oxides. J Phys Chem 59:421–425. doi: 10.1021/j150527a010

Brewer L, Mastick DF (1951) The stability of gaseous diatomic oxides. J Chem Phys 19:834–843. doi: 10.1063/1.1748392

Brewer L, Porter RF (1954) A thermodynamic and spectroscopic study of gaseous magnesium oxide. J Chem Phys 22:1867–1877

Brewer L, Rosenblatt GM (1969) Dissociation energies and free energy functions of gaseous monoxides. *In:*Eyring L (ed) Advances in High Temperature Chemistry, Elsevier BV, Amsterdam, 2:1–83

Brewer L, Searcy AW (1951) The gaseous species of the Al–Al_2O_3 system. J Am Chem Soc 73:5308–5314

Brittain RD, Lau KH, Hildenbrand DL (1982) Molecular species in the arsenic–oxygen system. J Phys Chem 86:5072–5075

Büchler A, Berkowitz-Mattuck JB (1963) Gaseous metaborates I. Mass-spectrometric study of the vaporization of lithium and sodium metaborates. J Chem Phys 39:286-291

Burnham AD, O'Neill HSC (2016) The effect of melt composition on mineral–melt partition coefficients: The case of beryllium. Chem Geol 442:139–147

Burns RP (1966) Systematics of the evaporation coefficient Al_2O_3, Ga_2O_3, In_2O_3. J Chem Phys 44:3307–3319. doi: 10.1063/1.1727229

Burns RP, DeMaria G, Drowart J, Grimley RT (1960) Mass spectrometric investigation of the sublimation of molybdenum dioxide. J Chem Phys 32:1363–1336. doi: 10.1063/1.1730922

Burns RP, DeMaria G, Drowart J, Inghram MG (1963) Mass spectrometric investigation of the vaporization of In_2O_3. J Chem Phys 38:1035–1036. doi: 10.1063/1.1733761

Byker HJ, Eliezer I, Howald RC, Ehlert TC (1979) Thermodynamic properties of potassium oxides. High Temp Sci 11:153–170

Cameron AGW (1995) The first ten million years in the solar nebula. Meteorit Planet Sci 30:133–161

Cameron AGW, Benz W (1991) The origin of the Moon and the single impact hypothesis IV. Icarus 92:204–216. doi: 10.1006/icar.1996.5642

Canup RM (2004) Simulations of a late lunar-forming impact. Icarus 168:433–456. doi: 10.1016/j.icarus.2003.09.028

Canup RM, Visscher C, Salmon J, Fegley Jr B (2015) Lunar volatile depletion due to incomplete accretion within an impact-generated disk. Nat Geosci 8:1–6. doi: 10.1038/ngeo2574

Caplan D, Cohen M (1961) The volatilization of chromium oxide. J Electrochem Soc 108:438-442

Carlson RW, Lugmair GW (1988) The age of ferroan anorthosite 60025: oldest crust on a young Moon? Earth Planet Sci Lett 90:119–130

Carmichael IS, Nicholls J, Spera FJ, Wood BJ, Nelson SA (1977) High-temperature properties of silicate liquids: applications to the equilibration and ascent of basic magma. Phil Trans R Soc Lond A 286:373–431

Carroll MR, Webster JD (1995) Solubilities of sulfur, noble gases, nitrogen, chlorine, and fluorine in magmas. Rev Mineral 30:231–279

Carter PJ, Leinhardt ZM, Elliott T, Stewart ST, Walter MJ (2018) Collisional stripping of planetary crusts. Earth Planet Sci Lett 484:276–286

Cater DE (1970) Measurement of the gross equilibrium vaporization rate (Knudsen Methods). *In:*Rapp RA (ed) Physicochemical Measurements in Metals Research. Interscience Publishers, New York, NY, pp 21–94

Chamberlain JW, Hunten DM (1989) Theory of Planetary Atmospheres, Academic Press, San Diego, CA 2nd edn

Chapman S, Cowling TG (1970) The Mathematical Theory of Non-Uniform Gases, 3rd edn. Cambridge University Press, Cambridge

Charles RJ (1967) Activities in Li_2O–, Na_2O–, and K_2O–SiO_2 solutions. J Am Ceram Soc 50:631–641

Charnoz S, Michaut C (2015) Evolution of the protolunar disk: Dynamics, cooling timescale and implantation of volatiles onto the Earth. Icarus 260:440–463. doi: 10.1016/j.icarus.2015.07.018

Chase MW (1998) NIST-JANAF Thermochemical Tables, 4th Edition. American Chemical Society, Washington, D.C

Chastel R, Bergman C, Rogez J, Mathieu JC (1987) Excess thermodynamic functions in ternary Na_2O–K_2O–SiO_2 melts by Knudsen cell mass spectrometry. Chem Geol 62:19–29. doi: 10.1016/0009-2541(87)90053-2

Chatillon C, Senillou C, Allibert M, Pattoret A (1976) High-temperature thermodynamical studies by a mass spectrometry device for measurements using multiple effusion cells. Rev Sci Inst 47:334–340

Chen C, Jahanshahi S (2010) Thermodynamics of arsenic in FeO_x–CaO–SiO_2 slags. Metall Mater Trans B 41B:1116–1174

Chervonnyi AD (2010) Composition of the gas phase over Al_2O_3 and the enthalpies of atomization of AlO, Al_2O, and Al_2O_2. Russ J Inorg Chem 55:556–559

Chervonnyi AD, Piven, VA, Kashireninov OE, Manelis GB (1977) Mass-spectrometric investigations of gas-phase equilibria over Al_2O_3 at high temperatures. High Temp Sci 9:99–108

Chipman J (1948) Metallic solutions. Activities in liquid metallic solutions. Discuss Faraday Soc 4:23–49
Chizhikov DM, Tsvetkov Y V., Kazenas EK (1971) Mass-spectrometric study of the dissociation of iron oxides. Izv Akad Nauk SSSR Met 3:55–61
Chizhikov DM, Tsvetkov YV, Kazenas EK, Tagirov VK (1972) Mass spectrometric study of the composition and vapor pressure of chromium oxide. Russ J Phys Chem 46:806–807
Chupka WA, Berkowitz J, Inghram MG (1957) Thermodynamics of the Zr–ZrO_2 system: The dissociation energies of ZrO and ZrO_2. J Chem Phys 26:1207–1210
Chupka WA, Berkowitz J, Giese CF (1959) Vaporization of beryllium oxide and its reaction with tungsten. J Chem Phys 30:827–834. doi: 10.1063/1.1730053
Churakov S, Tkachenko SI, Korzhinskii MA, Bocharnikov RE, Shmulovich KI (2000) Evolution of composition of high temperature fumarolic gasses from Kudryavy volcano, Iturup, Kuril Islands: the thermodynamic modeling. Geochemistry Int 38:436–451
Claasen A, Veenemans CF (1933) Dampfdruckbestimmungen von BaO, SrO, CaO and deren mischungen aus Verdampfungsgeschwindigkeitmessungen. Z Physik 80:342–351
Clapeyron B-PE (1834) Memoir sur la puissance motrice de la chaleur. J L'Ecole R Polytech 14:153–190
Colin R, Drowart J, Verhaegen G (1965) Mass-Spectrometric Study of the Vaporization of Tin Oxides. Dissociation energy of SnO. Trans Faraday Soc 61:364–1371
Copland EH, Jacobson NS (2010) Measuring thermodynamic properties of metals and alloys with Knudsen effusion mass spectrometry. NASA/TP-2010-216795
Cordfunke EHP, Meyer G (1962) The system iridium–oxygen I. Measurements on the volatile oxide of iridium. Rec Trav Chim Pays-Bas 81:495–504
Costa GCC, Jacobson NS, Fegley B (2017) Vaporization and thermodynamics of forsterite-rich olivine and some implications for silicate atmospheres of hot rocky exoplanets. Icarus 289:42–55. doi: 10.1016/j.icarus.2017.02.006
Cubicciotti D (1960) The equilibrium $2/3Bi_{(l)} + 1/3BiCl_{3(g)} = BiCl_{(g)}$ and the thermodynamic properties of BiCl gas. J Phys Chem 64:791–794
Cubicciotti D (1969) Some thermodynamic properties of the thallium oxides. High Temp Sci 1:11–17
Cubicciotti D (1970) The thermodynamics of vaporization of thallous oxide. High Temp Sci 2:213–220
Cubicciotti D, Keneshea FJ (1967) Thermodynamics of vaporization of thallic oxide. J Phys Chem 71:808–814
Darken LS, Gurry RW (1946) The system iron–oxygen. II. equilibrium and thermodynamics of liquid oxide and other phases. J Am Chem Soc 68:798–816
Dauphas N, Chaussidon M (2011) A perspective from extinct radionuclides on a young stellar object: The Sun and its accretion disk. Annu Rev Earth Planet Sci 39:351–386. doi: 10.1146/annurev-earth-040610-133428
Dauphas N, Poitrasson F, Burkhardt C, Kobayashi H (2015) Planetary and meteoritic Mg/Si and $\delta^{30}Si$ variations inherited from solar nebula chemistry. Earth Planet Sci Lett 427:236–248. doi: 10.1016/j.epsl.2015.07.008
Davis AM, Grossman L (1979) Condensation and fractionation of rare earths in the solar nebula. Geochim Cosmochim Acta 43:1611-1632
Davis AM, Richter FM (2014) Condensation and evaporation of solar system materials. *In:* Davis A (ed) Treatise on Geochemistry, Vol. 1, 2nd edn. Elsevier BV, Amsterdam, pp 335–360
DeMaria G, Piacente V (1969) Mass spectrometric study of rock that is like lunar surface material. Rend Sc fis mat e nat 47:525–536. doi: 10.1300/J108v05n03
DeMaria G, Burns RP, Drowart J, Inghram MG (1960) Mass spectrometric study of gaseous molybdenum, tungsten, and uranium oxides. J Chem Phys 32: 1373–1377
DeMaria G, Balducci G, Guido M, Piacente V (1971) Mass spectrometric investigation of the vaporization process of Apollo 12 lunar samples. Proc Second Lunar Sci Conf 2:1367–1380
Delsemme A-H (1960) Spectroscopie de flammes volcaniques. Bull des seances l'Academie R des Sci d'Outremer 6:507–519
Desch SJ, Taylor GJ (2013) Isotopic mixing due to the interaction between the protolunar disk and the Earth's atmosphere. 44th Lunar Planet Sci Conf:2566
Dingwell DB, O'Neill HSC, Ertel W, Spettel B (1994) The solubility and oxidation state of nickel in silicate melt at low oxygen fugacities: Results using a mechanically assisted equilibration technique. Geochim Cosmochim Acta 58:1967–1974
Distin PA, Whiteway SG, Masson CR (1971) Thermodynamics and constitution of ferrous silicate melts. Can Met Q 10:73–78
Dixon JE, Stolper EM, Holloway JR (1995) An experimental study of water and carbon dioxide solubilities in mid-ocean ridge basaltic liquids. Part I: Calibrations and solubility models. J Petrol 36:1607–1631. doi: 10.1093/oxfordjournals.petrology.a037268
Dohmen R, Chakraborty S, Palme H, Rammensee W (1998) Solid-solid reactions mediated by a gas phase: An experimental study of reaction progress and the role of surfaces in the system olivine + iron metal. Am Mineral 83:970–984
Donaldson CH (1979) Composition changes in a basalt melt contained in a wire loop of $Pt_{80}Rh_{20}$: effects of temperature, time, and oxygen fugacity. Mineral Mag 43:115–119

Doyle CD (1988) Prediction of the activity of FeO in multicomponent magma from known values in [SiO_2–$KAlO_2$–$CaAl_2Si_2O_8$]–FeO liquids. Geochim Cosmochim Acta 52:1827–1834
Dreibus G, Wanke H (1985) Mars, a volatile-rich planet. Meteoritics 20:367–381
Dreibus G, Wänke H (1979) On the chemical composition of the Moon and the eucrite parent body and a comparison with the composition of the Earth; the Case of Mn, Cr, and V. Lunar Planet Sci Conf 10:315–317
Dreibus G, Wänke H (1980) The bulk composition of the eucrite parent asteroid and its bearing on planetary evolution. Zeit für Naturforsch–Sect A J Phys Sci 35:204–216. doi: 10.1515/zna-1980-0206
Dreibus G, Wänke H (2001) Comment on: "Comparative geochemistry of basalts from the Moon, Earth, HED asteroid, and Mars: Implication for the origin of the Moon" by A. Ruzicka G.A. Snyder, L.A. Taylor (2001) Geochim Cosmochim Acta 65, 979–997. Geochim Cosmochim Acta 66:2631–2632
Drowart J, De Maria G, Inghram MG (1960) Thermodynamic study of Al_2O_3 using a mass spectrometer. J Chem Phys 32:1366–1372. doi: 10.1063/1.1744646
Drowart J, Colin R, Exsteen G (1965a) Mass-spectrometric study of vaporization of lead monoxide. Trans Faraday Soc 61:1376–1383. doi: Doi 10.1039/Tf9656101376
Drowart J, Degreve F, Verhaegen G, Colin R (1965b) Thermochemical study of the germanium oxides using a mass spectrometer. Trans Faraday Soc 61:1072–1085
Drowart J, Goldfinger P (1967) Investigation of inorganic systems at high temperature by mass spectrometry. Angew Chemie Int Ed 6:581–648
Drowart J, Coppens P, Smoes S (1969) Dissociation energy of the molecule $TiO_{(g)}$ and the thermodynamics of the system titanium–oxygen. J Chem Phys 50:1046-1048
Dulick M, Murad E, Barrow RF (1986) Thermochemical properties of the rare earth monoxides. J Chem Phys 85:385–390
Ebel DS (2004) Condensation of rocky material in astrophysical environments. *In:*Lauretta DS, Mcsween HY (eds) Meteorites and the Early Solar System II. University of Arizona Press, Tucson, pp 253–277
Edmunson J, Borg LE, Nyquist LE, Asmerom Y (2009) A combined Sm–Nd , Rb–Sr , and U–Pb isotopic study of Mg-suite norite 78238 : Further evidence for early differentiation of the Moon. Geochim Cosmochim Acta 73:514–527. doi: 10.1016/j.gca.2008.10.021
Edwards JG (1981) Automatic data acquisition by the torsion effusion method. *In:*Hastie JW (ed.) NBS Special Publication 561: Characterization of high temperature vapors and gases. National Bureau of Standards, Washington DC, pp. 67–82
Edwards JG, Ferro D, Weber JR (1989) The incongruent effusion of $ZnGa_8S_{13(s)}$. J Less Comm Met, 156:369–385
Ehlert TC (1977) Mass spectrometric investigations of the oxides of potassium. High Temp Sci 9:237–241
Eliezer I, Eliezer N, Howald RA, Verwolf MC (1978b) Calculation of activities in the $KO_{0.5}$–$AlO_{1.5}$–SiO_2 system. J Phys Chem 82:2688-2693
Eliezer N, Howald RA, Marinkovic M, Eliezer I (1978a) Vapor pressure measurements, thermodynamic parameters, and phase diagram for the system potassium oxide–silicon oxide at high temperatures. J Phys Chem 82:1021–1026
Ertel-Ingrisch W, Dingwell DB (2010) The Volatility and condensation behavior of elements in dependence of T and fO_2: a novel experimental approach. EGU Gen Assem Conf Abstr 12:11289
Ertel-Ingrisch W, Wombacher F, Dingwell DB, Kremser V, Seitz HM, Wennrich V, Heuser (2012) Experimental constraints on volatile element evaporation into air and CO–CO_2. Euro Mineral Conf 1:2012-610-1
Ewing MB, Lilley TH, Olofsson GM, Ratzsch MT, Somsen (1994) Standard quantities in chemical thermodynamics. Fugacities, activities and equilibrium constants for pure and mixed phases (IUPAC Recommendations 1994). Pure Appl Chem 66:533–552
Farber M, Srivastava RD (1976a) The dissociation energies of calcium oxide and strontium oxide. High Temp Sci 8:73–80
Farber M, Srivastava RD (1976b) The dissociation energy of magnesium oxide. High Temp Sci 8:195–201
Farber M, Srivastava RD, Uy OM (1972a) Mass spectrometric determination of the thermodynamic properties of the vapor species from alumina. J Chem Soc Faraday Trans 1 Phys Chem Condens Phases 68:249–258
Farber M, Uy OM, Srivastava RD (1972b) Effusion mass spectrometric determination of the heats of formation of the gaseous molecules V_4O_{10}, V_4O_8, VO_2, and VO. J Chem Phys 56:5312–5315. doi: 10.1063/1.1677037
Faktor MM, Carasso JI (1965) Tetragonal germanium dioxide and equilibria in the Ge–O–H system. J Electrochem Soc 112:817–822
Fedkin AV, Grossman L, Ghiorso MS (2006) Vapor pressures and evaporation coefficients for melts of ferromagnesian chondrule-like compositions. Geochim Cosmochim Acta 70:206–223. doi: 10.1016/j.gca.2005.08.014
Fegley B (1991) Thermodynamic models of the chemistry of lunar volcanic gases. Geophys Res Lett 18:2073–2076
Fegley B, Cameron AGW (1987) A vaporization model for iron/silicate fractionation in the Mercury protoplanet. Earth Planet Sci Lett 82:207–222. doi: 10.1016/0012-821X(87)90196-8
Fegley B, Lodders K (2017) Chemical Constraints on Formation of the Moon. 80th Ann Meeting Meteoritical Soc:6227
Fegley B, Palme H (1985) Evidence for oxidizing conditions in the solar nebula from Mo and W depletions in refractory inclusions in carbonaceous chondrites. Earth Planet Sci Lett 72:311–326. doi: 10.1016/0012-821X(85)90055-X
Fegley B, Schaefer L (2014) Chemistry of Earth's earliest atmosphere. *In:*Carlson RW (ed) Treatise on Geochemistry, vol. 2, 2nd edn. Elsevier, Amsterdam, pp 71–90

Fegley B, Zolotov MY (2000) Chemistry of sodium, potassium, and chlorine in volcanic gases on Io. Icarus 148:193–210. doi: 10.1006/icar.2000.6490

Fegley Jr B, Jacobson NS, Williams KB, Plane JM, Schaefer L, Lodders K (2016) Solubility of rock in steam atmospheres of planets. Astrophys J 824:103

Fincham CJB, Richardson FD (1954) The behavior of sulfur in silicate and aluminate melts. Proc R Soc Lond A 223:40–62

Floss C, El Goresy A, Zinner E, Kransel G, Rammensee W, Palme H (1996) Elemental and isotopic fractionations produced through evaporation of the Allende CV chondrite: Implications for the origin of HAL-type hibonite inclusions. Geochim Cosmochim Acta 60:1975–1997

Frantseva KE, Semenov GA (1969) Mass spectrometer study of the evaporation of certain vanadium oxides. Teplofiz Vys Temp 7:55–61

Fraser DG, Rammensee W (1987) Determination of the mixing properties of granitic and other alumino silicate melts by Knudsen cell mass spectrometry. *In:* Mysen BO (ed) Magmatic Processes: Physicochemical Principles, The Geochemical Society, Washington DC, pp 401–410

Fraser DG, Rammensee W, Jones RH (1983) The mixing properties of melts in the system $NaAlSi_2O_6$–$KAlSi_2O_6$ determined by Knudsen Cell mass spectrometry. Bull Miner 106:111–117

Fraser DG, Rammensee W, Hardwick A (1985) Determination of the mixing properties of molten silicates by Knudsen cell mass spectrometry-II. The systems $(NaK)AlSi_4O_{10}$, and $(Na–K)AlSi_5O_{12}$. Geochim Cosmochim Acta 49:349–359. doi: 10.1016/0016-7037(85)90028-6

Freeman RD (1967) Momentum sensors *In:* Margrave JL (ed) Characterization of High-Temperature Vapors, John Wiley and Sons, New York, Ch. 7

Friend P, Hezel DC, Palme H, Bischoff A, Gellissen M (2017) Complementary element relationships between chondrules and matrix in Rumuruti chondrites. Earth Planet Sci Lett 480:87–96

Frohberg M, Caune E, Kapoor ML (1973) Measurement of the activity of the oxygen ions in the liquid systems Na_2O–SiO_2 and K_2O–SiO_2. Arch Eisenhüttenwes 44:585–588

Frosch CJ, Thurmond CD (1962) The pressure of Ga_2O over Gallium–Ga_2O_3 mixtures. J Phys Chem 66:877–878

Gammie CF, Liao WT, Ricker PM (2016) A hot big bang theory: magnetic fields and the early evolution of the protolunar disk. Astrophys J 828:58

Genda H, Abe Y (2003) Modification of a proto-lunar disk by hydrodynamic escape of silicate vapor. Earth Planets Sp 53:53–57

Genda H, Abe Y (2005) Enhanced atmospheric loss on protoplanets at the giant impact phase in the presence of oceans. Nature 433:842–844

Geßmann CK, Rubie DC (1998) The effect of temperature on the partitioning of nickel, cobalt, manganese, chromium, and vanadium at 9 GPa and constraints on formation of the Earth's core. Geochim Cosmochim Acta 62:867–882

Ghiorso MS, Sack RO (1995) Chemical mass transfer in magmatic processes IV. A revised and internally consistent thermodynamic model for the interpolation and extrapolation of liquid-solid equilibria in magmatic systems at elevated temperatures and pressures. Contrib to Mineral Petrol 119:197–212. doi: 10.1007/BF00307281

Gibson EK, Hubbard NJ (1972) Thermal volatilization studies on lunar samples. Proc Third Lunar Sci Conf 2:2003–2014

Gilbert IGF, Kitchener JA (1956) The dissociation pressure of cadmium oxide. Trans Faraday Soc 52:3919–3921

Gilles PW, Franzen HF, Stone GD, Wahlbeck PG (1968) High temperature vaporization and thermodynamics of the titanium oxides. III Vaporization characteristics of the liquid phase. J Chem Phys 48:1938–1941

Glibin VP, King PL (2015) Prediction of the thermodynamic functions of mixing of binary oxide melts in the PbO–SiO_2, Al_2O_3–SiO_2 and CaO–Al_2O_3 systems by structure-based modification of the quasi-chemical model. Calphad 49:19–34

Glushko VP, Gurvich LV, Bergman GA, Veitz IV, Medvedev VA, Khachcurvzov GA, Yungman VS (1982) Thermodynamic properties of individual substances. Part IV, High Temperature Institute, Moscow

Glushko VP, Medvedev VA, Gurvich LV, Yungman VS (1999) Thermal Constants of Substances, 1st edn. John Wiley and Sons, New York

Goldstein HW, Walsh PN, White D (1961) Rare earths I. Vaporization of La_2O_3 and Nd_2O_3. Dissociation energies of gaseous LaO and NdO. J Phys Chem 65:1400–1404

Gomez M, Chatillon C, Allibert M (1982) Thermodynamics of gaseous and condensed indium oxides by mass spectrometry with controlled oxygen pressure. J Chem Thermo 14:447–459

Gooding JL, Muenow DW (1976) Activated release of alkalis during the vesiculation of molten basalts under high vacuum: implications for lunar volcanism. Geochim Cosmochim Acta 40:675–686. doi: 10.1016/0016-7037(76)90113-7

Govorchin SW (1986) Simultaneous Knudsen- and Torsion–Effusion Measurements of the Vapor Pressures of Triphenyl Aluminum and Triphenyl Boron. Masters Thesis, Dept. Chemistry, Western Michigan University

Green DH, Ringwood AE, Ware NG, Hibberson WO, Major A, Kiss E (1971) Experimental petrology and petrogenesis of Apollo 12 basalts. Proc 2nd Lunar Sci Conf:601–615

Grimley RT, Burns RP, Inghram MG (1960) Mass-spectrometric study of the osmium–oxygen system. J Chem Phys 33:308–309

Grimley RT, Burns RP, Inghram MG (1961a) Thermodynamics of the vaporization of Cr_2O_3: Dissociation energies of CrO, CrO_2, and CrO_3. J Chem Phys 34:664–667. doi: 10.1063/1.1701005

Grimley RT, Burns RP, Inghram MG (1961b) Thermodynamics of the vaporization of nickel oxide. J Chem Phys 35:551–554

Grimley RT, Burns RP, Inghram MG (1966) Mass-spectrometric study of the vaporization of cobalt oxide. J Chem Phys 45:4158–4162. doi: 10.1063/1.1727472

Grossman L (1972) Condensation in the primitive solar nebula. Geochim Cosmochim Acta, 36:597-619

Grossman L (1973) Refractory trace elements in Ca–Al-rich inclusions in the Allende meteorite. Geochim Cosmochim Acta 37:1119-1140

Grossman L, Larimer JW (1974) Early chemical history of the solar system. Rev Geophys 12:71–101. doi: 10.1029/RG012i001p00071

Grossman L, Beckett JR, Fedkin AV, Simon SB, Ciesla FJ (2008) Redox conditions in the solar nebula: observational, experimental, and theoretical constraints. Rev Mineral Geochem 68:93–140. doi: 10.2138/rmg.2008.68.7

Guillot B, Sator N (2007) A computer simulation study of natural silicate melts. Part I: Low pressure properties. Geochim Cosmochim Acta 71:1249–1265

Hampson PJ, Gilles PW (1971) High-temperature vaporization and thermodynamics of the titanium oxides. VII. Mass spectrometry and dissociation energies of $TiO_{(g)}$ and $TiO_{2(g)}$. J Chem Phys 55:3712–3729

Hans U, Kleine T, Bourdon B (2013) Rb–Sr chronology of volatile depletion in differentiated protoplanets: BABI, ADOR and ALL revisited. Earth Planet Sci Lett 374:204–214. doi: 10.1016/j.epsl.2013.05.029

Hashimoto A (1983) Evaporation metamorphism in the early solar nebula—evaporation experiments on the melt FeO–MgO–SiO_2–CaO–Al_2O_3 and chemical fractionations of primitive materials. Geochem J 17:111–145

Hashimoto A (1990) Evaporation kinetics of forsterite and implications for the early solar nebula. Nature 347:53–55

Hashimoto A (1992) The effect of H_2O gas on volatilities of planet-forming major elements: I. Experimental determination of thermodynamic properties of Ca-, Al-, and Si-hydroxide gas molecules and its application to the solar nebula. Geochim Cosmochim Acta 56:511–532

Hashizume A, Wasada N, Tsuchiya T (1966) A mass spectrometric study of phosphorus oxide. Bull Chem Soc Jpn 39:150–155

Hashizume K, Wang W-E, Olander DR (1999) Volatilization of urania in steam at elevated temperatures. J Nucl Mater 275:277–286

Hastie JW (1975) High Temperature Vapors. Academic Press, Cambridge, MA

Hastie JW (1981) NBS Special Publication 561: Characterization of High Temperature Vapors and Gases. National Bureau of Standards, Washington DC

Hastie JW, Bonnell DW (1985) A predictive phase equilibrium model for multicomponent oxide mixtures part II. Oxides of Na–K–Ca–Mg–Al–Si. High Temp Sci 19:275–306

Hastie JW, Plante ER, Bonnell DW (1982) Alkali vapor transport in coal conversion and combustion systems. *In:* J Gole and WC Stwalley (eds) Metal Bonding and Interactions in High Temperature Systems ACS Symposium Series, American Chemical Society, Washington DC, pp. 543–600

Hastie JW, Bonnell DW, Schenck PK (2000) Development and application of very high temperature mass spectrometry. Vapor pressure determinations over liquid refractories.Pure Appl Chem 72:2111–2126

Hauri EH, Saal AE, Rutherford MJ, Van Orman JA (2015) Water in the moon's interior: Truth and consequences. Earth Planet Sci Lett 409:252–264. doi: 10.1016/j.epsl.2014.10.053

Henley RW, Seward TM (2018) Gas–solid reactions in arc volcanoes: Ancient and modern. Rev Mineral Geochem 84:309–349

Hertz H (1882) Ueber die Verdunstung der Flüssigkeiten, insbesondere des Quecksilbers, im luftleeren Raume. Annalen der Physik 253:177-193.

Hezel DC, Palme H (2010) The chemical relationship between chondrules and matrix and the chondrule matrix complementarity. Earth Planet Sci Lett 294:85–93

Heyrman M, Chatillon C, Pisch A (2004) Congruent vaporization properties as a tool for critical assessment of thermodynamic data The case of gaseous molecules in the La–O and Y–O systems. CALPHAD 28:49-63

Hildenbrand DL (1975) Thermochemistry of molecular FeO, FeO^+ and FeO_2. Chem Phys Lett 34:352–354

Hildenbrand DL, Lau KH (1993) Mass spectrum and sublimation pressure of sodium oxide vapor: Stability of the superoxide molecule NaO_2. J Chem Phys 98:4076-4081. doi: 10.1063/1.465043

Hildenbrand DL, Lau KH (1994) Thermochemistry of gaseous manganese oxides and hydroxides. J Chem Phys 100:8377–8380

Hildenbrand DL, Murad E (1970) Dissociation energy of $NaO_{(g)}$ and the heat of atomization of $Na_2O_{(g)}$. J Chem Phys 53:3403–3408. doi: 10.1063/1.1674508

Hildenbrand DL, Murad E (1974) Mass spectrometric studies of gaseous ThO and ThO_2. J Chem Phys 61:1232–1237

Hildenbrand DL, Hall WF, Potter ND (1963) Thermodynamics of vaporization of lithium oxide, boric oxide, and lithium metaborate. J Chem Phys 39:296–301

Hilpert K, Gerads H (1975) Mass spectrometric investigation of the vaporization of BaO from Knudsen cells made of Mo, Pt, graphite, and Al_2O_3. High Temp Sci 7:11–19

Hin RC, Coath CD, Carter PJ, Nimmo F, Lai YJ, von Strandmann PA, Willbold M, Leinhardt ZM, Walter MJ, Elliott T (2017) Magnesium isotope evidence that accretional vapor loss shapes planetary compositions. Nature 549:511–515. doi: 10.1038/nature23899

Hincke WB (1930) The vapor pressure of antimony trioxide. J Am Chem Soc 52:3869–3877

Hirschmann MM, Ghiorso MS (1994) Activities of nickel, cobalt, and manganese silicates in magmatic liquids and applications to olivine/liquid and to silicate/metal partitioning Geochim Cosmochim Acta, 58:4109–4126

Hirth JP, Pound GM (1963) Condensation and evaporation—nucleation and growth kinetics. Pergamon Press, Oxford

Ho PH, Burns RP (1980) A mass spectrometric study of the AlO_2 molecule. High Temp Sci 12:31–39

Hoenig CL (1964) Vapor pressure and evaporation coefficient studies of stannic oxide, zinc oxide, and beryllium nitride. PhD thesis. University of California, Lawrence Radiation Laboratory, Livermore CA

Hoenig CL, Searcy AW (1966) Knudsen and Lanmguir evaporation studies of stannic oxide. J Am Ceram Soc 49:128–134. doi: 10.1300/J108v05n03

Holstein WL (1993a) Thermodynamics of the volatilization of Tl_2O from Tl_2O, Tl_4O_3, and Tl_2O_3. J Phys Chem 97:4224–4230

Holstein WL (1993b) Thermodynamic properties of thallium (I) hydroxide in the vapor state. J Chem Thermo 25:1287–1294

Holzheid A, Lodders K (2001) Solubility of copper in silicate melts as function of oxygen and sulfur fugacities, temperature, and silicate composition. Geochim Cosmochim Acta 65:1933–1951. doi: 10.1016/S0016-7037(01)00545-2

Holzheid A, Palme H, Chakraborty S (1997) The activities of NiO, CoO and FeO in silicate melts. Chem Geol 139:21–38

Horstmann A (1873) Theorie der Dissociation. Ann Chem Pharm 170:192-210; also see the English translation in Bull Hist Chem 34:73–82

Huebner JS (1987) Use of gas mixtures at low pressure to specify oxygen and other fugacities of furnace atmospheres. *In:* Ulmer GC, Barnes HL (eds) Hydrothermal Experimental Techniques. Wiley, New York, pp 20–60

Humayun M, Cassen P (2000) Processes determining the volatile abundances of the meteorites and terrestrial planets. *In:* Canup RM, Righter K (eds) The Origin of the Earth and Moon. University of Arizona Press, Tucson, pp 3–23

Humayun M, Crowther SA (2015) Elemental Volatility during Vacuum Melting of Martian Meteorite NWA 8114. *In:* 78th AnnMeeting Meteoritical Soc:5313

Humayun M, Koeberl C (2004) Potassium isotopic composition of Australasian tektites. Meteorit Planet Sci 39:1509–1516. doi: 10.1111/j.1945-5100.2004.tb00125.x

Hunten DM, Donahue TM (1976) Hydrogen loss from the terrestrial planets. Annu Rev Earth Planet Sci 4:256–292

Ikramuddin M, Binz CM, Lipschutz ME (1976) Thermal metamorphism of primitive meteorites-II. Ten trace elements in Abee enstatite chondrite heated at 400–1000 °C. Geochim Cosmochim Acta 40:133–142. doi: 10.1016/0016-7037(76)90170-8

Inghram MG, Chupka WA, Porter RF (1955) Mass spectrometric study of barium oxide vapor. J Chem Phys 23:2159–2165. doi: 10.1063/1.1740686

Inghram NG, Porter RF, Chupka WA (1956) Mass spectrometric study of gaseous species in the B–B_2O_3 system. J Chem Phys 25:498-501

Inghram MG, Chupka WA, Berkowitz J (1957) Thermodynamics of the Ta–O system: The dissociation energies of TaO and TaO_2. J Chem Phys 27:569–571

Ireland TR, Fegley B (2000) The solar system's earliest chemistry: systematics of refractory inclusions. Int Geol Rev 42:865–894

Jacobson NS, Myers DL (2011) High-temperature vaporization of $B_2O_{3(l)}$ under reducing conditions. J Phys Chem B 115:13253–13260

Jacobson NS, Opila EJ, Myers DL, Copland EH (2005) Thermodynamics of gas phase species in the Si–O–H system. J Chem Thermodyn 37:1130–1137. doi: 10.1016/j.jct.2005.02.001

Jacobson SA, Morbidelli A (2014) Lunar and terrestrial planet formation in the Grand Tack scenario. Phil Trans R Soc A 372:20130174

Jeans JH (1916) The Dynamical Theory of Gases. Cambridge University Press, Cambridge

Jochum K-P, Palme H (1990) Alkali elements in eucrites and SNC-meteorites: no evidence for volatility-related losses during magma eruption or thermal metamorphism. Meteoritics 25:373

Jolly WL, Latimer WM (1952) The equilibrium $Ge_{(s)} + GeO_{2(s)} = 2GeO_{(g)}$. The heat of formation of germanic oxide. J Am Chem Soc 74:5757-5758

Jones JH, Palme H (2000) Geochemical constraints on the origin of the Earth and Moon. *In:* Canup RM, Righter K (eds) The Origin of the Earth and Moon. University of Arizona Press, Tucson, pp 197–216

Joseph M, Sivakumar N, Darwin D, Raj A, Matthews CK (1996) Development of laser-induced vaporization mass spectrometry to study refractory materials. Rapid Comm Mass Spec 10:5–11

Joseph M, Sivakumar N, Manoravi P (2002) Laser-induced-vaporization mass spectrometry studies on UO_2, UC, and ThO_2. High Temp High Press 34:411–424

Kamegashira N, Matsui T, Harada M, Naito K (1981) Vaporization of niobium dioxide by mass—effusion and mass—spectrometric methods. J Nucl Mater 101:207–216

Kassis N, Frischat GH (1981) Dampfdrucke von Glasschmelzen des Mischalkalisystems Na_2O–Rb_2O–SiO_2. Glastech Ber 54:89–98
Kay DAR, Taylor J (1960) Activities of silica in the lime+alumina+silica system. Trans Faraday Soc 56:1372–1386
Kazenas EK, Petrov AA (1996) Thermodynamics of processes of vaporization, dissociation, and gas-phase reactions in vapors over PbO system. Russ Metall 22–27
Kazenas EK, Petrov AA (1997) Thermodynamics of processes of phosphorus oxides and arsenic. Russ Metall 29–34
Kazenas EK, Tagirov VK (1995) Thermodynamics of vaporization of the oxides FeO, CoO, and NiO. Metally 31–37
Kazenas EK, Chizhikov DM, Tsvetkov YV (1969) The dissociation pressures of copper oxides. Russ Metall 46–48
Kazenas EK, Chizhikov DM, Tsvetkov YV, Vasyuta YuV (1973) Mass spectrometric study of the sublimation of germanium dioxide. Russ J Phys Chem 47:389–390
Kazenas EK, Samoilova IO, Zviadadze GN (1983) Thermodynamics of the Dissociation and Sublimation of Magnesium Oxide. Russ J Inorg Chem 57:1571–1572
Kazenas EK, Zviadadze GN, Bol'shikh MA (1984a) Mass spectrometric study of the dissociation and vaporization thermodynamics of cadmium and zinc oxides. Russ Metall 67–70
Kazenas EK, Tagirov VK, Zviadadze GN (1984b) Mass spectroscopic investigation of the dissociation and sublimation of manganese oxide. Russ Metall 58–59
Kazenas EK, Zviadadze GN, Bol'shikh MA (1985) Thermodynamics of sublimation, dissociation and gas-phase reactions of vapors over silicon dioxide. Metally 46–48
Kazenas EK, Petrov AA, Samoilova IO (1994) Evaporation of Ta_2O_5. Russ Metall 16–19
Kazenas EK, Bol'shikh MA, Petrov AA (1996) Thermodynamics of evaporation, dissociation and gas phase reactions in vapor over the tin–oxygen system. Metally 36–42
Kim Y-W, Belton GR (1974) The thermodynamics of volatilization of chromic oxide: Part I. The species CrO_3 and CrO_2OH. Metall Trans 5:1811–1816
Kim SS, Sanders TH Jr. (1991) Thermodynamic modeling of phase diagrams in binary alkali silicate systems. J Am Ceram Soc 74:1833–1840
Kimura H, Asano M, Kubo K (1980) Thermochemical study of the vaporization of $Li_2O_{(c)}$ by mass spectrometric Knudsen effusion method. J Nucl Mater 92:221–228. doi: 10.1016/0022-3115(80)90106-3
Kiseeva ES, Wood BJ (2015) The effects of composition and temperature on chalcophile and lithophile element partitioning into magmatic sulfides. Earth Planet Sci Lett 424:280–294. doi: 10.1016/j.epsl.2015.05.012
Kitchener JA, Ignatowicz S (1951) The reduction equilibria of zinc oxide and zinc silicate with hydrogen. Trans Faraday Soc 47:1278–1286
Kite ES, Fegley B Jr., Schaefer L, Gaidos E (2016) Atmosphere–interior exchange on hot, rocky exoplanets. Astrophys J 828:80
Kleine T, Touboul M, Bourdon B, Nimmo F, Mezger K, Palme H, Jacobsen SB, Yin QZ, Halliday AN (2009) Hf–W chronology of the accretion and early evolution of asteroids and terrestrial planets. Geochim Cosmochim Acta 73:5150–5188. doi: 10.1016/j.gca.2008.11.047
Knudsen M (1909) Die Gesetze der Molekularströmung und der inneren Reibungsströmung der Gase durch Röhren. Ann Phys 333:75–130
Kobertz D, Müller M, Molak A (2014) Vaporization and caloric studies on lead titanate. Calphad 46:62–79
Kodera K, Kusunoki I, Shimizu S (1968) Dissociation Pressures of Various Metallic Oxides. Bull Chem Soc Jpn 41:1039–1045
Koeberl C (1986) Geochemistry and tektites and impact glasses. Ann Rev Earth Planet Sci 14:323–350. doi: doi:10.1146/annurev.ea.14.050186.001543
Kofstad P (1964) Low-pressure oxidation of tantalum at 1300–1800 °C. J Less Common Met 7:241–266
Kohn SC, Schofield PF (1994) The importance of melt composition in controlling trace-element behavior: an experimental study of Mn and Zn partitioning between forsterite and silicate melts. Chem Geol 117:73–87
Kornacki AS, Fegley B (1986) The abundance and relative volatility of refractory trace elements in Allende Ca , Al-rich inclusions : implications for chemical and physical processes in the solar nebula. Earth Planet Sci Lett 19:217–234
Kracek FC (1930) The cristobalite liquidus in the alkali oxide–silica systems and the heat of fusion of cristobalite. J Am Chem Soc 52, 1436–1442
Krawczynski MJ, Sutton SR, Grove TL, Newville M (2009) Titanium oxidation state and coordination in the lunar high-titanium glass source mantle. Lunar Planet Sci Conf 40th:2164
Kreutzberger ME, Drake MJ, Jones JH (1986) Origin of the Earth's Moon: Constraints from alkali volatile trace elements. Geochim Cosmochim Acta 50:91–98
Krikorian OH, Carpenter JH (1965) Enthalpies of formation of gaseous tantalum oxide and tantalum dioxide. J Phys Chem 69:4399–4401
Kröger FA (1964) The Chemistry of Imperfect Crystals. North-Holland, Amsterdam
Kröger C, Sörström L (1965) Dampfdruck von Silicatgläsern und deren Bestandteilen. Glastech Berichte 38:313–322
Krönert W, Boehm A (1972) Messungen des Dampfdruckes bei freier Verdampfung an Aluminiumoxid un Magnesiumoxid. Glas-Email-Keramo-Technik 23:319–323
Kubaschewski O, Alcock CB (1979) Metallurgical Thermochemistry, 5th edn. Pergamon Press, Oxford

Kudo H, Wu CH, Ihle HR (1978) Mass-spectrometric study of the vaporization of $Li_2O_{(s)}$ and thermochemistry of gaseous LiO, Li_2O, Li_3O, and Li_2O_2. J Nucl Mater. 78:380–389
Kushiro I (1975) On the nature of silicate melt and its significance in magma genesis; regularities in the shift of the liquidus boundaries involving olivine, pyroxene, and silica minerals. Am J Sci 275:411–431
L'vov B (2007) Thermal Decomposition of Solids and Melts, 1st edn. Springer Netherlands
Lamoreaux RH, Hildenbrand DL (1984) High temperature vaporization behavior of oxides. I. Alkali metal binary oxides. J Phys Chem Ref Data 13:151–173
Lamoreaux RH, Hildenbrand DL, Brewer L (1987) High-temperature vaporization behavior of oxides II. Oxides of Be, Mg, Ca, Sr, Ba, B, Al, Ga, In, Tl, Si, Ge, Sn, Pb, Zn, Cd, and Hg. J Phys Chem Ref Data 16:419–443. doi: 10.1063/1.555799
Lange RA, Navrotsky A (1992) Heat capacities of Fe_2O_3-bearing silicate liquids. Contrib Min Pet 110:311–320
Lange RA, Navrotsky A (1993) Heat capacities of TiO_2-bearing silicate liquids: Evidence for anomalous changes in configurational entropy with temperature. Geochim Cosmochim Acta 57:3001–3011
Langhoff SR, Bauschlicher Jr CW (1988) Ab initio studies of transition metal systems. Ann Rev Phys Chem, 39:181–212
Langmuir I (1916) The evaporation, condensation and reflection of molecules and the mechanism of adsorption. Phys Rev, 8:149–176
Langmuir (1932) Vapor pressures, evaporation, condensation and adsorption. J Am Chem Soc 54:2798–2832
Larimer JW (1967) Chemical fractionations in meteorites-I. Condensation of the elements. Geochim Cosmochim Acta 31:1215–1238
Larimer JW, Bartholomay M (1979) The role of carbon and oxygen in cosmic gases: some applications to the chemistry and mineralogy of enstatite chondrites. Geochim Cosmochim Acta 43:1455–1466
Lellouch E, Paubert G, Moses JI, Schneider NM, Strobel DF. (2003) Volcanically emitted sodium chloride as a source for Io's neutral clouds and plasma torus. Nature 421:45–47. doi: 10.1038/nature01292
Levelt Sengers JMH, Klein M, Gallaher JS (1972) Pressure–volume–temperature relationships of gases; virial coefficients. *In:* American Institute of Physics Handbook, 3rd edn. McGraw-Hill, New York, pp 204–221
Lewis GN (1906) Equilibrium in the deacon process. J Am Chem Soc 28:1380–1395. doi: 10.1021/ja01976a008
Littlewood R, Rideal E (1956) On the evaporation coefficient. Trans Faraday Soc 52:1598–1608. doi: 10.1039/tf9565201598
Lock SJ, Stewart ST (2017) The structure of terrestrial bodies: Impact heating, corotation limits, and synestias. J Geophys Res Planets 122:950–982. doi: 10.1002/2016JE005239
Lock SJ, Stewart ST, Petaev MI, Leinhardt Z, Mace MT, Jacobsen SB, Cúk M (2018) The origin of the Moon within a terrestrial synestia. J Geophys Res Planets 123:910-951
Lodders K (1994) Retention of alkali elements during planetary accretion and differentiation. Meteoritics 29:492–493
Lodders K (2003) Solar system abundances and condensation temperatures of the elements. Astrophys J 591:1220–1247
Lodders K (2008) The solar argon abundance. Astrophys J 674:607-611
Lodders K, Fegley B (1998) The Planetary Scientist's Companion. Oxford University Press, Oxford
Lodders K, Fegley B (1999) Condensation Chemistry of Circumstellar Grains in Asymptotic Giant Branch Stars, eds. T. Le Bertre, A. Lèbre and C. Waelkens IAU Symposium No. 191, Astronomical Society of the Pacific, San Francisco, CA, pp. 279–291
Loeb LB (1961) The Kinetic Theory of Gases. 3rd edn. Dover, NY, pp 301–388
Lopatin SI, Shugurov SM (2014) Thermodynamic properties of the Lu_2O_3–ZrO_2 solid solutions by Knudsen effusion mass spectrometry at high temperature. J Chem Thermo 72:85–88
Mack E, Osterhof GG, Kraner HM (1923) Vapor pressure of copper oxide and of copper. J Am Chem Soc 45, 617–623
Macris CA, Badro J, Eiler J, Stolper EM (2016) High temperature, controlled-atmosphere aerodynamic levitation experiments with applications in planetary science. AGU Fall Meet Abs P22A07
Mann U, Frost DJ, Rubie DC (2009) Evidence for high-pressure core–mantle differentiation from the metal–silicate partitioning of lithophile and weakly-siderophile elements. Geochim Cosmochim Acta 73:7360–7386. doi: 10.1016/j.gca.2009.08.006
Margrave JL (1967) The Characterization of High Temperature Vapors. John Wiley and Sons, New York
Markova OM, Yakovlev OI, Semenov GA, Belov AN (1986) Evaporation of natural melts in a Knudsen chamber. Geokhimiya 11:1559–1568
Marushkin KN, Kalinin VB, Alikhanyan AS (2000) Mass spectrometric study of vapor composition over the Ce–O system. Inorg Mater 36:793–798
Mason B, Taylor SR (1982) Inclusions in the Allende Meteorite. Smithsonian Contribution to the Earth Sciences No. 25, 33 pp. Smithsonian Institution Press, Washington DC
Masuda A, Tanaka T (1979) Experimental studies on behaviors of major and minor lithophile elements in vaporization under evacuated condition. Meteoritics 14:13-28
Mather TA, Witt ML, Pyle DM, Quayle BM, Aiuppa A, Bagnato E, Martin RS, Sims KW, Edmonds M, Sutton AJ, Ilyinskaya E (2012) Halogens and trace metal emissions from the ongoing 2008 summit eruption of Kīlauea volcano, Hawaìi. Geochim Cosmochim Acta 83:292–323. doi: 10.1016/j.gca.2011.11.029
Mathieu R, Khedim H, Libourel G, Podor R, Tissandier L, Deloule E, Faure F, Rapin C, Vilasi M (2008) Control of alkali-metal oxide activity in molten silicates. J Non-Crys Solids 354:5079-5083

Mathieu R, Libourel G, Deloule E, Tissandier L, Rapin C, Podor R (2011) Na_2O solubility in CaO–MgO–SiO_2 melts. Geochim Cosmochim Acta 75:608-628
Matousek J (1998) Chemical reactions taking place during vaporization from silicate melts. Ceramics-Silikaty 42:74–80
Matraszek A, Miller M, Singheiser L, Hilpert K (2004) Thermodynamic vaporization studies of the manganese oxide –yttria stabilized zirconia (YSZ) solid solution. J Eur Ceram Soc 24:2649–2656
Matsui T, Naito K (1982) Vaporization study of the niobium monoxide and niobium metal systems by mass spectrometric methods. J Nucl Mater 107:83–89
Matsui T, Naito K (1983) High temperature vaporization studies on the niobium–oxygen system by mass spectrometric method. Int J Mass Spec Ion Phys 47:253–256
Matsui T, Naito K (1985) Vaporization study on UO_2 and $(U_{1-y}Nb_y)O_{2+x}$ by mass spectrometric method. J Nucl Mater 136:69–77
Matsumoto K, Sata T (1981) A study of the calcium oxide–water vapor system by means of the transpiration method. Bull Chem Soc Jpn 54:674–677
Matza SD, Lipschutz ME (1977) Thermal metamorphism of primitive meteorites. VI-Eleven trace elements in Murchison C2 chondrite heated at 400–1000 °C. Lunar Planet Sci Conf Proc 8:161–176
McCreary JR, Thorn RJ (1968) Heat and entropy of sublimation of nickel dichloride, dibromide, and diiodide; dissociation energies of gaseous $NiCl_2$ and $NiBr_2$. J Chem Phys 48:3290–3297
McCubbin FM, Vander Kaaden KE, Tartèse R, Klima RL, Liu Y, Mortimer J, Barnes JJ, Shearer CK, Treiman AH, Lawrence DJ, Elardo SM (2015) Magmatic volatiles (H, C, N, F, S, Cl) in the lunar mantle, crust, and regolith: Abundances, distributions, processes, and reservoirs. Am Mineral 100:1668–1707
McDonald JD, Margrave JL (1968) Mass spectrometric studies at high temperatures XVI. Sublimation and vaporization of chromium trioxide. J Inorg Nucl Chem 30:665–667. doi: 10.1016/0022-1902(68)80495-6
Melosh HJ (1990) Giant impacts and the thermal state of the early Earth. *In:* Newsom HE, Jones JH (eds) Origin of the Earth. Oxford University Press, New York, pp 69–83
Merten U, Bell WE (1967) The transpiration method. *In:* Margrave JL (ed) The Characterization of High Temperature Vapors. John Wiley and Sons, Inc., New York, N.Y., pp 91–114
Meschter PJ, Opila EJ, Jacobson NS (2013) Water vapor–mediated volatilization of high-temperature materials. Ann Rev Mater Res 43:559–588. doi: 10.1146/annurev-matsci-071312-121636
Meschi DJ, Chupka WA, Berkowitz J (1960) Heterogeneous reactions studied by mass spectrometry. I. Reaction of $B_2O_{3(s)}$ with $H_2O_{(g)}$. J Chem Phys 33:530–533
Messier DR (1967) Vapor pressure of Gd_2O_3 from 2350 to 2590 K. J Am Ceram Soc 50:665–668
Miller AR (1975) The vaporization of cadmium oxide by Knudsen effusion. High Temp Sci 7:126–130
Milushin MI, Emel'yanov AM, Gorokhov LN (1987) Enthalpies of formation for $Al_2O_{(g)}$ and $Al_2O_{2(g)}$. High Temp 25:46–51
Mittlefehldt DW, Lindstrom MM (1990) Geochemistry and genesis of the angrites. Geochim Cosmochim Acta 54:3209–3218
Moullet A, Lellouch E, Moreno R, Gurwell M, Black JH, Butler B (2013) Exploring Io's atmospheric composition with apex: First measurement of $^{34}SO_2$ and tentative detection of KCl. Astrophys J. 776:32 doi: 10.1088/0004-637X/776/1/32
Moynier F, Fegley B (2015) The Earth's building blocks. *In:* Badro J and Walter M (eds) The Early Earth: Accretion and Differentiation. AGU, Wiley NY. p. 27–47. doi: 10.1002/9781118860359.ch2
Moynier F, Yin Q, Jacobsen B (2007) Dating the first stage of planet formation. Astrophys J 671:181–183
Muan A, Osborn EF (1965) Phase equilibria among oxides in steelmaking. Addison-Wesley Pub Co, New York
Muenow DW, Uy OM, Margrave JL (1970) Mass spectrometric studies of the vaporization of phosphorus oxides. J Inorg Nucl Chem 32:3459–3467
Munir ZA, Searcy AW (1964) Torsion effusion study of the vapor pressure and heat of sublimation of gallium. J Electrochem Sco, 111:1170–1173
Murad E, Hildenbrand DL (1975) Thermochemical properties of gaseous ZrO and ZrO_2. J Chem Phys 63:1133–1139
Murata KJ (1960) Occurrence of CuCl emission in volcanic flames. Am J Sci 258:769–772
Myers DL, Kulis MJ, Horwath JP, Jacobson NS, Fox DS (2016) Interactions of Ta_2O_5 with water vapor at elevated temperatures. J Am Ceram Soc 100:2353–2357
Mysen BO, Kushiro I (1988) Condensation, evaporation, melting, and crystallization in the primitive solar nebula; experimental data in the system MgO–SiO_2–H_2 to 1.0×10^{-9} bar and 1870 °C with variable oxygen fugacity. Am Mineral 73:1–19
Mysen BO, Virgo D (1980) Trace element partitioning and melt structure: an experimental study at 1 atm pressure. Geochim Cosmochim Acta 44:1917–1930
Nagahara H (2018) Kinetics of gas–solid reactions in the Solar System and beyond. Rev Mineral Geochem 84:461–497
Nagahara and Kushiro (1989) Vaporization experiments in the system plagioclase–hydrogen. Proc NIPR Symp Antarc Meteorites 2:235–251
Nagahara H, Ozawa K (1994) Vaporization rate of forsterite in hydrogen gas. Meteoritics, 29:508–509
Nagai S-I, Niwa K, Shinmei M, Yokokawa T (1973) Knudsen effusion study of silica. J Chem Soc Faraday Trans Phys Chem Condens Phases 69:1628–1634

Nakajima M, Stevenson DJ (2014) Investigation of the initial state of the Moon-forming disk: Bridging SPH simulations and hydrostatic models. Icarus 233:259–267. doi: 10.1016/j.icarus.2014.01.008
Nakajima M, Stevenson DJ (2018) Inefficient volatile loss from the Moon-forming disk: Reconciling the giant impact hypothesis and a wet Moon. Earth Planet. Sci. Lett. 487:117–126
Naughton JJ, Derby JV, Lewis VA (1971) Vaporization from heated lunar samples and the investigation of lunar erosion by volatilized alkalis. Proc Second Lunar Sci Conf 1:449–457
Nesmeyanov AnN, Firsova LP (1960) Equilibrium vapor pressure of solid silicon dioxide. Russ J Phys Chem 34:906–907
Neufeld PD, Janzen AR, Aziz RA (1972) Empirical equations to calculate 16 of the transport collision integrals $\Omega(l, s)^*$ for the Lennard–Jones (12–6) Potential. J Chem Phys, 57:1100–1102
Newbury RS, Barton GW Jr., Searcy AW (1968) Vapor species of the barium – oxygen system. J Chem Phys 48:793–800
Nicolosi SL, Tang I, Munkelwitz H (1979) High-temperature mass spectrometry study of cesium oxide and rubidium oxide. Report NUREG/CR -0867, BNL-NUREG-51030, Brookhaven National Laboratory
Nguyen QN, Baauschlicher CW Jr., Myers DL, Jacobson NS, Opila EJ (2017) Computational and experimental study of thermodynamics of the reaction of titania and water at high temperatures. J Phys Chem A 121:9508–9517
Norris CA, Wood BJ (2017) Earth's volatile contents established by melting and vaporization. Nature 549:507–510. doi: 10.1038/nature23645
Notsu K, Onuma N, Nishida N (1978) High temperature heating of the Allende meteorite. Geochim Cosmochim Acta 42:903-907
Nussinov MD, Chernyak YB (1975) On volatilization in vacuum of the elements from the planet surface soil melts. The Moon 13:377–394
O'Hara MJ, Biggar GM, Richardson SW, Ford CE, Jamieson BG (1970) The nature of seas, mascons and the lunar interior in the light of experimental studies. Proc Apollo 11 Lunar Sci Conf: 695–710
Ohse R (1966) High-temperature vapor-pressure studies of UO_2 by the effusion method and its thermodynamic interpretation. J Chem Phys 44:1375–1378
Ohta H, Suito H (1995) Activities of MnO in $CaO–SiO_2–Al_2O_3–MnO$ (<10 Pct) Fe_tO (<3 Pct) slags saturated with liquid iron. Metall Mater Trans B 26B:295–303
O'Neill HSC (1987) Quartz–fayalite–iron and quartz–fayalite–magnetite equilibria and the free energy of formation of fayalite (Fe_2SiO_4) and magnetite (Fe_3O_4). Am Mineral 72:67–75
O'Neill HSC (1991) The origin of the Moon and the early history of the Earth —A chemical model. Part 1: The Moon. Geochim Cosmochim Acta 55:1135–1157
O'Neill HSC (2005) A method for controlling alkali-metal oxide activities in one-atmosphere experiments and its application to measuring the relative activity coefficients of $NaO_{0.5}$ in silicate melts. Am Mineral 90:497–501. doi: 10.2138/am.2005.1792
O'Neill HSC, Eggins SM (2002) The effect of melt composition on trace element partitioning : an experimental investigation of the activity coefficients of FeO, NiO, CoO, MoO_2 and MoO_3 in silicate melts. Chem Geol 186:151–181
O'Neill HSC, Palme H (2008) Collisional erosion and the non-chondritic composition of the terrestrial planets. Philos Trans A Math Phys Eng Sci 366:4205–4238. doi: 10.1098/rsta.2008.0111
O'Neill HSC, Berry AJ, Eggins SM (2008) The solubility and oxidation state of tungsten in silicate melts: Implications for the comparative chemistry of W and Mo in planetary differentiation processes. Chem Geol 255:346–359
Oniyama E, Wahlbeck PG (1998) Phase equilibria in the bismuth–oxygen system. J Phys Chem B 102:4418–4425
Osborn EF, Tait DB (1952) The system diopside–forsterite–anorthite. Am J Sci, 250:413–433
Otto EM (1964) Equilibrium pressures of oxygen over $Mn_2O_3–Mn_3O_4$ at various temperatures. J Electrochem Soc 111:88–92
Otto EM (1965) Equilibrium pressures of oxygen over $MnO_2–Mn_2O_3$ at various temperatures. J Electrochem Soc 112:367–370
Otto EM (1966a) Equilibrium pressures of O_2 over $Ag_2O–Ag$ at various temperatures. J Electrochem Soc 113:643–645
Otto EM (1966b) Equilibrium pressures of O_2 over oxides of lead at various temperatures. J Electrochem Soc 113:525–527
Pack A, Kremer K, Albrecht N, Simon K, Kronz A (2010) Description of an aerodynamic levitation apparatus with applications in Earth sciences. Geochem Trans 11:4
Palme H, Larimer JW, Lipschutz ME (1988) Moderately volatile elements. *In:* Kerridge JF, Matthews MS (eds) Meteorites and the Early Solar System. University of Arizona Press, Tucson, pp 436–461
Palme H, O'Neill HSC (2014) Cosmochemical estimates of mantle composition. *In:* Carlson RW (ed) Treatise on Geochemistry, Vol. 3: The Mantle and Core, 2nd edn. Elsevier B.V., Amsterdam, pp 1–39
Panish MB (1961a) Vaporization of several rare earth oxides. J Chem Phys 34:1079–1080
Panish MB (1961b) Vaporization of the rare earth oxides. J Chem Phys 34:2197–2198
Panish MB, Reif L (1963) Thermodynamics of the vaporization of Hf and HfO_2: Dissociation energy of HfO. J Chem Phys 38:253–256
Parker EN (1960) The hydrodynamic theory of solar corpuscular radiation and stellar winds. Astrophys J 132:821–866
Partington JR (1950) Thermodynamics: A Modern Introduction to General Thermodynamics and its Application to Chemistry and Physics. 4th edn. Constable, London
Paule RC (1976) Mass spectrometric studies of Al_2O_3 vaporization processes. High Temp Sci 8:257–266

Paulina L, Swinbourne DR, Kho TS (2013) Distribution of bismuth between copper and FeO_x–CaO–SiO_2 slags under copper converting conditions. Trans Inst Min Metall C 122:79-87

Pedley JB, Marshall EM (1983) Thermochemical data for gaseous monoxides. J Phys Chem Ref Data 12: 967–1031

Pelchowitch I, (1954) A study of the evaporation products of alkaline earth oxides. Philips Res Reports 9:42–79

Peleg M, Alcock CB (1966) Application of the torsion technique for the measurement of vapor pressures in the temperature range 1500–2500 °C. J Sci Instrum 43:558–565

Pelton AD, Degterov SA, Eriksson G, Robelin C, Dessureault Y (2000). The modified quasichemical model I—Binary solutions. Metall Mat Trans B 31:651–659

Penzhorn R-D, Ihle HR, Schuster P, Zmbov K (1988) The evaporation process of solid lithium metasilicate. J Nucl Mater 155-157:471–475

Persad AH, Ward CA (2016) Expressions for the Evaporation and Condensation Coefficients in the Hertz-Knudsen Relation. Chem Rev 116:7727–7767. doi: 10.1021/acs.chemrev.5b00511

Petaev MI, Jacobsen SB, Huang S (2016) Testing models of the Moon's origin, III: Phase diagram of a proto-lunar disk and condensation of trace elements. Lunar Planet Sci Conf 47th:2468–2469

Pflieger R, Colle J-Y, Iosilevskiy I, Sheindlin M (2011) Urania vapor composition at very high temperatures. J Appl Phys 109:033501 doi:10.1063/1.3533439

Piacente V, Bardi G, Malaspina L, Desideri A (1973) Dissociation energy of CeO_2 and Ce_2O_2 molecules. J Chem Phys 59:31–36

Piacente V, Desideri A, Bardi G (1972) Torsion effusion determination of sodium partial pressure over Na_2O. J Electrochem Soc 119:75–76

Plante ER (1981) Vapor pressure measurements of potassium over K_2O–SiO_2 solutions by a Knudsen effusion, mass spectrometric method. *In:* Hastie JW (ed.) NBS Special Publication 561: Characterization of High Temperature Vapors and Gases. National Bureau of Standards, Washington DC., pp 265–281

Plante ER, Hastie JW, Kowalska M (1992) Activity of FeO in the FeO–MgO–SiO_2 system determined by high temperature mass spectrometry. ISIJ Int 32:1276–1279

Pokrovski GS, Borisova AY, Bychkov AY (2013) Speciation and transport of metals and metalloids in geological vapors. Rev Mineral Geochemistry76:165–218

Popovič A, Bencze L, Koruza J, Malič B, Kosec M (2012) Knudsen effusion mass spectrometric approach to the thermodynamics of Na_2O–Nb_2O_5 system. Int J Mass Spec 309:70–78

Porter RF, Schissel P, Inghram MG (1955a) A mass spectrometric study of gaseous species in the Al–Al_2O_3 system. J Chem Phys 23:339–342

Porter RF, Chupka WA, Inghram MG (1955b) On the dissociation energies of SrO and MgO molecules. J Chem Phys 23:1347–1348

Porter RF, Chupka WA, Inghram MG (1955c) Mass spectrometric study of gaseous species in the Si–SiO_2 system. J Chem Phys 23:216–217

Pratt JN, Aldred AT (1959) Torsion-effusion apparatus for the study of vapor pressures of alloys. J Sci Inst 36:465–468

Presnall DC, Dixon SA, Dixon JR, O'donnell TH, Brenner NL, Schrock RL, Dycus DW (1978) Liquidus phase relations on the join diopside–forsterite–anorthite from 1 atm to 20 kbar: their bearing on the generation and crystallization of basaltic magma. Contrib Mineral Petrol, 66:203–220

Pretorius EB, Muan A (1992) Activity-Composition Relations of Chromium Oxide in Silicate Melts at 1500 °C under Strongly Reducing Conditions. J Am Ceram Soc 75:1364–1377

Quisefit JP, Toutain JP, Bergametti G, Javoy M, Cheynet B, Person A (1989) Evolution versus cooling of gaseous volcanic emissions from Momotombo Volcano, Nicaragua: Thermochemical model and observations. Geochim Cosmochim Acta 53:2591–2608

Rammensee W, Fraser DG (1982) Determination of activities in silicate melts by Knudsen cell mass spectrometry—I. The system $NaAlSi_3O_8$–$KAlSi_3O_8$. Geochim Cosmochim Acta 46:2269–2278. doi: 10.1016/0016-7037(82)90200-9

Rau H, Schnedler E (1984) Standard molar enthalpy of formation of $GeO_{(g)}$ from flow measurements. J Chem Thermo, 16:673–682

Rego DN, Sigworth GK, Philbrook WO (1985) Thermodynamic study of Na_2O–SiO_2 melts at 1300 °C and 1400 °C. Met Trans 16B:313–323

Rein RH, Chipman J (1965) Activities in liquid solution SiO_2–CaO–MgO–Al_2O_3 at 1600 °C. Trans Metall Soc AIME 233:415

Renggli CJ, King PL, Henley RW, Norman MD (2017) Volcanic gas composition, metal dispersion and deposition during explosive volcanic eruptions on the Moon. Geochim Cosmochim Acta 206:296–311. doi: 10.1016/j.gca.2017.03.012

Reyes RA, Gaskell DR (1983) The Thermodynamic Activity of ZnO in Silicate Melts. Metall Trans B 14B:725-731

Richet P, Bottinga Y (1986) Thermochemical properties of silicate glasses and liquids: a review. Rev Geophys 24:1-25

Richter FM, Davis AM, Ebel DS, Hashimoto A (2002) Elemental and isotopic fractionation of type B calcium-, aluminum-rich inclusions: Experiments, theoretical considerations, and constraints on their thermal evolution. Geochim Cosmochim Acta 66:521–540. doi: 10.1016/S0016-7037(01)00782-7

Richter FM, Janney PE, Mendybaev RA, Davis AM, Wadhwa M (2007) Elemental and isotopic fractionation of Type B CAI-like liquids by evaporation. Geochim Cosmochim Acta 71:5544–5564. doi: 10.1016/j.gca.2007.09.005

Richter FM, Mendybaev RA, Christensen JN, Ebel D, Gaffney A (2011) Laboratory experiments bearing on the origin and evolution of olivine-rich chondrules. Meteorit Planet Sci 46:1152–1178. doi: 10.1111/j.1945-5100.2011.01220.x
Ringwood AE (1966) Chemical evolution of the terrestrial planets. Geochim Cosmochim Acta 30:41–104
Ringwood AE (1979) Origin of the Earth and Moon. Springer-Verlag, New York, N.Y
Ringwood AE, Essene E (1970) Petrogenesis of Apollo 11 basalts, internal constitution and origin of the moon. Proc Apollo 11 Lunar Sci Conf:769–799
Ringwood AE, Kesson SE (1977) Basaltic magmatism and the bulk composition of the moon. Moon 16:425–464.
Rosenblatt GM, Birchenall CE (1961) Vapor pressure of antimony by the torsion–effusion method. J Chem Phys, 35:788–794
Rostai M, Wahlbeck PG (1999) Dissociation energy of gaseous scandium monoxide. J. Chem. Thermo. 31:255–261
Rubin AE, Fegley B, Brett R (1988) Oxidation State in Chondrites. *In:* Kerridge J and Matthews MS (Eds) Meteorites and the Early Solar System, University of Arizona Press, Tucson, pp 488-511
Ruzicka A, Snyder GA, Taylor LA (2001) Comparative geochemistry of basalts from the Moon, Earth, HED asteroid, and Mars: Implications for the origin of the Moon. Geochim Cosmochim Acta 65:979–997
Ryerson FJ (1985) Oxide solution mechanisms in silicate melts: Systematic variations in the activity coefficient of SiO_2. Geochim Cosmochim Acta 49:637–649
Safarian J, Engh TA (2013) Vacuum evaporation of pure metals. Metall Mater Trans A 44:747–753. Doi: 10.1007/s11661-012-1464-2
Samoilova IO, Kazenas EK (1994) Thermodynamics of dissociation and sublimation of strontium oxide. Metally 36–39
Samoilova IO, Kazenas EK (1995) Thermodynamic dissociation and sublimation of calcium oxide. Russ Metall 1:30–33
Sanders DM, Haller WK (1981) A High-temperature transpiration apparatus for the study of the atmosphere above viscous, incongruently vaporizing melts. *In:* Hastie JW (ed) NBS Special Publication 561: Characterization of High Temperature Vapors and Gases. National Bureau of Standards, Washington DC, pp 111–124
Sano N, Belton GR (1974) The thermodynamics of volatilization of chromic oxide: Part II. The species CrO_2Cl_2. Metall Trans 5:2151–2154
Sasamoto T, Mizushima K, Sata T (1979) Transpiration study of the reaction of water vapor with barium oxide. Bull Chem Soc Jpn 52:2127–2129
Sata T, Sasamoto T, Lee HL, Maeda E (1978) Vaporization processes from magnesia materials. Rev Int Haut Temp 15:237–248
Sata T, Sasamoto T, Matsumoto K (1982) High-temperature vaporization of calcium oxide. High Temp –High Press 14:399–408
Saunders N, Miodownik AP (1998) CALPHAD (calculation of phase diagrams): a comprehensive guide (Vol. 1). Elsevier B.V. Amsterdam
Schaefer L, Fegley B (2004a) A thermodynamic model of high temperature lava vaporization on Io. Icarus 169:216–241
Schaefer L, Fegley B (2004b) Heavy metal frost on Venus. Icarus 168:215–219. doi: 10.1016/j.icarus.2003.11.023
Schaefer L, Fegley B (2009) Chemistry of silicate atmospheres of evaporating super-earths. Astrophys J 703:L113-L117
Schaefer L, Fegley B (2010) Volatile element chemistry during metamorphism of ordinary chondritic material and some of its implications for the composition of asteroids. Icarus 205:483–496. doi: 10.1016/j.icarus.2009.08.025
Schaefer L, Lodders K, Fegley B (2012) Vaporization of the earth: Application to exoplanet atmospheres. Astrophys J 755:41. doi: 10.1088/0004-637X/755/1/41
Schuhmann R, Ensio PJ (1951) Thermodynamics of iron silicate slags: Slag saturated with gamma iron. Trans AIME 191:401–411
Shapiro E (1952) Vapor pressure of thorium oxide from 2050 to 2250 K. J Am Chem Soc 74:5233–5235
Schissel PO, Trulson OC (1966) Mass-spectrometric study of the oxidation of tungsten. J Chem Phys 43:737–743
Schmid-Fetzer R, Andersson D, Chevalier PY, Eleno L, Fabrichnaya O, Kattner UR, Sundman B, Wang C, Watson A, Zabdyr L, Zinkevich M (2007) Assessment techniques, database design and software facilities for thermodynamics and diffusion. Calphad 31:38–52
Schönbächler M, Carlson RW, Horan MF, Mock TD, Hauri EH. Schönbächler M, Carlson RW, Horan MF, Mock TD, Hauri EH (2010) Heterogeneous accretion and the moderately volatile element budget of Earth. Science 328:884–7. doi: 10.1126/science.1186239
Schrage RW (1953) Theoretical study of interphase mass transfer. Columbia University Press, New York
Semenov GA (1969) Evaporation of titanium oxide. Inorg Mater 5:54-59
Semenov GA, Frantseva KE, Aurova OA (1983) Mass-spectrometric study of Antimony oxide evaporation. Izv Vyss Uchebnyk Zaved Khimiya I Khimicheskaya Tekhnologiya 26:66–70
Shaffer EE, Jurewicz AJG, Jones JH (1991) Experimental studies of the volatility of V and Mn. *In:* Lunar Planet Sci XXII:1221–1222
Shapiro E (1952) Vapor pressure of thorium oxide from 2050 to 2250 °K. J Am Chem Soc 74:5233–5235
Shchedrin WM, Kulikov IS, Vas'kin VN, Teleguin AA (1978) Vaporization of magnetite and wüstite in neutral vacuum with mass-spectrometric analysis of gaseous phase. J Chem Thermodyn 10:9–18
Shchukarev SA, Semenov GA, Rat'kovskii IA (1961a) Determination of the saturation vapor pressure of thallic oxide. Russ J Inorg Chem 6:2817–2818

Shchukarev SA, Semenov GA, Rat'kovskii IA, Perevoshchikov VA (1961b) Determination of the saturated vapor pressure of indium oxide. Russ J Gen Chem 31:1952–1954

Shchukarev SA, Semenov GA, Frantseva KE (1966) A thermodynamic study of the volatilization of the lower oxides of niobium. Russ J Inorg Chem 11:129-135

Shchukarev SA, Semenov GA, Rat'kovskii IA (1969) A thermal investigation of the evaporation of gallium and indium oxides. Russ J Inorg Chem 14:1–5

Shimaoka T, Nakamura N (1989) Vaporization of sodium from partially molten chondritic material. Proc NIPR Symp Antarct Meteorites 2:252–267

Shimaoka T, Nakamura (1991) The effect of total pressure on vaporization of alkalis from partially molten chondritic material. *In:*Levasseur-Regourd AC, Hasegawa H (eds) Origin and Evolution of Interplanetary Dust. Kluwer Academic Publishers, Dordrecht, pp 79–82

Shimaoka TK, Miyano N, Baba T, Yamamoto K, Nakamura N (1994) Volatilization of alkali metals from the heated Murchison (CM2) Meteorite. Proc NIPR Symp Antarct Meteorites 7:164–177

Shimazaki E, Matsumoto N, Niwa K (1957) The vapor pressure of germanium dioxide. Bull Chem Soc Jpn 30:969–971

Shornikov SI (2015) Vaporization coefficients of oxides contained in the melts of Ca–Al-inclusions in chondrites. Geochemistry Int 53:1080–1089. doi: 10.1134/S0016702915100055

Shornikov SI, Archakov IY, Shul'ts MM (1998) Mass spectrometric study of vaporization and thermodynamic properties of silicon dioxide. I. Composition of the gas phase and partial vapor pressures of the molecular forms over silicon dioxide. Russ J Gen Chem 68:1171–1177

Shuva MAH, Rhamdhani MA, Brooks GA, Masood S, Reuter MA (2016) Thermodynamics behavior of germanium during equilibrium reactions between FeO_x–CaO–SiO_2–MgO slag and molten copper. Metall Mater Trans B 47B:2889-2903

Sidorov LN, Minayeva II, Zasorin EZ, Sorokin ID, Borshchevskiy AYa (1980) Mass spectrometric investigation of gas-phase equilibria over bismuth trioxide. High Temp Sci 12:175-196

Siebert J, Sossi PA, Blanchard I, Mahan B, Badro J, Moynier F (2018) Chondritic Mn/Na ratio and limited post-nebular volatile loss of the Earth. Earth Planet Sci Lett 485:130–139. doi: 10.1016/j.epsl.2017.12.042

Sime RJ, Gregory NW (1960) Vapor pressures of $FeCl_2$, $FeBr_2$ and FeI_2 by the torsion effusion method. J Phys Chem, 64:86–89

Simmons LL, Lowden LF, Ehlert TC (1977) A mass spectrometric study of K_2CO_3 and K_2O. J Phys Chem 81:706-709

Skinner HB, Searcy AW (1973) Mass spectrometric studies of Rhenium. J Phys Chem 77:1578–1585. doi: 10.1149/04601.0039ecst

Smoes S, Drowart J (1984) Determination of the dissociation energies of gaseous iron monoxide and manganese monoxide by the mass spectrometric Knudsen cell method. *In:*Margrave JL, (ed) Modern High Temperature Science. Humana Press, Clifton, NJ, pp 31–52

Smoes S, Drowart J, Myers CE (1976) Determination of the atomization energies of the molecules $TaO_{(g)}$ and $TaO_{2(g)}$ by the mass-spectrometric Knudsen cell method. J Chem Thermo 8:225–239

Sossi PA, Klemme S, O'Neill HSC, Berndt J, Moynier F (2016a) Volatility of the elements and the role of oxygen fugacity. EMPG XV, ETH Zürich, Switzerland, 5–8 June

Sossi PA, Nebel O, Anand M, Poitrasson F (2016b) On the iron isotope composition of Mars and volatile depletion in the terrestrial planets. Earth Planet Sci Lett 449:360–371

Sossi PA, Nebel O, O'Neill HSC, Moynier F (2018) Zinc isotope composition of the Earth and its behavior during planetary accretion. Chem Geol. 477:73–84

Speelmans I (2014) The behavior of moderately volatile elements during partial melting. Masters Thesis, Rheinische Friedrich-Wilhelms-Universität Bonn

Srivastava RD, Farber M (1981) The evaporation coefficients of the Al_2O_3 vapor species. J Chem Sci 90:257–259

Stafford FE, Berkowitz J (1964) Mass-spectrometric study of the reaction of water vapor with solid barium oxide. J Chem Phys 40:2963–2969

Stebbins JF, Carmichael ISE, Moret LK (1984) Heat capacities and entropies of silicate liquids and glasses. Contrib Min Pet 86 :131-148

Stolyarova VL (2001) A mass spectrometric study of the thermodynamic properties of oxide melts. Glass Phys Chem 27:3–15

Stolyarova VL, Lopatin SI, Fabrichnaya OB, Shugurov SM (2014) Mass spectrometric study of thermodynamic properties in the Yb_2O_3– ZrO_2 system at high temperatures. Rapid Commun Mass Spectrom 28:109–114

Storey WC (1973) Volatilization studies on a terrestrial basalt and their applicability to volatilization from the lunar surface. Nat Phys Sci 241:154–157

Suito H, Inoue R (1984) Manganese equilibrium between molten iron and MgO-saturated CaO–Fe_tO–SiO_2–MnO slags. ISIJ 24:257–265

Symonds RB, Reed MH (1993) Calculation of Multicomponent chemical equilibria in gas–solid–liquid systems: Calculation methods, thermochemical data, and applications to studies of high-temperature volcanic gases with examples from Mount St. Helens. Am J Sci 293:758–864

Symonds RB, Rose WI, Bluth GJS, Gerlach TM (1994) Volcanic gas studies: Methods results, and applications. Rev Mineral 30:1–66

Symonds RB, Rose WI, Reed MH, Lichte FE, Finnegan DL (1987) Volatilization, transport and sublimation of metallic and non-metallic elements in high temperature gases at Merapi Volcano, Indonesia. Geochim Cosmochim Acta 51:2083–2101

Takeda Y, Yazawa, A (1989) Dissolution loss of copper, tin and lead in FeO_n-SiO_2-CaO slag. *In:*Koch M, Taylor JC (eds.) Productivity and Technology in the Metallurgical Industries, The Minerals, Metals and Materials Society, Pittsburgh, PA, pp. 227– 240

Tartèse R, Anand M, Barnes JJ, Starkey NA, Franchi IA, Sano Y (2013) The abundance, distribution, and isotopic composition of Hydrogen in the Moon as revealed by basaltic lunar samples: Implications for the volatile inventory of the Moon. Geochim Cosmochim Acta 122:58–74. doi: 10.1016/j.gca.2013.08.014

Taylor GB, Hulett GA (1913) The dissociation of mercuric oxide. J Phys Chem 17:565–591

Taylor GJ, Wieczorek MA (2014) Lunar bulk chemical composition: a post-Gravity Recovery and Interior Laboratory reassessment. Philos Trans R Soc A Math Phys Eng Sci 372:20130242

Taylor SR, Taylor GJ, Taylor LA (2006) The Moon: A Taylor perspective. Geochim Cosmochim Acta 70:5904–5918. doi: 10.1016/j.gca.2006.06.262

Tetenbaum M (1975) High temperature vaporization behavior of the neodymium sesquioxide phase. High Temp Sci 7:37–43

Theard LP, Hildenbrand DL (1964) Heat of formation of $Be_2O_{(g)}$ by mass spectrometry. J Chem Phys 41:3416–3420

Tissandier L, Libourel G, Toplis MJ, Chaussidon M (1998) Alkali volatilization at high temperature in silicate melts. Meteorit Planet Sci 33:A154–A155

Torgesen T (1989) Terrestrial helium degassing fluxes and the atmospheric helium budget: Implications with respect to the degassing processes of continental crust. Chem Geo 79:1-14

Tower LK (1969) Estimated gas compositions in equilibrium with condensed phases of the Cs–O system. NASA Technical Memorandum TM X-52702, Lewis (Glenn) Research Center, Cleveland, OH

Trinquier A, Birck JL, Allègre CJ, Göpel C, Ulfbeck D (2008) ^{53}Mn–^{53}Cr systematics of the early Solar System revisited. Geochim Cosmochim Acta 72:5146–5163. doi: 10.1016/j.gca.2008.03.023

Tsuchiyama A, Nagahara H, Kushiro I (1981) Volatilization of sodium from silicate melt spheres and its application to the formation of chondrules. Geochim Cosmochim Acta 45:1357–1367. doi: 10.1016/0016-7037(81)90228-3

Turkdogan ET (2000) Assessment of P_2O_5 activity coefficients in molten slags. ISIJ Intl 40:964-970

Valderraman J, Jacob KT (1977) Vapor pressure and dissociation energy of In_2O. Thermochim Acta 21:215–224

Visscher C, Fegley B (2013) Chemistry of impact-generated silicate melt–vapor debris disks. Astrophys J 767:L12

Viswanadham P, Edwards JG (1975) High-temperature thermodynamic properties of MnS by the dynamic Knudsen–torsion effusion method. J Chem Phys 62:3875–3882

Volmer M (1931) Molargewichtsbestimmung im Gaszustand bei sehr niedrigen Drucken nach den Experimentalarbeiten von S. Heller und K. Neumann. Zeitschrift für Phys Chemie 863–873

Wahlbeck PG (1986) Comparison and interrelations of four methods of measurement of equilibrium vapor pressures at high temperatures. High Temp Sci 21:189–232

Wahlbeck PG, Gilles PW (1967) Dissociation energy of $TiO_{(g)}$ and the high-temperature vaporization and thermodynamics of the titanium oxides. II. Trititanium Pentoxide. J Chem Phys 46:2465–2473.

Wahlbeck PG, Myers DL (1997) Thermodynamics of the Tl–O system and Tl-superconductors. J Chem Phys 106:10383–10384

Wahlbeck PG, Richards RR, Myers DL (1991) Vaporization of thallium (III) oxide and thallium activities in thallium superconductors. J Chem Phys 95:9122–9127. doi: 10.1063/1.461191

Wahrenberger C, Seward TM, Dietrich V (2002) Volatile trace-element transport in high-temperature gases from Kudriavy volcano (Iturup, Kurile Islands, Russia). *In:* Hellmann R, Wood SA (eds) The Geochemical Society Special Publication No. 7. Water–Rock Interactions, Ore Deposits and Environmental Geochemistry. The Geochemical Society, Washington, DC, pp 307–327

Walsh PN, Goldstein HW, White D (1960) Vaporization of rare-earth oxides. J Am Ceram Soc 43:229–233

Wang M-S, Lipschutz ME (2005) Thermal metamorphism of primitive meteorites—XII. The enstatite chondrites revisited. Env Chem 2:215–226

Wang J, Davis AM, Clayton RN, Hashimoto A (1999) Evaporation of single crystal forsterite: Evaporation kinetics, magnesium isotope fractionation, and implications of mass-dependent isotopic fractionation of a diffusion-controlled reservoir. Geochim Cosmochim Acta 63:953–966

Wang H, Stolyarova VL, Lopatin SI, Kutuzova ME, Seetharaman S (2010) High-temperature mass spectrometric study of the vaporization processes of V_2O_3 and vanadium-containing slags. Rapid Comm Mass Spec 24:2420–2430

Wänke H, Dreibus G, Jagoutz E (1984) Mantle chemistry and accretion history of the Earth. *In:*Kröner A, Hanson GN, Goodwin AM (Eds.) Archaean Geochemistry, Springer, Berlin, Heidelberg, pp 1–24

Washburn CA (1963) Vaporization of iron oxides. Report UCRL-10991, Lawrence Radiation Laboratory, Berkeley CA

Wasson JT, Kallemeyn GW (1988) Compositions of chondrites. Philos Trans R Soc A Math Phys Eng Sci 325:535–544

Webster JD (1997) Chloride solubility in felsic melts and the role of chloride in magmatic degassing. J Petrol 38:1793–1807. doi: 10.1093/petroj/38.12.1793

Wetzel S, Pucci A, Gail H-P (2012) Vapor pressure and evaporation coefficient measurements at elevated temperatures with a Knudsen cell and a quartz crystal microbalance: new data for SiO. J Chem Eng Data 57:1594–1601

White D, Seshadri KS, Dever DF, Mann DE, Linevsky MJ (1963) Infrared spectra and the structures and thermodynamics of gaseous LiO, Li_2O, and Li_2O_2. J Chem Phys 39:2463–2473

Witt-Eickschen G, Palme H, O'Neill HSC, Allen CM (2009) The geochemistry of the volatile trace elements As, Cd, Ga, In and Sn in the Earth's mantle: New evidence from in situ analyses of mantle xenoliths. Geochim Cosmochim Acta 73:1755–1778. doi: 10.1016/j.gca.2008.12.013

Wolff EG, Alcock CB (1962) The volatilization of high-temperature materials in vacuo. Trans Br Ceram Soc 61:667–684

Wolf R, Anders E (1980) Moon and Earth: compositional differences inferred from siderophiles, volatiles, and alkalis in basalts. Geochim Cosmochim Acta 44:2111–2124. doi: 10.1016/0016-7037(80)90208-2

Wolf R, Richter GR, Woodrow AB, Anders E (1980) Chemical fractionations in meteorites—XI. C2 chondrites. Geochim Cosmochim Acta 44:711–717

Wombacher F, Rehkämper M, Mezger K, Bischoff A, Münker C (2008) Cadmium stable isotope cosmochemistry. Geochim Cosmochim Acta 72:646–667

Woolum DS, Cassen P (1999) Astronomical constraints on nebular temperatures: Implications for planetesimal formation. Meteorit Planet Sci 34:897–907. doi: 10.1111/j.1945-5100.1999.tb01408.x

Wood BJ, Halliday AN (2010) The lead isotopic age of the Earth can be explained by core formation alone. Nature 465:767–70. doi: 10.1038/nature09072

Wood BJ, Wade J (2013) Activities and volatilities of trace components in silicate melts: a novel use of metal–silicate partitioning data. Contrib Mineral Petrol 166:911–921. doi: 10.1007/s00410-013-0896-z

Wood BJ, Kiseeva ES, Mirolo FJ (2014) Accretion and core formation: the effects of sulfur on metal-silicate partition coefficients. Geochim Cosmochim Acta 145:248–267. doi: 10.1016/j.gca.2014.09.002

Wu HY, Wahlbeck PG (1972) Vapor pressures of $TiO_{(g)}$ in equilibrium with $Ti_2O_{3(s)}$ and $Ti_3O_{5(s,\beta)}$; Dissociation energy of $TiO_{(g)}$. J Chem Phys 56: 4534–4540

Wu P, Eriksson G, Pelton AD (1993) Optimization of the thermodynamic properties and phase diagrams of the Na_2O–SiO_2 and K_2O–SiO_2 Systems. J Am Ceram Soc 76:2059–2064

Wulf AV, Palme H, Jochum KP (1995) Fractionation of volatile elements in the early solar system: evidence from heating experiments on primitive meteorites. Planet Space Sci 43:451–468

Wyllie G (1949) Evaporation and surface structure of liquids. Proc R Soc Lond A 197:383–395

Xiao B, Stixrude L (2018) Critical vaporization of $MgSiO_3$. PNAS 115:5371–5376

Yazhenskikh E, Hack K, Müller M (2006) Critical thermodynamic evaluation of oxide systems relevant to fuel ashes and slags Part 2: alkali oxide–alumina systems. CALPHAD 30:397-404

Yazhenskikh E, Hack K, Müller M (2011) Critical thermodynamic evaluation of oxide systems relevant to fuel ashes and slags Part 5: Potassium oxide–alumina–silica. CALPHAD 35:6-19

Yan S Swinbourne DR (2003) Distribution of germanium under lead smelting conditions. Miner Process Extr Metall 112:75–80

Yu Y, Hewins RH, Wang J (2003) Experimental study of evaporation and isotopic mass fractionation of potassium in silicate melts. Geochim Cosmochim Acta 67:773–786.

Zahnle KJ, Catling DC (2017) The cosmic shoreline: The evidence that escape determines which planets have atmospheres, and what this may mean for Proxima Centauri B. Astrophys J, 843:122

Zaitsev AI, Mogutnov BM (1995) Thermodynamic properties and phase equilibria in the MnO–SiO_2 system. J Mater Chem 5:1063–1073

Zaitsev AI, Mogutnov BM (1997) Thermodynamics of CaO–SiO_2 and MnO–SiO_2 Melts: I. Experimental Study. Inorg Mater 33:707–714

Zaitsev AI, Shelkova NE, Lyakishev NP, Mogutnov BM (1999) Thermodynamic properties and phase equilibria in the Na_2O–SiO_2 system. Phys Chem Chem Phys 1:1899–1907. doi: 10.1039/a809003c

Zaitsev AI, Shelkova NE, Lyakishev NP, Mogutnov BM (2000) Modeling of the thermodynamic properties of silicate melts and calculation of phase equilibria in the K_2O–SiO_2 system. Russ J Phys Chem 74:1033–1038

Zaitsev AI, Arutyunyan NA, Shaposhnikov NG, Zaitseva NE, Burtsev VT (2006) Experimental study and modeling of the thermodynamic properties of magnesium silicates. Russ J Phys Chem 80:335–344. doi: 10.1134/S0036024406030058

Zanda B (2004) Chondrules. Earth Planet Sci Lett 224:1–17

Zelenski M, Taran Y (2012) Volcanic emissions of molecular chlorine. Geochim Cosmochim Acta 87:210–226. doi: 10.1016/j.gca.2012.03.034

Zelenski ME, Fischer TP, de Moor JM, Marty B, Zimmermann L, Ayalew D, Nekrasov AN, Karandashev VK (2013) Trace elements in the gas emissions from the Erta Ale volcano, Afar, Ethiopia. Chem Geol 357:95–116. doi: 10.1016/j.chemgeo.2013.08.022

Zimmermann E, Koenigs S, Neuschuetz D (1999) Mass Spectrometric Determination of the Partial Pressures of SnO, Sn_2O_2 and O_2 in Equilibrium with Solid SnO_2. Zeit Phys Chemie 209:271–280

Zmbov KF, Ames LL, Margrave JL (1973) A mass spectrometric study of the vapor species over silicon and silicon oxides. High Temp Sci 5:235–240